Synthesis, Characterization, and Performance Assessment of a Novel Thiazine-Fe_3O_4-TiO_2-SiO_2-Bentonite Nanocomposite for Asphaltene Precipitation Inhibition

By

Yuliya Ten

Thesis submitted to the School of Mining and Geosciences of Nazarbayev University in Partial Fulfillment of the Requirements for the Degree of

Master of Science in Petroleum Engineering

Nazarbayev University

April 2023

Acknowledgments

I would like to extend my profound gratitude to everyone who helped to complete my dissertation. I want to start by expressing my gratitude to my supervisor Dr. Ali Shafiei for his essential advice, astute criticism, and unwavering support throughout the study process. Furthermore, I would like to thank my co-supervisor Dr. Timur Atabaev for his guidance, support, and access to his research laboratory, which enabled completion of my experimental program. I also would like to thank Dr. Simin Tazikeh, postdoctoral fellow and research group member, who helped me a lot during my studies especially with my experiments and interpretation of the results.

I also would like to thank Dr. Sohrab Zendehboudi (MUN, Canada) and Dr. Sonny Irawan for serving in my thesis committee. I appreciate their constructive feedback, which contributed to the improvement of quality of this dissertation.

The present work was a part of Collaborative Research Proposal Faculty grant project (091019CRP2103) entitled: "A comprehensive study on asphaltene characterization and screening asphaltene deposition inhibitors for Kazakhstan crude oils." I would like to acknowledge the financial support I received from Nazarbayev University through this grant.

I also want to thank the School of Mining and Geosciences staff and faculty at Nazarbayev University for giving me a top-notch academic setting, access to tools and opportunities, and for their encouragement and support. Finally, I would like to thank my fellow students Kamilya Arstanova and Alisher Rakhmetullin for their efforts, who gave me helpful comments, ideas, and motivation throughout the study process.

I want to thank my family and friends from the bottom of my heart for their unwavering love, support, and inspiration throughout my academic career. Their unfailing believe in me and support has given me courage and inspiration during this journey.

Originality Statement

I, Yuliya Ten, hereby declare that this submission is my own work and to the best of my knowledge it contains no materials previously published or written by another person or substantial proportions of material which have been accepted for the award of any other degree or diploma at Nazarbayev University or any other educational institution, except where due acknowledgment is made in the thesis.

Any contribution made to the research by others, with whom I have worked at NU or elsewhere is explicitly acknowledged in the thesis.

I also declare that the intellectual content of this thesis is the product of my own work, except to the extent that assistance from others in the project's design and conception or in style, presentation, and linguistic expression is acknowledged.

Signed on **15.04.2023**

_____

Nomenclature

Acronyms and Abbreviations

AOP	Asphaltene onset point
BET	Brunauer-Emmett-Teller
CII	Colloidal instability index
EOR	Enhanced oil recovery
IFT	Interfacial tension
IUPAC	International Union of Pure and Applied Chemistry
n-heptane	Normal heptane
NP	Nanoparticle
NC	Nanocomposite
SARA	Saturate, Aromatics, Resin, Asphaltene
SEM	Scanning electron microscope
TGA	Thermogravimetric analysis
XRD	X-ray diffraction
EDAX	Energy dispersive X-ray analysis

Symbols

A	Surface area of NC, m^2/g
A_d	Asphaltene absorbance after dilution
A_i	Initial absorbance of asphaltene
C_d	Concentration of asphaltene after dilution
C_0	Initial asphaltene concentration, mg/L
C_e	Equilibrium asphaltene concentration, mg/L
C_{NP}	Nanoparticle concentration, g/L
K_F	Freundlich constant

K_L	Langmuir constant
M	Mass of asphaltene, mg
m	Mass of NC, g
$\frac{m_{NP}}{C_0}$	NP mass per Initial Asphaltene Concentration, $\frac{\text{g}}{\text{mg/L}}$
m_{ads}	Mass of adsorbed asphaltene, g
$m_{TGA(ads+NP)}$	Mass of adsorbed asphaltene and NP from TGA, g
$m_{TGA(NP)}$	Final mass of NP, g
V_1	Volume of synthetic oil, ml
V_2	Volume of toluene, ml
MW	Molecular Weight, mol/g
q_{eq}	Equilibrium asphaltene concentration, mg/g
Q_e	Equilibrium asphaltene amount per surface area, c
Q_m	Maximum amount of adsorbed asphaltene per surface area, s the equilibrium adsorbate uptake per surface area of the adsorbent (mg/m^2),
SD_i	Standardized Deviation, %

Greek Letters

ε	Molar absorption coefficient, $M^{-1}cm^{-1}$
λ	Spectrophotometry wavelength, nm

Metric Conversion Factors

1 ppm	1 mg/L
1 min	60 sec
1 hour	3600 sec
1 mD	9.869×10^{-16} m^2
1 bbl	0.159 m^3
1 nm	10^{-9} m

Abstract

Asphaltene precipitation and deposition in petroleum industry presents a big challenge. Major issues with asphaltene deposition include clogging of pores, flow impairment in pipelines, and surface facilities and production equipment. Nanoparticles exhibited excellent properties to prevent asphaltene precipitation. In this research work, a novel nanocomposite (NC) of Thiazine-Fe_3O_4-SiO_2-TiO_2-Bentonite was synthesized, characterized, and tested as a novel agent for asphaltene precipitation inhibition. The NC was characterized using various techniques including scanning electron microscopy (SEM), energy dispersive spectroscopy (EDS), Brunauer–Emmett–Teller analysis (BET), X-ray diffraction (XRD), and Fourier-Transform infrared spectroscopy (FTIR). The particle size of the NC determined by using SEM is on the range of 38-74 nm. The crystallite size of the NC calculated from XRD is 46 nm showing good match with SEM measurements. The surface area of the NC was determined using BET analysis as 43.84 m^2/g. Asphaltene was extracted from a paraffinic heavy crude oil from West Kazakhstan using indirect IP-143 standard method. UV-spectroscopy was used to investigate asphaltene onset point (AOP) in absence and presence of the NC. The research results demonstrated that the assessed NC can effectively delay the asphaltene onset point in a 0.5 wt% asphaltene synthetic oil. The new NC works best at 0.3 wt% concentration of NC, increasing AOP from 40 to 45 vol% of *n*-heptane. The Langmuir model fitted best to the experimental adsorption isotherms data for the NC suggesting a monolayer asphaltene adsorption. Thermogravimetric analysis (TGA) was used to assess thermal stability of the NC, to investigate adsorption kinetics of the asphaltene-NC system, oxidation behavior, and catalytic effect of the NC. Asphaltene adsorption and obtain adsorption kinetics isotherms. TGA analysis also revealed that asphaltene adsorbed on the NC and pure asphaltene both oxidize. When the NC was added, this significantly lowered the temperature at which asphaltene oxidizes proving that the novel NC has a catalytic effect. TGA analysis confirmed that the main function of the NC in process of asphaltene oxidation is to assist the process by increasing its surface exposure in addition to acting as a catalyst. Overall, the results showed that the novel NC performed well under laboratory conditions and prevented asphaltene precipitation, effectively. The outcomes of this research work can help in development and testing new nano-inhibitors leading to higher rates of oil recovery and trouble free production and transportation of problematic crude oils.

Keywords: Asphaltene precipitation, asphaltene adsorption, asphaltene precipitation, AOP shift, nanocomposite, nano-inhibitors, adsorption kinetics.

Table of Contents

List of Figures

List of Tables

1 INTRODUCTION

In this chapter, a brief background on the nature of asphaltene, their molecular structure, adsorption properties, and the application of ion nanocomposites site as inhibitors for asphaltene precipitation inhibition is provided. Then, the problem statement, aims, objectives, and methods used for the proposed research and their relevance to the oil industries are presented. Finally, the thesis structure and organization are introduced at the end of the background chapter.

Uninterrupted crude oil production is a major force that keeps the world economy running smoothly, as most countries either produce or import crude oil to develop their economic system [1]. Flow assurance issues such as wax deposition, hydrate formation, and asphaltene precipitation are all conditions that threaten the crude oil supply, with asphaltene being the most damaging of them all [2]. As a result, the study of asphaltene has gotten much attention in the oil and gas industry. McMullen [3] discusses the industry's flow assurance challenges, emphasizing the need to manage and build confidence in the areas of erosion, wax and asphaltene deposition, corrosion, and hydrate formation, all of which are dependent on fluid mechanics, oil field chemistry, process instrumentation, and control, and heat transfer.

Asphaltene management has relied solely on empirical methods, with a few successful field trials but no robust analytical model to forecast its onset and deposition. Asphaltene remains ambiguous because a minor is recognized explicitly about the molecule. Asphaltene is the highest molecular weight oil fraction, usually by their solubility. Based on the solubility approach, asphaltene dissolves in aromatic solvents (e.g., toluene) and precipitates in paraffinic solvents like *n*-heptane [4]. Asphaltene is composed of hydrocarbons and heteroatoms such as sulfur (S), nitrogen (N), oxygen (O), and trace metals such as nickel (Ni) and vanadium (V) [4]. Asphaltene is thought to be encased in resin that act as peptizing agents, keeping the asphaltene in a colloidal dispersion (rather than a solution) within the crude oil [5]. They can precipitate as the oil's temperature, pressure, or composition changes. When the equilibrium has shifted, the resin surrounding the asphaltene tend to move into the non-polar part of the oil to restore the equilibrium [5]. In such cases, asphaltene particles overcome Brownian forces and form nanoaggregates. Pressure is the most critical factor influencing asphaltene precipitation/deposition in isotherm system. Typically, asphaltene and light ends compete for solubility in oil. When the reservoir pressure is reduced to saturation pressure, light oil ends in

a gas state, and asphaltene has more opportunities to dissolve in oil. Therefore, as the pressure decreases, it can be argued that asphaltene is stabilized in oil [5].

There are several techniques available to mitigate asphaltene precipitation and deposition. Figure 1-1 depicts different asphaltene deposition treatment methods. They include mechanical, chemical, thermal, ultrasonic, bacterial, and nanotechnology-based techniques. The mechanical method includes using slicklines or coil tubing to clean the wellbore. However, this method is time-consuming and expensive, especially if the deposits are hard and long. Another method is the application of chemicals (aromatic solvents) to dissolve the deposited asphaltene. This method's limitation is the aromatic solvent's low flash point, which can be very dangerous. Aromatic solvents such as xylene and toluene have flash points of 28°C and 5°C, respectively [6]. The low ignition temperature implies a high risk of explosion and fire. When any ignition or spark source appears, aromatic solvents can instantly ignite since their ignition temperature is near room temperature. The thermal method decreases the viscosity of crude oil and helps to ease the flow of asphaltic crude oil. The thermal method includes the application of steam or downhole heaters, requiring lots of electrical energy [6]. Pu et al. conducted several experiments and concluded that ultrasonic waves could be used to treat the formation damage [7] .R. Rezaei Dehshibi et al. investigated the removal effect of ultrasonic waves on asphaltene deposition [8] The ultrasonic technique may positively affect the reversibility of asphaltene deposition, so asphaltene molecules deposited on the walls could dissolve in the oil again. According to the R. Rezaei Dehshibi et al. study, around 70% of deposited asphaltene will not precipitate using the ultrasonic method [8]. Large aggregate asphaltene could be separated from its surface by vibration of ultrasound waves and moved into the main flow path.

As all of the methods mentioned above suffer from some limitations, there is a need for a new alternative method to provide more effective and efficient inhibition. The application of nanotechnology was introduced as a new solution to mitigate issues caused by asphaltene deposition. Asphaltene precipitation in porous media has enhanced oil recovery implications, as well. There is an asphaltene adsorption phenomenon when molecules of asphaltene tend to adhere to the walls of porous media, changing the wettability of the formation from a water-wet to an oil-wet. Adsorption of asphaltene onto the surface of NPs can decrease the chance of asphaltene precipitation/deposition enhancing the flow of oil in porous media and increasing the oil recovery via wettability alteration (Figure 1-2) [9]. The most significant advantage of using NPs is their high surface-to-volume ratio, meaning they can absorb a high amount of

asphaltene molecules [10]. In addition, NPs can quickly move through the pore channels because of their small size. However, research shows that NPs can only slow down the deposition of asphaltene, and complete prevention of precipitation is not feasible [11]. The main advantages and disadvantages of asphaltene deposition prevention techniques are summarized in Table 1.

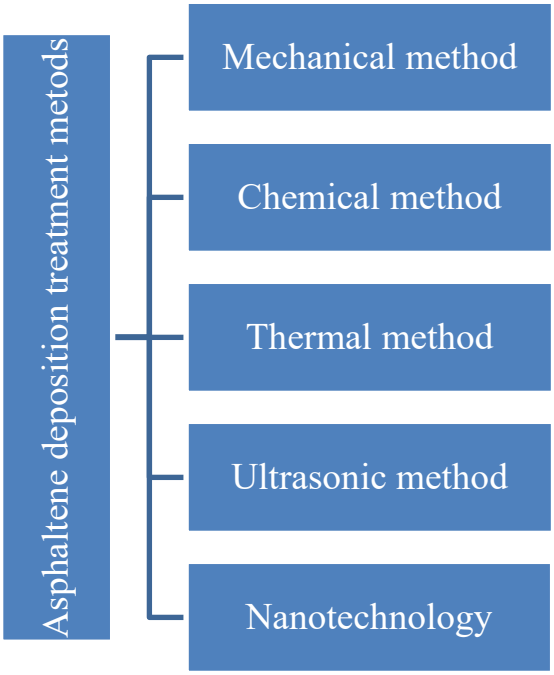

Figure 1-1 Asphaltene deposition treatment techniques

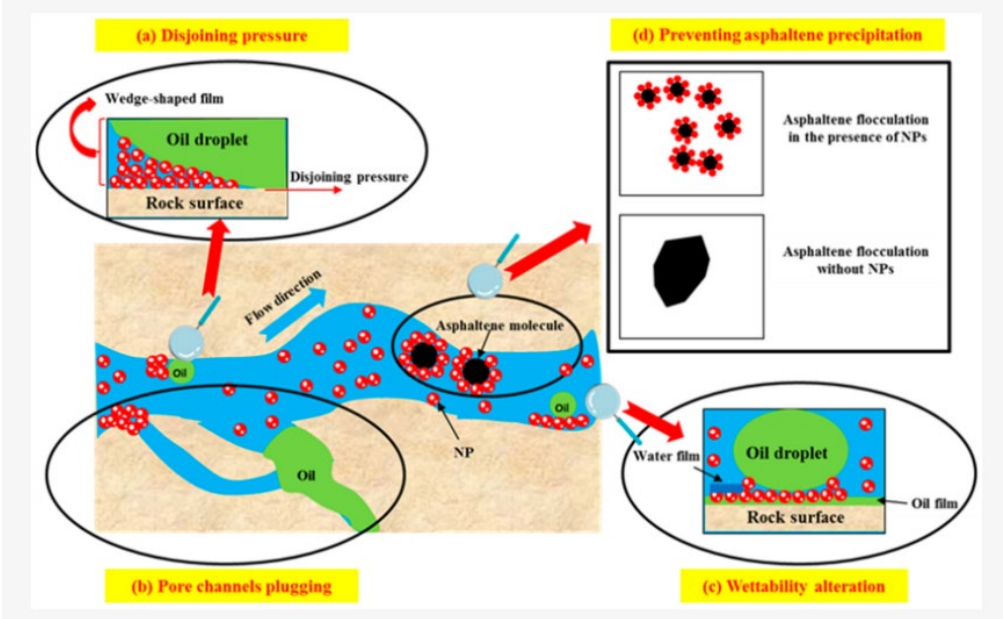

Figure 1-2. Schematic mechanisms of nanofluid [9].

Table 1-1. Advantages and disadvantages of asphaltene deposition mitigation techniques.

Treatment techniques	Advantages	Disadvantages
Mechanical	Simple technique	Expensive Time-consuming [6]
Chemical	The high solubility of asphaltene in aromatic solvents	Risk of explosions [6] Corrosion Environmental hazards
Thermal	Improves the flow of oil. Decreases viscosity of crude oil.	It may cause formation damage High cost Availability of electricity
Ultrasonic	No harm to the reservoir and ecology Low operation costs	A small area of effect [8]
Nanotechnology	High removal efficiency	Recyclability [6]

1.1 Problem statement

Asphaltene precipitation is generally accepted to cause serious flow assurance challenges. The research on asphaltene science contains lots of evidence of NPs being used effectively to inhibit asphaltene precipitation. Nowadays, most mitigation measures deal with the negative consequences of the asphaltene deposition problem. Various chemical and mechanical methods require additional costs and time, and there is a possibility that the precipitation will be repeated. Hence, it is ineffective, as there is no guarantee that pressure and temperature will not change with time in the field and that asphaltene will not deposit again. NPs have benefits not only from the technical side, including their specific properties, such as the high surface area to volume ratio, but it is also advantageous from the economic and environmental aspects [5]. Previous studies have shown the positive impact of NPs on asphaltene aggregation. The nano-inhibition process is required to treat the asphaltene deposition problem, as it deals with this problem on a molecular level. Nassar et al. investigated the fast adsorption of asphaltene aggregates to the surface of aluminum oxide (γ-Al_2O_3) NPs [12]. In another study, Nassar et al. reported that NiO > Co_3O_4 > Fe_3O_4 is the order in which transition metal oxide NPs lose their affinity for adhering to asphaltene [13]. Specific NPs improve the specific area of oil production; however, combining different nano-substances allows for simultaneously improving different aspects of oil production. The new nanocomposite will not only adsorb

asphaltene but also consider such factors as acidity and solution stabilization. The main novelty of this work is that few studies were conducted to investigate the asphaltene inhibition properties of NPs, and even less studies were performed on nanocomposites as nano-inhibitors. There is a still huge gap between the factors affecting performance of NPs as asphaltene inhibitor. These factors include the size, surface chemistry, and concentration of nanocomposite. Furthermore, there is a need to optimize the use of NPs to achieve maximum inhibition while minimizing any negative effects on the oil and gas production process.

1.2 Relevance to the industry

The US Energy Information Administration (EIA) forecasts that worldwide energy consumption will increase by nearly 50% between 2018 and 2050 in its latest International Energy Outlook 2019 (IEO2019) Reference case [14]. The petroleum industry remains the most significant energy supplier, as nearly half of the world's primary energy source will be fossil fuels. Asphaltene deposition is a crucial problem for the oil and gas industry.

Most techniques for inhibition/removing asphaltene precipitation deal with the problem on a production level, removing asphaltene deposits from the pipes and tubes and not affecting the rate of asphaltene precipitation in the formation. The relevance of the thesis is that the new nano-inhibitors will not correct the negative consequences of asphaltene aggregation but will prevent this process in the reservoir itself. As a result, the employment of NPs in the oil sector to prevent asphaltene precipitation is regarded as a valuable and efficient technology from an economic and environmental standpoint.

1.3 Research objectives

The present research aims to evaluate the effectiveness of a novel nanocomposite Thiazine-Fe_3O_4-TiO_2-SiO_2-Bentonite for inhibiting asphaltene precipitation of an asphaltene extracted from a Kazakhstani crude oil. The main novelty of the work is not only the application of such types of NPs but the use of their combination of them. Each nanoparticle has its functions, and using nanocomposite allows for influencing several issues simultaneously. For example, silica oxide keeps asphaltene suspended, changes wettability and reduces IFT to improve oil recovery. Metal oxides are proven suitable asphaltene adsorbents. Bentonite is responsible for improving the physical and thermal properties of the nanocomposite. The thesis mainly focuses on the characterization of the novel nanoinhibitor and evaluation of its efficiency. There are several objectives to achieve the aim of a research project as listed below:

- To determine physical and chemical properties of the NC using SEM, EDAX, BET, XRD, FTIR and TGA techniques,
- To determine asphaltene onset point (AOP) for different NC concentrations using UV-spectroscopy,
- To determine asphaltene adsorption isotherms using UV-spectroscopy,
- To determine the catalytic effect of NC for adsorbed asphaltene's oxidation using thermogravimetric analysis (TGA).

1.4 Research methodology

The following research methodology is designed in four different phases to conduct the present research work:

- Phase 1. Asphaltene extraction. This phase describes the origin of crude oil and its specification. In addition, it includes the procedure of asphaltene extraction using the IP 143 technique and the preparation of synthetic oil.
- Phase 2. Nano-composite synthesis.
- Phase 3. Nano-composite characterization. This section describes laboratory experiments on nano-composite characterization techniques (TEM, SEM, BET, FTIR, XRD).
- Phase 4. Evaluation of performance of the nano-inhibitor. It provides the procedure of UV spectroscopy and TGA techniques to evaluate effectiveness of the NC in inhibition of asphaltene precipitation.

1.5 Thesis structure

The thesis is organized in five chapters. In Chapter 1, after a brief introduction on the importance of asphaltene precipitation and disposition and the issues causes, the relevance of the proposed research work to the oil industry, the problem statement, the am, and objectives of the thesis project, the research methodology, and the structure of the dissertation are described. A critical analysis of the previous research works, and studies related to the asphaltene deposition and application of nano-inhibitors in the flow assurance field is presented in Chapter 2 as a literature review. The experimental procedures used for this research work are described in Chapter 3. The results of the present research work, plus a discussion of the limitations of the research work and some nuances of procedure and characterization of

nanocomposite extracted from the crude oil, are presented, and discussed in Chapter 4. Then, a summary of the significant findings and outcomes of the conducted research and some recommendations for further studies are presented in Chapter 5.

2 LITERATURE REVIEW

The petroleum industry has been the primary energy source worldwide for decades. However, most conventional reservoirs have already been developed, and their number is much smaller than unconventional reservoirs. Figure 2-1 illustrates that conventional reservoirs comprised only 30% of world oil reserves [15]. As most of the oil reserves are unconventional, tight oil cannot be extracted with conventional Enhanced oil recovery (EOR) methods and is required to introduce novel methods. Most unconventional crude oil contains asphaltene, which causes devastating problems connected with flow assurance. In this chapter, first an overview of asphaltene, their molecular and chemical structure, asphaltene aggregation, and various views on mechanism of their aggregation is provided. Then, possible factors influencing asphaltene deposition are discussed. Nanotechnology-based asphaltene precipitation inhibitors are introduced, and the results of different research works are discussed. A critical analysis of the experiments carried out and their findings and limitations will also help to identify the gaps in this field of research.

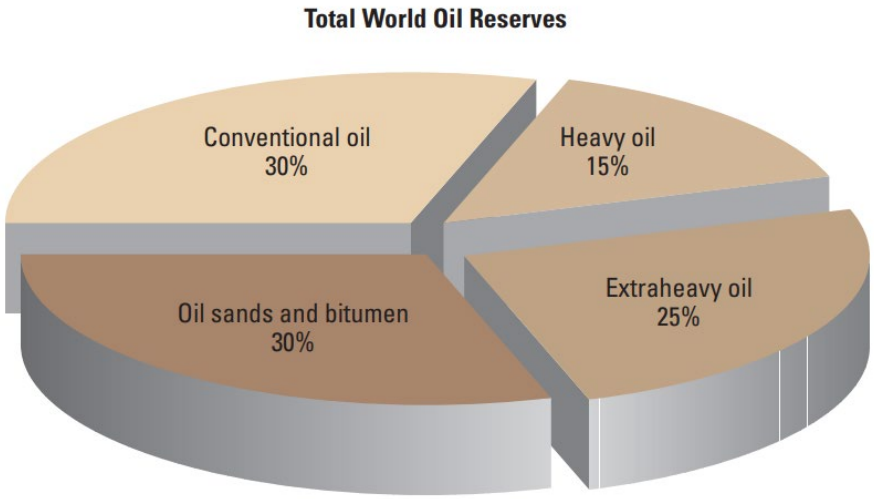

Figure 2-1. Total World oil reserves [15]

2.1 Asphaltene

2.1.1 Definition of asphaltene

Asphaltene is one of the four main constituents of crude oil. The term asphaltene were introduced in 1837 by J.B. Boussingault as a final residue of bitumen distillation that dissolves in turpentine and does not dissolve in alcohol [16]. The modern definition of asphaltene is similar to the initial; they can be distinguished by their ability to dissolve in aromatic solvents

(e.g., toluene) and precipitate in light paraffinic solvents (e.g., *n*-heptane and *n*-pentane). Because the asphaltene fraction defines by its solubility properties, it is still challenging to identify the specific composition of this heavy crude oil fraction [4]. However, at high temperatures, it can decompose, forming carbonaceous residue. Asphaltene is constructed from highly condensed polyaromatic and naphthenic rings, including heteroatoms (e.g., sulfur, oxygen, nitrogen) and trace metals (Iron, vanadium, and nickel). It exists as a suspension surrounded by resin in crude oil [17].

Due to the changes in temperature, pressure, and oil composition, the equilibrium condition is shifted, and asphaltene has a trend to precipitate. Several conditions may promote asphaltene precipitation—for example, gas-lift, miscible flooding, or acid performing. The problems of asphaltene deposition cover all stages during production. Particles of asphaltene adhere to the walls of the pipes, increasing pressure drop and decreasing the radius of pipes at production facilities. Asphaltene particles start to precipitate when the pressure decreases to the bubble point. They may cause problems not only at the production level but also plug the pores in the reservoir, decreasing the relative permeability of oil and oil production rate in general. However, with a strong flow, the forces acting on the asphaltene particles can exceed the attraction to the walls. As a result, the deposited particles can be carried further by the flow [18].

2.1.2 Molecular Composition of Asphaltene

When using *n*-pentane as a precipitant, it was reported that the hydrogen-to-carbon ratio of asphaltene is almost the same, varying in a range between 1.15 ± 0.5%, corresponding to the carbon-to-hydrogen atomic ratio [19]. It shows that the hydrogen-to-carbon ratio varies in a narrow range; this fact talks about a definite composition of unchanged asphaltene from crude oil, even if there are many possible permutations using heteroatoms [19]. There is an opinion that hydrocarbon solvents reinitiate the precipitation of asphaltene not only because of the solubility properties but also because of the specific constant composition of asphaltene [19].

Dickie et al. reported that asphaltene contains hydrogen and carbon molecules that construct fused and naphthenic rings and some naphthenic chains. As mentioned before, except for hydrocarbons, they are composed of low concentrations of heteroatoms (oxygen, nitrogen, sulfur) and trace metals (nickel and vanadium) [20]. Rogel et al. observed that the fractions with lower solubility contain more aromatic hydrocarbons and heteroatoms while the ratio of

hydrogen to carbon decreases [21]. The most polar fractions have high concentrations of vanadium and nickel. A high hydrogen deficiency and uneven components distribution lead to asphaltene's instability. In addition, they compared the fractionated asphaltene from the oil field with asphaltene extracted from the same crude oil by *n*-heptane. Investigations concluded that asphaltene extracted by heptane are not the best way for kinetic/thermodynamic modeling of asphaltene precipitation because, according to the results, heptane asphaltene had higher solubility and lower aromaticity compared to asphaltene from the deposit [21]. Furthermore, deposit asphaltenes comprise more oxygen-containing species and fewer nitrogen-containing species than heptane asphaltenes [21].

According to research, the dominant sulfur in asphaltene is thiophene, followed by sulfide. Asphaltene contains aromatic nitrogen in pyrrolic and pyridine forms [20]. Oxygen in asphaltene is mainly present as a phenolic hydroxyl group. The high oxygen content compensates for the low aromaticity. Vanadium and nickel present significant difficulties since they are in a highly aromatic, polar asphaltene fraction. Heteroatoms in the form of polar groups upset the balance of charge density. For example, sulfur atoms increase the degree of condensation, and the size of asphaltene can increase due to sulfide bridging. Nitrogen and oxygen atoms are responsible for hydrogen bond acceptor and donor forms [20].

The molecular weight of asphaltene is a property that is difficult to estimate accurately. First, asphaltene contains molecules of metals, hetero-elements, and hydrocarbons, which, in turn, are found in various compounds (cyclic, double bonds). Consequently, the molecular weight of 2 bonds differs from cyclic ones, which creates certain difficulties in calculating the concentration of constituent substances, their types of bonds, and molecular weight. Second, self-aggregate is another reason that causes complexity in molecular weight calculation. Asphaltene molecules can combine to form long chains of monomers, thereby increasing the molecular weight. Nanoaggregates are formed from six to eight asphaltene molecules [22].

Molina et al. stated that monomers' molecular weight varies from 500 g/mol to 1,000 g/mol [23]. Yarranton et al. reported that molecular weight for asphaltene aggregation is about 3,000 g/mol to 10,000 g/mol depending on the sample, sometimes reaching 50,000 g/mol [24]. Therefore, it can be concluded that molecular weight is not the best property to identify asphaltene. Molecular mass increases with decreasing temperature and aromaticity of solvent; asphaltene start to aggregate more intensively with the rise of their concentration [25].

2.1.3 Asphaltene architecture

The structure of asphaltene has been causing questions and conflicting opinions for many years. However, knowing that asphaltene contains alkyl and aromatic functional groups. Two structural models of asphaltenes have been proposed: island and archipelago [26]. The island or "continental" asphalting model is represented in Figure 2-2a, where aromatic rings condense together and form a fused aromatic core surrounded by alkyl chains. This model was proposed by Yen and other scientists in the 1960s using the X-ray diffraction method [27]. Figure 2-2b illustrates the "archipelago" model, where the asphaltene contains more than one aromatic core connected by aliphatic bridges [28]. The main issue is which of the model dominant in the asphaltene structure. Molecular imaging techniques and fluorescence depolarization confirm the hypothesis about the domination of the asphaltene island structure.

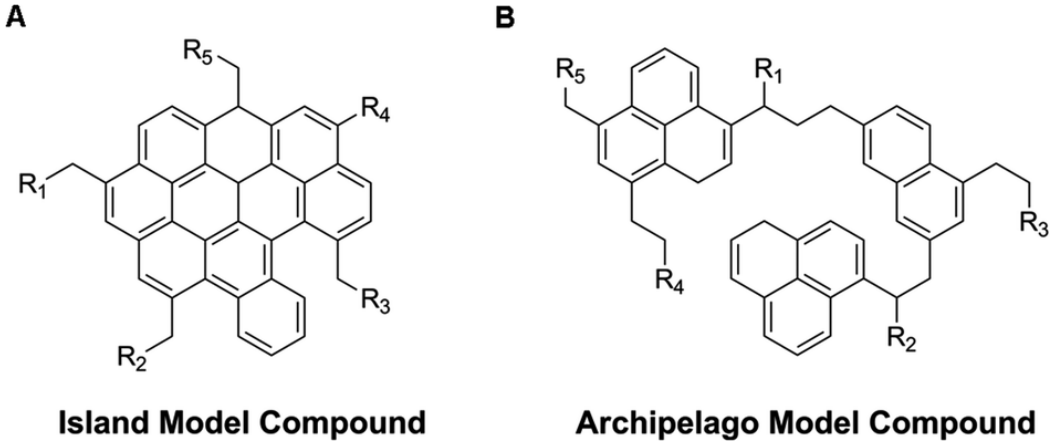

Figure 2-2. Examples of asphaltene's architecture: island (a) and archipelago (b) [29]

2.1.4 Asphaltene phase behavior

Leontaritis noted that asphaltene start to precipitate when the flowing pressure in the wellbore decreases below a certain point pressure [17]. Leontaritis and Mansoori observed that asphaltene cease to deposit when the pressure increases above the bubble point [30] and that the asphaltene precipitation depends on the pressure changes. Moreover, Leontaritis was found at high oil production rates. The well's initial pressure (Po) is lower than at lower rates [17]. Subsequently, the pressure of asphaltene precipitation depends on the temperature, and asphaltene phase behavior is a function of pressure and temperature.

Asphaltene deposition envelope (ADE) is the disposition of thermodynamic points on a phase diagram where asphaltene starts to flocculate. It can be seen from Figure 2-3 that there is no critical point for the asphaltene's phase envelope. For asphaltene, this point does not exist.

Because to have a critical point reservoir, the fluid should have dew and bubble points; however, asphaltene do not tend to vaporize. This point is the main difference between asphaltene and black oil reservoirs. The Asphaltene deposition envelope represents the bubble point line, ADE's lower and upper boundary. Above the ADE upper boundary, only liquid is usually under reservoir conditions. In the region between the bubble point line and ADE upper boundary, there is a presence of liquid and asphaltene phases. The region between the bubble point line and the ADE lower boundary has 3 phases: liquid, vapor, and asphaltene. Some asphaltene molecules tend to flocculate irreversibly. For example, when the asphaltene passes through the upper boundary due to production, they will not return to stable suspension, changing the thermodynamic way. It is impossible to determine the lower boundary for asphaltene because asphaltene will not cross this line [17].

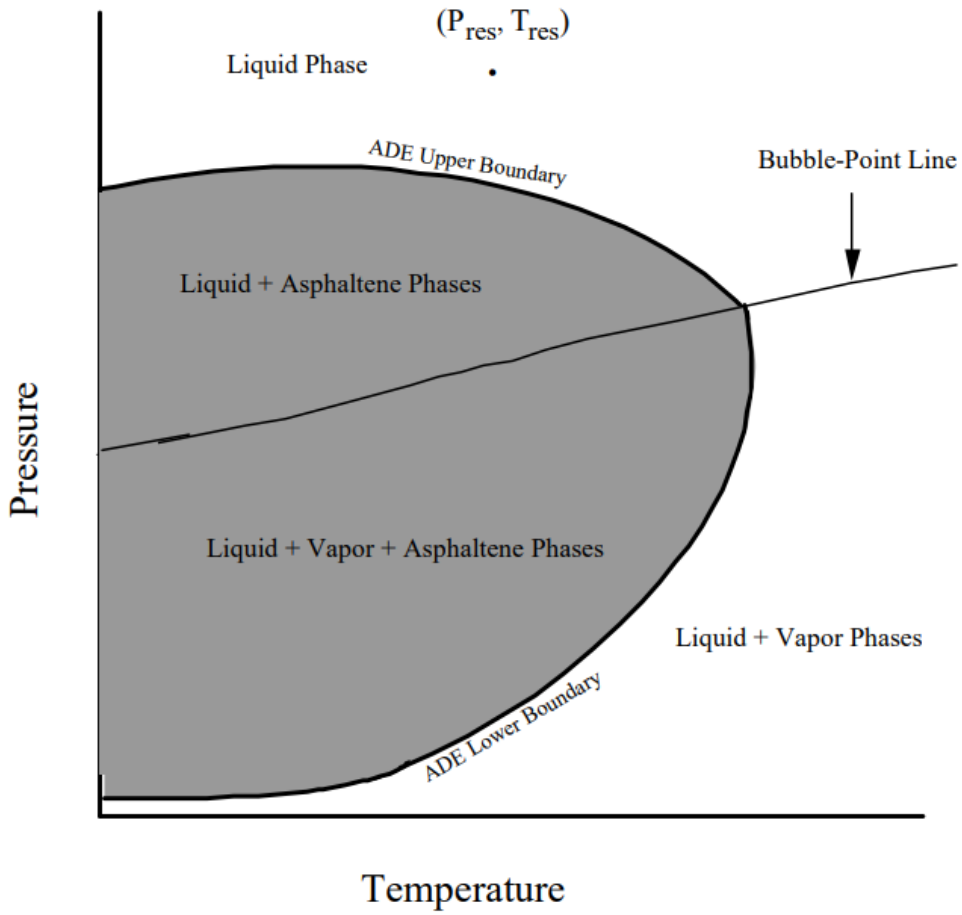

Figure 2-3 A typical P-T asphaltene's deposition envelope [17].

2.1.5 Asphaltene aggregation

To describe the process of asphaltene precipitation, it is necessary to understand the structure of crude oil and how the main fractions of petroleum are connected. Figure 2-4 illustrates how saturated aromatic, resin, and asphaltene (SARA) fractions interact. Through heteroatoms, using hydrogen bonding, resin is attached to asphaltene molecules surrounding them. They are creating a polar part of petroleum. Aromatic and saturated hydrocarbons are the non-polar part of the oil. However, the presence of paraffin in resin composition makes it possible to be present in the non-polar part of crude oil. Aromatic fractions can dissolve heavy fractions of resin and asphaltene [5].

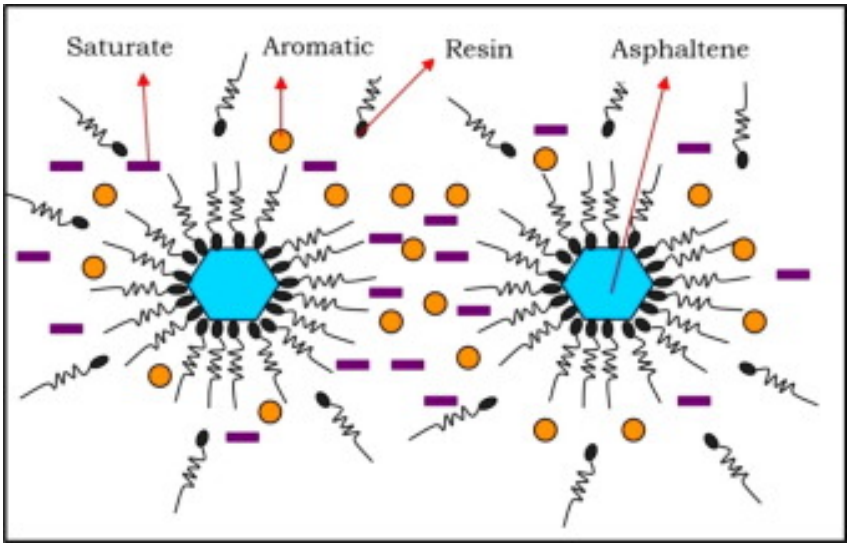

Figure 2-4. A simplified view of crude oil fractions [31]

Asphaltene aggregation can be explained using the Yen-Mullins or supramolecular models [32], [33]. Figure 2-5 illustrates a simple Yen-Mullins model that describes the asphaltene aggregation process. In the first stage, due to π- π interactions, aromatic cores of 6-9 molecules stack together, creating a nano-aggregate with a size of 2-3 nm [34]. In the second stage, when equilibrium conditions change, approximately ten nano-aggregates tend to form a 5-10 nm size cluster. Moreover, the weak nuclear forces between the aliphatic side-chain contribute to cluster formation [35]. In the third stage, the flocculation stage occurs because clusters of asphaltene is unstable and start precipitating [36]. Asphaltene self-association tends to have the exact mechanism of micelle formation from surfactants. Mullins et al. explored different ways to determine a “critical cluster concentration.” However, the main limitation is that asphaltene structure is not the same as surfactants causing troubles with experiments and

results. Figure 2-6 illustrates the growth of asphaltene aggregation due to its concentration. As the asphaltene concentration reaches the "critical cluster concentration," asphaltene aggregate.

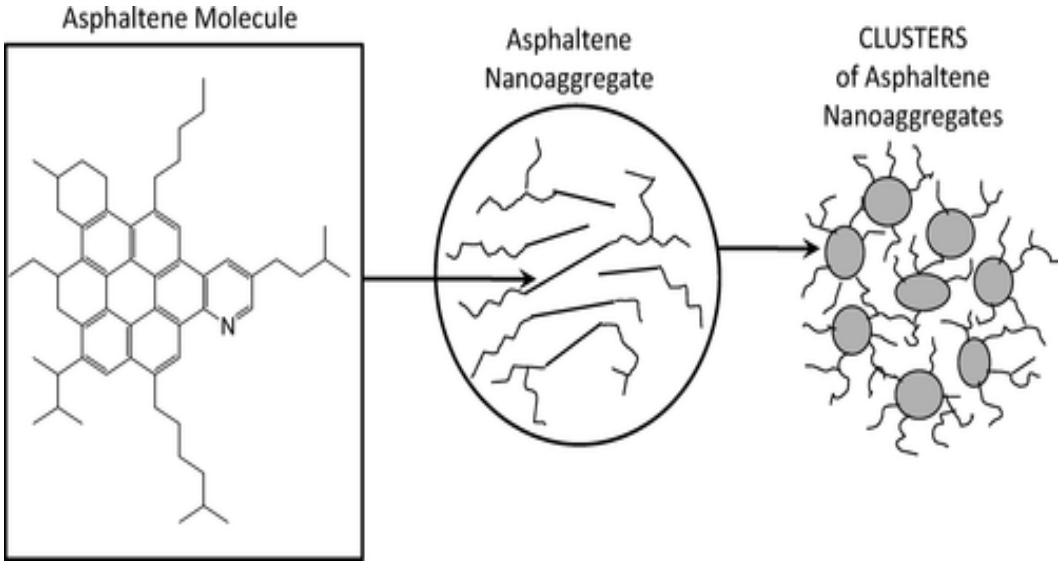

Figure 2-5. Yen-Mullins model of asphaltene aggregation [33]

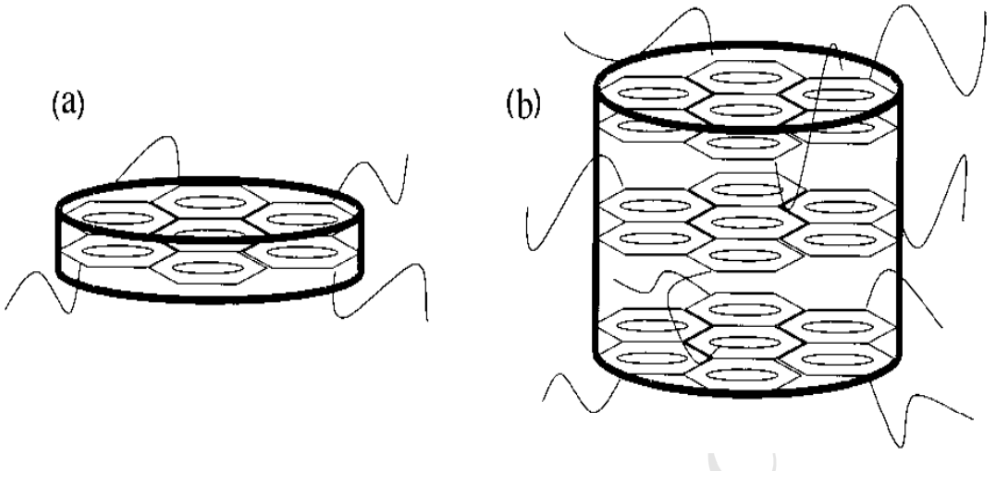

Figure 2-6. Representation of growth of asphaltene aggregation; (a) asphaltene and (b) aggregates [37]

2.1.6 Factors affecting the asphaltene aggregation process

Asphaltene molecules begin to aggregate and deposit when the equilibrium conditions are shifted. Various factors provoke asphaltene, creating unstable conditions and forcing them to deposit. This section will discuss factors that may affect asphaltene depositions and increase their rates, such as pressure, temperature, and composition of crude oil.

2.1.6.1 Effect of crude oil composition on asphaltene aggregation

The system is in equilibrium when resin and asphaltene are soluble in crude oil. However, this equilibrium can shift when adding substances with different compositions and structures. For example, to reduce viscosity, saturated hydrocarbons are added to the oil solution, which shifts the thermodynamic equilibrium, changing the properties of the oil. The resin, in turn, try to detach from the surface of the asphaltene by passing into the non-polar part of the oil, trying to restore balance. The similar process when after desorption of resin, molecules of asphaltene overcome Brownian motions and create high-weight nano-aggregates that start to deposit is demonstrated on Figure 2-7 [38]. The precipitated asphaltene depends on the composition and amount of solvent in crude oil. Figure 2-8 shows how asphaltene precipitation relates to the carbon number of added solvents. Short titrants with less carbon number contribute to the intensive deposition of asphaltene and resin [39]. While long *n*-alkanes contribute to low amount of dry precipitated asphaltene without resin.

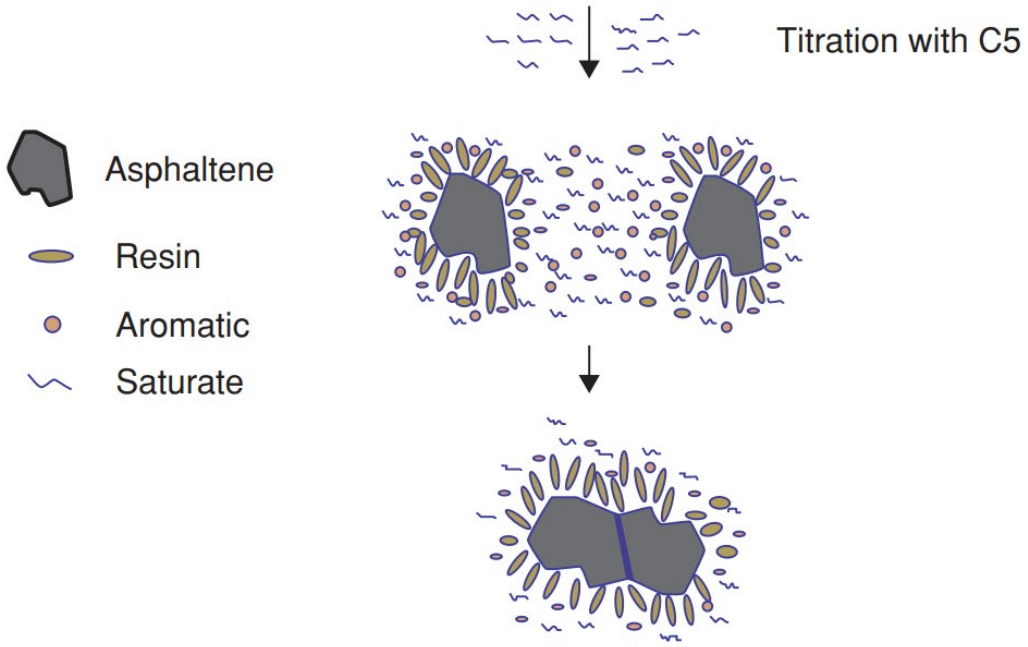

Figure 2-7. Schematic of asphaltene flocculation mechanism due to titration with *n*-C_5 [5]

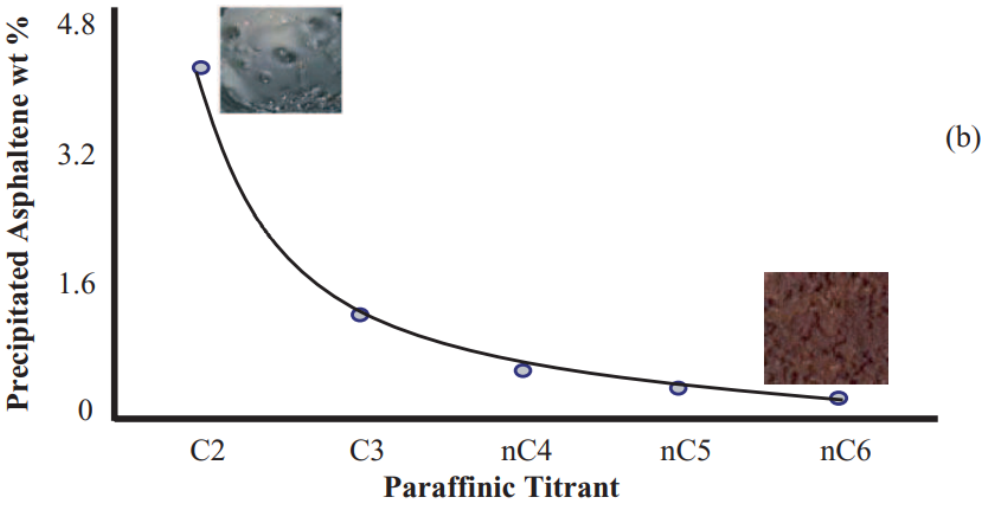

Figure 2-8. Effect of paraffinic Titrant carbon number on the number of precipitated asphaltene [5]

The stability of asphaltene can be evaluated quantitatively by Colloidal Instability Index (CII), which is based on interactions between SARA fractions [40]. Loeber et al. (1988) created a formula to define the stability of asphaltene (see Equation 2-1)[41]. Ashoori et al. (2016) reported that if CII is less than 0.7, then asphaltene is stable. On the other hand, if the CII value is higher than 0.9, then unstable conditions present in crude oil and asphaltene molecules tends to precipitate [15]:

$$\text{CII} = \frac{\text{asphaltene [wt\%]+saturates [wt\%]}}{\text{resin [wt\%]+aromatics [wt\%]}} \qquad \text{Equation 2-1}$$

Asphaltene can behave differently at different production stages. For example, light fractions leave crude oil at primary production due to natural depletion, increasing density. As a result, the rate of asphaltene aggregation decreases. However, during secondary and tertiary recovery, this rate may increase significantly. It depends on applied EOR methods. For example, if the miscible gas injection is used, oil becomes rich with light substances, and asphaltene flocculation rises [42].

2.1.6.2 *Effect of pressure on asphaltene aggregation*

Different fractions of crude oil have different compressibility properties. As illustrated in Figure 2-9, as pressure declines during production and its values become near the saturation pressure, the molar volume of light hydrocarbons increases significantly. In contrast, the volume of asphaltene does not change rapidly [5]. As pressure drops, asphaltene can precipitate due to the

destabilization of micro colloids. Crude oil is very sensitive to asphaltene precipitation under pressure. Usually, the reservoir pressure is much higher than the bubble pressure, and crude oil cannot extract gas up to a high-pressure drop. From the moment that gas begins to evolve from the oil sphere, asphaltene begins to stabilize because the solvating ability of oil increases with a decrease in the concentration of light hydrocarbons in the liquid phase. In addition, oil containing asphaltene can compress, followed by a decrease in pressure, and the dielectric constant decreases [43]. The solvating ability of oil is associated with a decrease in pressure; therefore, the physical and chemical properties of the oil can vary depending on the pressure. For example, in 1965, in Hassi Messaoud's field, it was reported that at a pressure lower than the bubble p, point problems with asphaltene deposition disappeared [44]. It can be explained by the fact that light fractions of oil competed at bubble point pressure for the solvency change phase from liquid to gas [44].

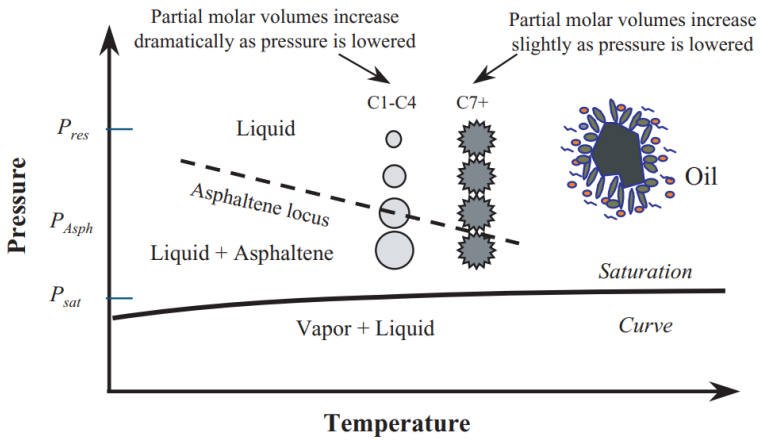

Figure 2-9. Effect of pressure on the partial molar volume of petroleum components [5]

2.1.6.3 Effect of temperature on asphaltene aggregation

The temperature may affect the deposition of asphaltene from different sides. Firstly, temperature influences oil composition as light fractions expand and oil solubility decreases. Hence, asphaltene aggregates more intensively as they become less soluble in oil. Secondly, oil viscosity becomes lower at high temperatures, which may accelerate the deposition of asphaltene. Thirdly, with temperature increase, the solubility of asphaltene increases [45]. Considering all factors, it can be concluded that asphaltene tends to precipitate at high temperatures but not in big portions.

2.1.6.4 Effect of aqueous phase on asphaltene aggregation.

Another factor that may affect the stability of asphaltene is the presence of water in the reservoir [40]. Usually, brine is used for the completion and injection stages, and formation water contains salts with differently charged particles, so they can interact with some substances that compose asphaltene. Some formation water or brine droplets are presented with asphaltene in an emulsion phase. Asphaltene particles can be attracted to the interface because of hydrogen bonds between water and nitrogen/ oxygen-containing groups of asphaltene. The presence of heteroatoms in asphaltene can change the aquaphobic property of asphaltene to hydrophilic. Such a change can occur when heteroatoms interact with water molecules, forming hydrogen bonds. In addition, the rate of asphaltene aggregation can be reduced due to sodium chloride in the aqueous phase. According to studies, the amount of asphaltene migrating to the interface depends on the composition of the aqueous phase [20].

2.1.7 Asphaltene precipitation/deposition reversibility

Hammami et al. discovered that asphaltene can re-dissolve in crude oil at a pressure higher than the bubble-point pressure [46]. Andersen used a gravimetric method to study the reversibility of asphaltene precipitation using a mixture of toluene and n-heptane as the solvent [46]. Asphaltene precipitation was first measured by adding a mixture of toluene and n-heptane to crude oil. The resulting asphaltene precipitate was then dissolved in the same mixture, and the asphaltene dissolution was measured. It turned out that during precipitation, the number of precipitated asphaltene was higher than during dissolution, as a result of which a hysteresis curve appeared. Despite this, the experiment's results cannot fully reflect the reversibility of asphaltene precipitation since crude oil was used for precipitation, and only asphaltene obtained during precipitation were used for dissolution [47]. In their research, Clarke and Pruden noted the difference between true potency and methods for redissolving asphaltene in aromatic solutions. They conducted experiments at constant temperature by adding and removing *n*-heptane. It turned out that the asphaltene redissolved in the crude oil as the n-heptane was removed. However, a hysteresis curve appeared, indicating that the dissolution of asphaltene did not follow the same deposition trajectory. It has been suggested that the aggregation process is faster than the asphaltene segregation process [48]. Complete reversibility of asphaltene precipitation is possible when the solution is treated with ultrasound for several hours. It has also been reported that partial reversibility occurs even after 24 hours [49].

2.2 Nanotechnology

Nanotechnology is a rapidly developing field that involves investigation, manipulation, and functionalization of matter at the nanoscale, which is roughly one billionth of a meter in size [50]. Nanotechnology organizes both living things and artificial systems' atoms and molecules at the first level. All systems' characteristics and capabilities are defined here. The development of precise molecular-scale machines and components is promised by nanotechnology. A greater surface area, higher reactivity, and enhanced mechanical, electrical, and optical properties are just a few examples of the distinctive properties that materials display at this scale that are absent at larger scales [51]. Nanotechnology has much potential for use in various fields, including electronics, medicine, energy, and the environment [52]–[55].

2.2.1 Nanoparticles

Compared to corresponding bulk counterparts, NPs have improved physical, chemical, and biological properties that are unique [56]. Therefore, they can be combined with other materials to create unique functionalization with uses other than their behavior [57]. Thus, in the physics of composites, NPs are promising candidates for integration into appropriate matrices to form high-performance composite materials [58]. Thus, the key characteristics of both the carrier and the NPs are mixed. Therefore, individual properties of NPs require a comprehensive study to extract the maximum benefit in research and innovative research. Khan and Hossain [51] stated that the three significant interrelated physical characteristics lead to the distinctive characteristics of NPs. First, because NPs possess a remarkably substantial specific surface area (to area-to-volume ratio), they are highly susceptible to electronic activity and external influences. Second, they move around a lot, both in free states and in porous media. Finally, NPs show a quantum effect because their size is similar to the wavelength of the electron wave function. NPs can be classified according to their origin, dimension, and chemical composition [51].

2.2.2 Nanoparticles in the oil and gas industry

Nanoparticles have gained attention as potential additives in petroleum engineering due to their unique physicochemical properties. Various studies have explored the application of metal oxide, silica, and other NPs in enhanced oil recovery (EOR), flow assurance, drilling fluids, and cementing materials. Nanoparticles or nano-sized particles possess various unique qualities, including a huge surface area and the potential for surface functionalization. In

addition, they offer various properties depending on the composition, synthesis technique, size, and surface structure. The selective adsorption of undesirable components from liquid streams is one of several [59] applications made possible by NPs' physicochemical affinity for particular surfaces. For example, NPs with a surface affinity for asphaltene and the capacity to be present at the oil-water interface are needed to demulsify stable crude oil emulsions successfully. Another strategy involves creating nanocomposites or irreversibly bonding functional NPs to a carrier matrix. Due to the interaction of NPs with the matrix, nanocomposites have higher mechanical stability, are more easily manufactured, and offer some advantages over NPs [59].

Nanoparticles have gained widespread attention and found use in oil and gas fields due to their distinctive physical and chemical properties. The petroleum industry uses silica (SiO_2) [60] and metal oxides such as magnesium oxide (MgO) [61], [62], alumina (Al_2O_3)[62], titanium dioxide (TiO_2) [63], [64], and iron oxide (Fe_2O_3) [65], [66] most frequently. Drilling [67], [68], exploration [69], completion [70], enhanced production [60], [71], and stimulation techniques[72] all make use of materials based on nanotechnology. They are suitable for regulating subtle instability and migration and can control formation damage, reducing wellbore risk.

Ehtesabi et al. discovered that adding TiO_2 NPs to hydrophobic sandstones boosted oil recovery by 80% [73]. At the same time, Shah looked at the effectiveness of employing CuO NPs for oil recovery. The findings show that CuO NPs boost oil recovery by 71% [74]. Furthermore, oil recovery by using nanofluids containing modified carbon NPs were investigated by Kang et al. They discovered that carbon-based fluorescent NPs boosted oil recovery in carbonate reserves by more than 96% [74], [75]. Finally, to restore formation damaged by asphaltene deposition under static conditions, Lopez et al. studied Al_2O_3 nanomaterials [76]. They concluded that asphaltene self-association, which could precipitate and deposit in the porous system due to the neutralization of polar forces from asphaltene affinity, could be prevented by the interaction of the nanoparticle with asphaltene [77]. Iron oxide NPs, conversely, can remove asphaltene deposits in porous media, according to a study by Parsaei et al. [78].

2.2.3 Mechanism of inhibition of asphaltene precipitation using nanoparticles.

One of the ways to remove asphaltene is to use their adsorption phenomenon as a benefit. Nassar et al. reported that asphaltene can be adsorbed on the surfaces of metal oxide NPs [79]. The

presence of NPs prevents the coalescence of asphaltene particles and the formation of larger molecules. It adsorbs the asphaltene particles on its surface, disaggregating high-weighted molecules. In addition, the absorption of asphaltene by NPs prevents the accumulation of asphaltene on the surface of a porous medium, but it cannot completely prevent these accumulations. By removing asphaltene from oil, NPs also reduce viscosity and interfacial tension, which can change rock wettability and change permeability. Such nano-sized particles usually have a high absorbing capacity and catalytic activity. Nanoparticles have two main functions, catalytic and thermal [80]. The catalytic feature of NPs makes it possible to improve oil mobility and prevent the aggregation and precipitation of asphaltene due to their high absorption capacity. The thermal function of the NPs facilitates the removal of asphaltene from heavy oils by catalytic removal [80].

The ways by which asphaltene disaggregates when it is exposed to NPs are shown in Figure 2-10. Typically, aliphatic and aromatic molecules make up the molecular structure of asphaltene. The aliphatic segment contains alkyl chains of various lengths, with the first area encircled by the second. The aromatic component is a polynuclear aromatic moiety. The H-bond interactions between the aromatic structures cause the attraction of the asphaltene molecules. On the other hand, aliphatic chains attract aromatic sheets to one another. It suggests that the existence of polar and nonpolar groups facilitates their amphiphilic nature and self-association. Asphaltene often adsorb onto solid surfaces as single molecules or colloidal aggregates of different sizes due to their carboxylic and phenolic acid groups. The principal functional groups of asphaltene, such as carbonyl, pyrrolic, pyridinic, sulfite, and Thiophene interact with the functional groups of the NPs and increase the preferential adsorption of the asphaltene over NPs [81]. Typically, aliphatic and aromatic molecules make up the molecular structure of asphaltene. The aliphatic segment contains alkyl chains of various lengths, with the first area encircled by the second. The aromatic component is a polynuclear aromatic moiety. The H-bond interactions between the aromatic structures cause the attraction of the asphaltene molecules. On the other hand, aliphatic chains attract aromatic sheets to one another. It suggests that the existence of polar and nonpolar groups facilitates their amphiphilic character and self-association [81].

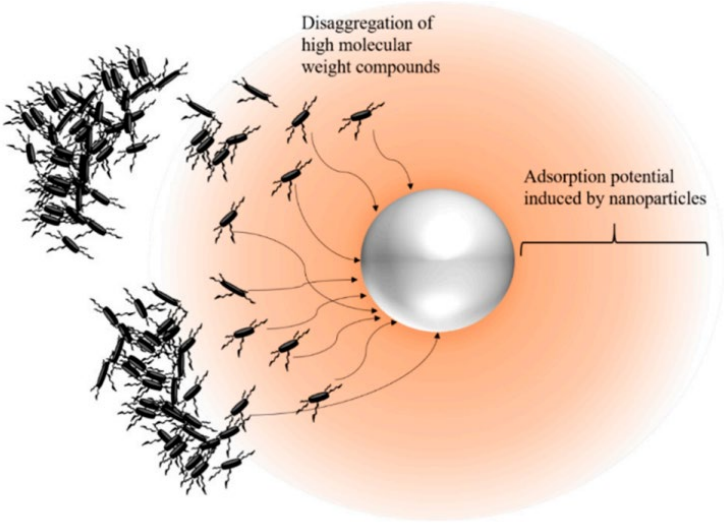

Figure 2-10. Asphaltene disaggregation by NPs [81]

2.2.4 Nanoparticles as inhibitors of asphaltene precipitation

Nanoparticles proved to be suitable asphaltene precipitation inhibitors. Due to their catalytic capacity, they have a significant potential for selectively enriching adsorbed asphaltene [82]. The high adsorption capacity and fast kinetics of NPs can be attributed to their great surface area [83]. First, Setoodeh et al. [84] confirmed that NPs are effective and eco-friendly. Then, Nassar et al. studied asphaltene adsorption from the Athabasca oil field using alumina NPs in 2010 [12]. They concluded that Al_2O_3 NPs adsorb asphaltene quickly reaching equilibrium in less than 2 hours. After that, in 2011, Nassar et al. investigated the effect of alumina particle size on asphaltene adsorption [12]. Al_2O_3 NPs less than 50 nm in size adsorb asphaltene more than the 50-200 μm Al_2O_3 particles. Furthermore, alumina NPs fit the Langmuir model by having a monolayer asphaltene adsorption, while alumina microparticles better-fit multilayer adsorption. Another research work conducted by Shayan and Mirzayi [11] on Maghemite (γ-Fe_2O_3) and hematite (Fe_2O_3) nano-inhibitor for asphaltene precipitation. As a result, due to the small size, high surface area, and acidity of Maghemite, it has a higher adsorption capacity than hematite, 108.1 mg/g and 45.8 mg/g, respectively. Additionally, Nassar et al. confirmed that iron oxide (III) NPs are a great adsorbent for removing asphaltene, dramatically decreasing the oxidation temperature of asphaltene [85].

2.2.4.1 SiO_2 as a part of nanocomposite

Nanoparticles play the role of not only inhibitors but also displacing agents since, with the introduction of particles, the volume of the injected fluid increases, displacing more and more

oil. According to Betancur et al., silica NPs increase oil recovery due to strong acidity [86]. Due to its distinct properties, silicon dioxide, also known as SiO_2, is a commonly used nanomaterial in the nanocomposite. It is a naturally occurring mineral found in sand, quartz, and opal, among other forms.

Silica NPs have a wide range of applications. For example, Rayeni et al. investigated interfacial tension (IFT) reduction and wettability improvement when adding SiO_2 to the oil [87]. Similarly, Ahmadi et al. concluded that nano SiO_2 could improve oil recovery by decreasing the IFT between oil and water [88]. SiO_2 NPs also have a high surface area-to-volume ratio, which makes them powerful asphaltene molecule adsorbents. The NPs can adsorb the asphaltene, preventing their deposition on the pipeline walls. This mechanism is beneficial in locations where asphaltene tends to deposit and fluid velocity is low. Furthermore, according to Alemi et al., SiO_2 NPs positively affect the beginning of asphaltene precipitation, increasing AOP [89]. Besides this, SiO_2 NPs are a powerful addition to nanocomposite materials that can stop asphaltene from depositing in oil and gas pipelines. There are several studies where SiO_2 was added to nanocomposite with iron oxide (Fe_2O_3) [89], cobalt oxide (Co_3O_4) [90], cardanol [76], calcium carbonate ($CaCO_3$) [91], zinc oxide (ZnO) [92]. SiO_2 can be considered a desirable candidate for creating anti-asphaltene nanocomposites due to its distinctive properties, dispersant, and adsorbent qualities.

2.2.4.2 *TiO_2 as a part of nanocomposite*

Titanium dioxide performs a crucial role in asphaltene adsorption. Nassar et al. [93] in 2011 compared six metal oxide NPs, Co_3O_4, Fe_3O_4, MgO, CaO, TiO_2, and NiO; among them, titanium dioxide has the highest surface area of 183 m^2/g from BET measurements and particle size of less than 25 nm. In 2014 Nassar, Natan, and Vitale studied the asphaltene adsorption onto TiO_2, ZrO_2, and CeO_2 [64]. They also measured the surface area from BET, and particle sizes were 183 m^2/g and 8 nm, respectively. So, TiO_2 NPs have a high surface area and small particle size; as a result, the surface area-to-volume ratio of titanium dioxide NPs is very high, making them suitable for adsorbing asphaltene molecules. In addition, several studies indicate the positive effect of combining titanium dioxide with silica NPs. For example, Mohammadi et al. investigated nanofluid of 80 wt% of TiO_2 and 20 wt% of SiO_2 [94]; they reported that TiO_2 contributed more to increasing asphaltene onset point rather than silica NPs.

2.2.4.3 Fe_3O_4 as a part of nanocomposite

Iron oxide (III) is a naturally occurring mineral compound that has been reported to have potential as an asphaltene deposition nano-inhibitor. Therefore, studies were performed to investigate whether iron oxide NPs could improve asphaltene adsorption. Studies have shown that iron oxide (III) NPs can effectively inhibit asphaltene deposition under various conditions. For example, in a study conducted by Ansari et al., magnetite and hematite NPs adsorb asphaltene better than dolomite and calcite NPs [95]. At the same time, Kazemzadeh et al. reported that a higher mass fraction of Fe_3O_4 NPs enhanced the performance of the tried solutions in stopping precipitation of asphaltene [96]. Furthermore, the effectiveness of iron oxide (III) NPs as asphaltene deposition nano-inhibitors can be improved by modifying the surface of the NPs with various functional groups. In addition, Setoodeh et al. compared the uncoated and polythiophene-coated Fe_3O_4 NPs [97]. As a result, Fe_3O_4-PT and Fe_3O_4 MNPs had average adsorption efficiencies of 78.98 and 65.94%, respectively. By analogy with a solution of synthetic asphaltene in toluene, the experiments on crude oil demonstrated that Fe_3O_4-PT MNPs could adsorb asphaltene from crude oil.

2.2.4.4 Bentonite and thiazine as parts of nanocomposite

Clays, called bentonites, are found in large quantities in deposits worldwide. Their properties are ultimately determined by montmorillonite, the primary clay mineral in their makeup. It was possible to create nanocomposites with enhanced mechanical, thermal, and hydrophobic properties for various applications in food technology, pharmaceuticals, packaging, coatings, etc., by adding bentonite to polymer matrices [98]–[100]. In the ring structure of the heterocyclic compound thiazine, there are sulfur and nitrogen atoms. Organic compounds known as thiazine derivatives are created by changing the structure of thiazine [101]. It has been reported that thiazine derivatives, including methylene blue and toluidine blue, can effectively stabilize and reduce metal oxides [102]. Because of their interactions with the metal ions on the surface of metal oxide particles, these substances can create stable bonds that stop further oxidation and aggregation. Thiazine also may act as a stabilizing agent preventing NPs to precipitate in the solution.

2.2.5 Asphaltene adsorption

The asphaltene adsorption phenomenon at the borders of liquid-liquid and solid-liquid interfaces leads to undesirable issues during the production and transportation stages.

Asphaltene may affect the wettability of reservoir rock [103] and aggregation of asphaltene can occur due to attractive forces during the interaction of asphaltene with various surfaces. Therefore, the adsorption of asphaltene can be seen as a negative phenomenon, but at the same time, this phenomenon can be used as a selective removal of asphaltene from oil[82]. The use of asphaltene adsorption as an oil treatment makes it possible to obtain a product with a lower probability of precipitation and a decrease in coke yield while increasing the amount of liquid coming out [104].

2.2.5.1 Asphaltene adsorption on metals

The adsorption capacity of asphaltene on metal surfaces has a similar trend as on minerals. Stainless steel is the main component of pipelines, the highest adsorption of asphaltene (2.7 mg/m^2) is observed on it, the lowest adsorption of 0.25 mg/m^2 is observed for aluminum, iron has an average adsorption capacity of 1.35 mg/m2 [82]. Alboudwarej, H. et al., using scanning electron microscopy, reported that adsorption capacity varies for metals due to the differences in their surface morphology [105].

According to the studies of Gonzales et al., asphaltene adsorption isotherms follow the Langmuir model, where the adhesion of asphaltene molecules forms the monolayer on the porous media of reservoir rock. In addition, its maximum capacity is 1-2 mg/m^2 [105]. However, some investigations showed multi-layer adsorption in the formation [106]. Based on the general shape of the isotherm, many scientists concluded the type of adsorption of asphaltene. When Marczewski and Szymula insisted that asphaltene adsorption does not everywhere follow the Langmuir behavioral model [107], indeed, there is evidence that asphaltene adsorption for some mineral surfaces is type 1. Still, these same asphaltene may have a more complex multilayer adsorption process on other surfaces. This suggests that the adsorption of asphaltene is affected not only by their origin but also by the surface on which they are adsorbed.

2.2.5.2 Asphaltene Adsorption on metal oxides

Metal oxide NPs are becoming more popular because they can catalyze activity to enhance adsorption asphaltene [77], [108]. It has been shown that the catalytic steam cracking of asphaltene adsorbing to metal oxide NPs is comparatively mild. Furthermore, it has been proven that the NPs' adsorption capacity and the catalysts' activity are related. Nassar concluded that

the adsorption of asphaltene could be as single molecules or colloidal aggregates with different sizes if there are phenolic or carboxylic weak acids in the composition of asphaltene [79].

Considering the adsorption of asphaltene on the surfaces of various metal oxides, it is worth paying attention to iron oxide because it is often found at various stages of oil production. Iron oxide can form in pipelines and refinery stages due to corrosion [82]. It has been studied that the presence of iron oxide can increase the amount of adsorbed asphaltene. Dubey & Waxman concluded that iron-free chlorite adsorbs three times less asphaltene on its surface than iron-containing chlorite [109]. Adams cited Alvarez-Ramirez et al. work, where they reported that Fe_2O_3 may attract aromatic parts of asphaltene [82]. The adsorption properties of metal oxides can be improved by impregnation with other metal oxides. Faus et al. studied the adsorption capacity of aluminum oxide with the deposition of molybdenum and cobalt on its surface [110]. It turned out that the number of porphyrins adsorbed on the surface of $CoMoAl_2O_3$ was greater than on the surface of conventional metal oxides [110]. Adams cited Xing et al. that the adsorption capacity of the adsorbent has a strong relationship with the acidity of the surface of metal oxides. The higher the acidity, the more asphaltene can be adsorbed on the surface of the oxide. For example, the adsorption capacity for iron oxide and nickel oxide is 1.1 and 0.6 mg/m^3 relative [82].

Asphaltene adsorption on the surface of metal oxides can be affected by several parameters demonstrated in Figure 2-11, such as the properties of metal oxide NPs and asphaltene and external factors. The acidity and basicity of the surface of metal oxides strongly affects asphaltene adsorption and it is considered as the main mechanism due to acid-base interactions. Nassar et al. investigated the adsorption properties of basic (CaO, MgO), amphoteric (Fe_3O_4, Co_3O_4), and acid (NiO, TiO_2) metal oxides. They reported that acid oxides' adsorption affinity was greater, whereas basic and amphoteric demonstrated higher adsorption capacity. It means that adsorption affinity cannot be correlated with adsorption capacity according to the acidity and basicity of metal oxides [79]. Betancur et al. concluded that the amount of adsorbed asphaltene could be correlated with surface acidity. They treated the SiO_2 NPs with different acid, base, and neutral approaches and reported that the highest adsorption capacity is directly related to the highest surface acidity of NPs [86]. Therefore, the NPs' surface area and size may contribute to asphaltene adsorption. Olaitan et al. investigated that nickel oxide (NiO) NPs had more adsorption affinity than iron and cobalt oxides (Fe_3O_4 and

Co_3O_4, respectively). Because NiO has a larger surface area than Fe_3O_4 and Co_3O_4, so it has higher adsorption efficiency [111].

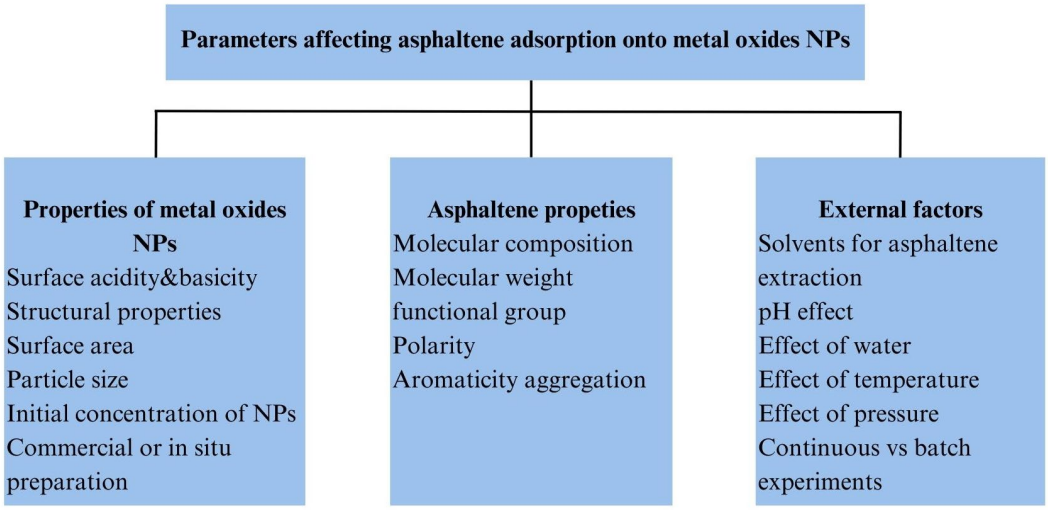

Figure 2-11. Parameters affecting asphaltene adsorption onto metal oxides NPs

2.2.6 Factors affecting asphaltene adsorption

Sorbents come in many forms, including clay minerals, rock minerals, silica, alumina, glass, metals, metal oxides, carbon, and, more recently, polymers. The adsorption capacity for many materials was limited to under 4 mg/m^2, and at low concentrations or for surfaces with a very poor affinity for asphaltene; the adsorption capacities could be below 0.2 mg/m^2 [112]. Simple adsorption isotherms were observed for asphaltene solutions with the nanoaggregate concentration, around 3,000-5,000 mg/L or less (in suitable solvents such as aromatics, CH_2Cl_2, CS_2, etc.). Above the 3,000 mg/L cutoff (and in weak solvents such as heptane toluene mixtures), multilayer formation is frequent. Depending on the level of asphaltene aggregation, several adsorption regimes can take place, with adsorption levels reaching 100 mg/m^2 feasible [107].

Saturated hydrocarbons, aromatic hydrocarbons, and resin that make up crude oil have different chemical and physical properties that can affect the rate of asphaltene aggregation and, consequently, the adsorption process [82]. According to previous studies, the adsorption of isolated asphaltene was almost the same compared to the adsorption of whole crude oil. This conclusion shows that asphaltene mostly affect the adsorption behavior of crude oil [113]. Studies show that when combining resin and asphaltene, the adsorption layer becomes larger. This may be due to the introduction of resin into the aggregates and their swelling [114]. It has

been suggested that resin can limit asphaltene surfaces to form into a denser structure [114]. Temperature is another factor affecting asphaltene adsorption. The size of aggregates adsorbed onto surfaces is proportional to the temperature dependency on aggregate size in asphaltene solutions: increasing the temperature decreases adsorption [115]. Other researchers have reported that adsorption reduces or is unchanged as the temperature rises.

Aromaticity is another factor that may affect asphaltene adsorption. The high solvent concentration decreases the size of asphaltene, and consequently, the number of adsorbed materials reduces [49]. Nevertheless, some studies contradict those results. For example, saint et al. showed a comparatively low rate of asphaltene adsorption in pyridine solvent, whereas, in toluene, it was much higher [50]. Water in reservoir rock can also decrease the adsorption of asphaltene as it may compete with asphaltene for the adsorption on the rock surface. As the concentration of water increases, the adsorption of asphaltene decreases at the same time [51].

2.3 Evaluation of the performance of nanocomposite as nano-inhibitors

2.3.1 Adsorption isotherms

2.3.1.1 IUPAC classification of adsorption isotherms

The process of asphaltene adsorption is investigated using adsorption isotherm models. The graphs represent the relationship between the amount of adsorbed substance and relative pressure at a constant temperature. The IUPAC adsorption isotherm classification is based on nitrogen adsorption in solids. Nitrogen fills the pores of solids and begins to adsorb on them. The proposed adsorption isotherms can reflect the behavior of various liquids concerning solids. Figure 2-12 illustrates the classification of adsorption isotherms according to UIPAC. Type one characterizes the formation of a monolayer on the adsorbent's surface and the process's reversibility. Types a and b differ from each other in the pore size of the adsorbent. Type 1a is characterized by pores smaller than 1 nm, while type 1b characterizes adsorbent pores larger than 2.5 nm. Type 2 of the reversible isotherm demonstrates gas adsorption on materials with large or no pores. Type 2 differs from the first one in that the linear section gradually transforms into a curved line, which indicates the beginning of multilayer adsorption. Isotherm 3 shows that the interaction forces between adsorbent and adsorbate become weaker, and the adsorbed molecules begin to cluster. Type 4 isotherm shows the process of adsorption in mesopores, where monolayer and multilayer adsorption turns into pore condensation, i.e., the gas in the pores begins to condense and turn into a liquid phase. The main feature of type 4 isotherm is

the final saturation plateau of variable length. The isotherm itself is subdivided into two types, which differ in the shape of the pores. Isotherm 4b is fully reversible; while, isotherm 4a is accompanied by hysteresis. Isotherm type 5 is similar in shape to isotherm three at low relative pressure; however, the pores fill up as the relative pressure increases. 6, the reversible isotherm reflects layer-by-layer adsorption on non-porous surfaces of the material [116].

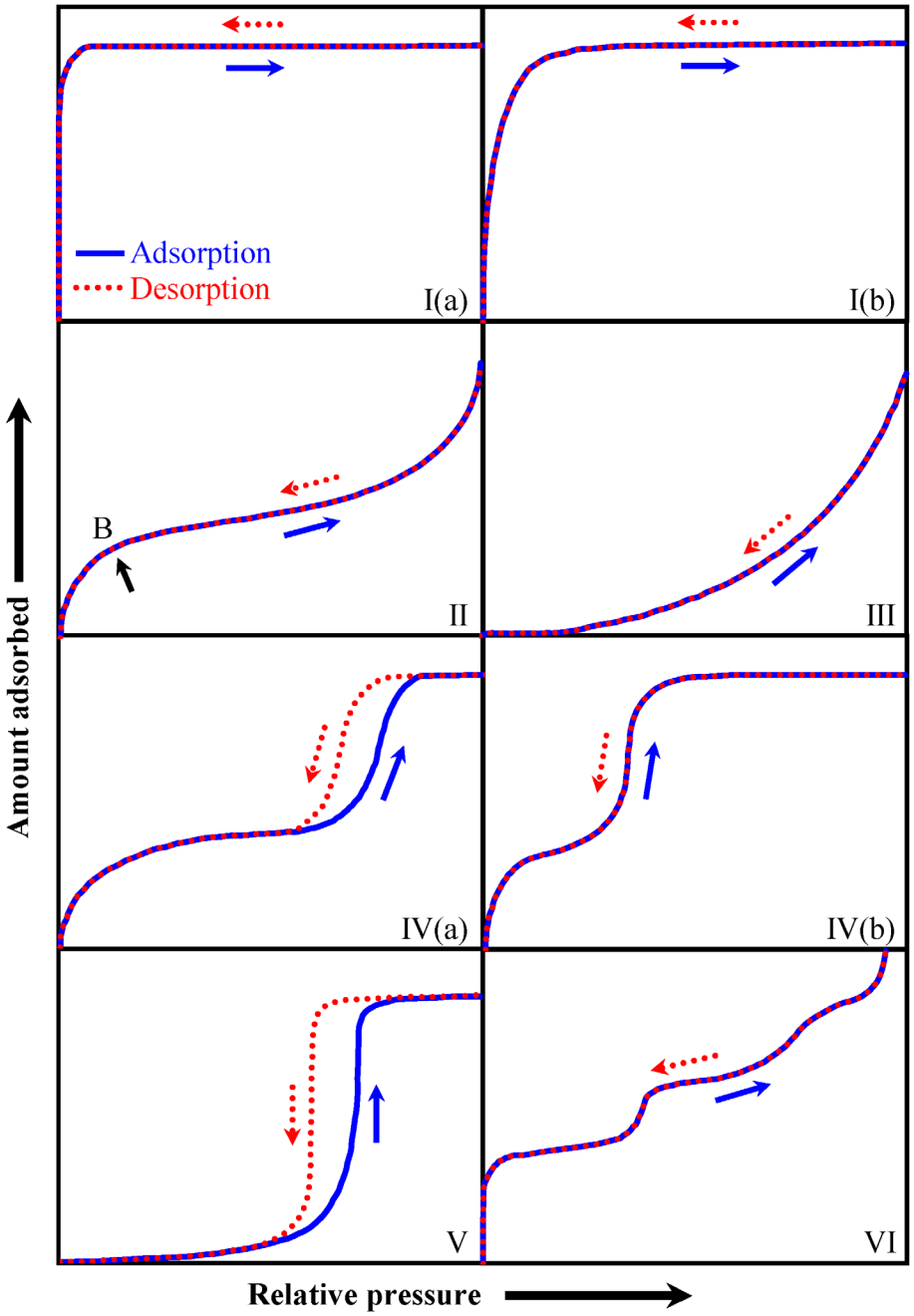

Figure 2-12. IUPAC classification of adsorption isotherms [117]

2.3.1.2 Adsorption isotherm models

Generally, there are two most common models of asphaltene adsorption mechanisms as presented in Figure 2-16. Langmuir model represents the adsorption of asphaltene as a monolayer onto a homogeneous material [12], [118], [119]. It assumes that adsorbate behaves as an ideal gas. It shows the maximum amount of gas the surface can cover at specific pressure and temperature [82]. The two-parameter Langmuir adsorption isotherms were initially created to characterize gas-solid phase adsorption on a homogeneous surface [120]. The Langmuir model is based on the theoretical equation as shown below [121]:

$$Q_e = Q_m \frac{K_L C_e}{1+K_L C_e} \qquad \text{Equation 2–2}$$

$$\frac{C_e}{Q_e} = \frac{1}{Q_m K_L} + \frac{C_e}{Q_m} \qquad \text{Equation 2–3}$$

where Q_e is the ratio of adsorbed asphaltenes mass and the surface area of the nanocomposite obtained from the BET analysis (mg/m^2), C_e is the equilibrium asphaltene concentration of the supernatant solution (mg/L), K_L is the Langmuir constant, Q_m is the maximum amount of asphaltene adsorbed on the surface of nanocomposite (mg/m^2). Figure 2-13 depicts the Langmuir model, there is no a direct relationship between Q_e and C_e from Equation 2-2. After modification of Equation 2-2 to Equation 2-3 the direct relationship between C_e/Q_e vs C_e was established. The Figure 2-14 shows this relationship.

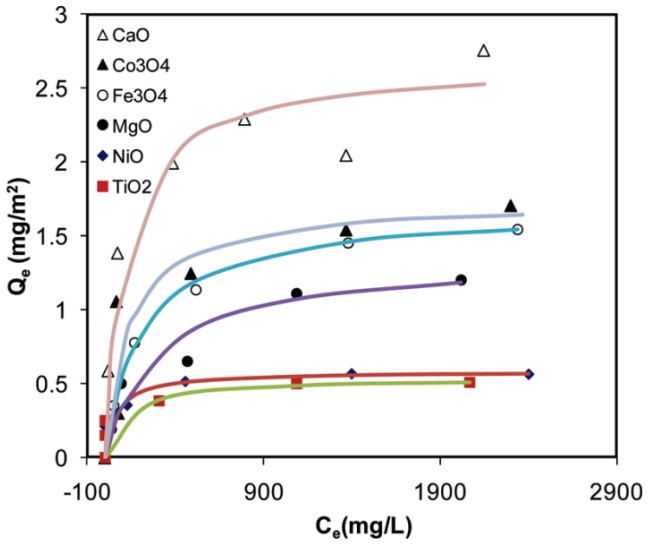

Figure 2-13. Example of Langmuir model for asphaltene adsorption isotherm on the surface of different NPs [93]

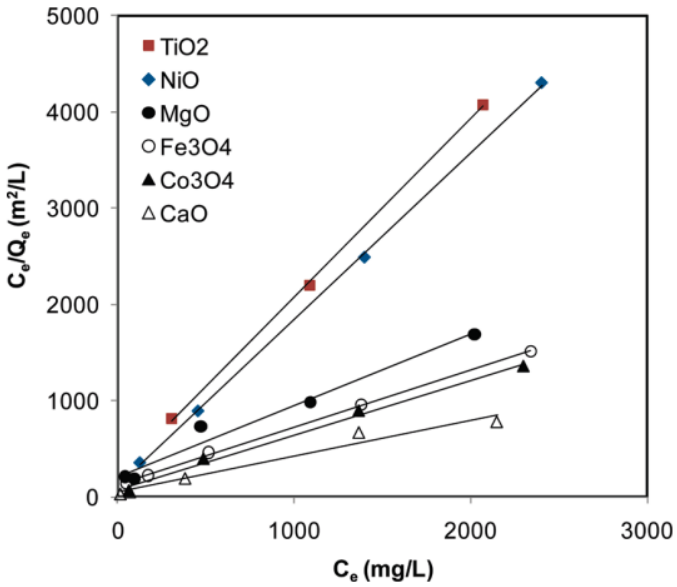

Figure 2-14. Example of Langmuir adsorption isotherms [93]

The Freundlich model allows predicting the amount of adsorbed gas by a solid adsorbent when changing pressure but at a constant temperature. In this case, only the pressure and amount of gas change, while the mass of the adsorbent and the temperature are constant. The adsorption isotherm model represents the non-uniform absorbance of asphaltene molecules. The main difference between the two models is that the Freundlich adsorption isotherm model is based on an empirical equation, whereas the Langmuir model is based on a theoretical equation [82]. The equation described by the Freundlich model is represented below:

$$Q_e = K_F C_e^{1/n} \qquad \text{Equation 2–4}$$

$$log(Q_e) = log(K_F) + \frac{1}{n} log(C_e) \qquad \text{Equation 2–5}$$

where K_F and n are Freundlich constants. Q_e and C_e have a logarithmic relationship for the Freundlich isotherm model. Figure 2-15 shows the example of the Freundlich isotherm model for asphaltene adsorption onto different NPs.

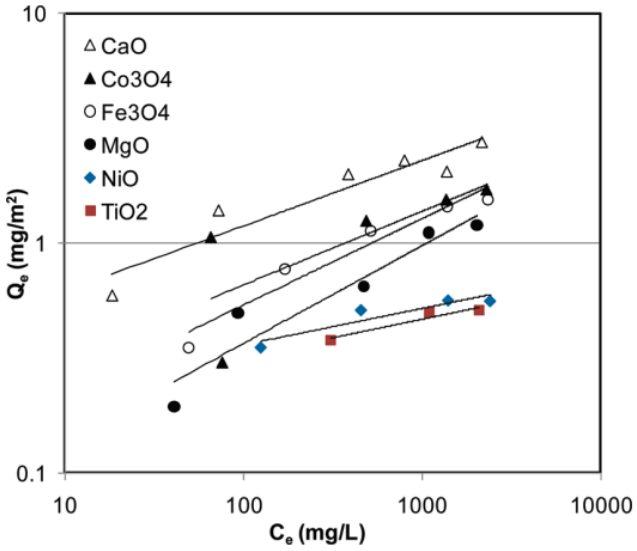

Figure 2-15. Example of Freundlich adsorption isotherms [93]

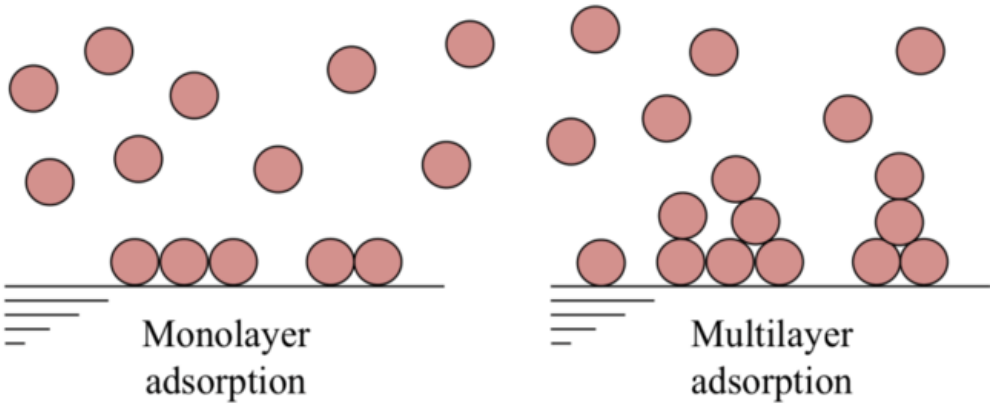

Figure 2-16. Main mechanisms of asphaltene adsorption [122]

2.3.2 UV-vis spectroscopy for asphaltene onset point (AOP) determination

Ultraviolet (UV) spectroscopy is a physical method of optical spectroscopy that uses light in the visible, ultraviolet, and near-infrared ranges and is based on the Beer-Lambert law, according to which the absorption of a solution is directly proportional to the concentration of absorbing particles in the solution and the path length. Thus, for a fixed path length, it can be used to determine the absorbent concentration in the solution. It is necessary to know how quickly the absorbance changes with concentration. UV-visible spectroscopy has been widely used over the past several decades and it has become the most important analytical tool in the modern laboratory investigations [123].

UV spectroscopy is a powerful analytical technique used to investigate the presence of chromophores in a sample. Chromophores are molecules that absorb light in the

electromagnetic spectrum's ultraviolet (UV) region. Their presence can be used to determine the onset point of asphaltene in a sample [123]. UV spectroscopy is a fast, accurate, and non-destructive method for determining the onset point of asphaltene in crude oil. Asphaltene molecules are heavy, complex molecules in crude oil and can cause numerous problems in oil production and processing. The onset point of asphaltene refers to the concentration at which these molecules start to precipitate out of the oil and form a solid phase. This onset point is an essential parameter in oil production, as it can affect the stability and flow properties of the oil. Beer-Lambert law expresses the relationship between the absorption, concentration, path length, and extinction coefficient [124]:

$$A = \varepsilon l c \qquad \text{Equation 2–6}$$

where A is absorbance determined by UV spectroscopy, ε is extinction coefficient, c is the concentration of absorbing chromophores, and l is the path length. According to the Beer–Lambert law, the absorbance and concentration of the absorbing species are directly proportional. Therefore, as soon as the deviation from Beer–Lambert law happens, asphaltene precipitate and asphaltene onset point can be determined. For example, Tazikeh et al. investigated the effect of coated iron oxide (III) NPs on AOP, determining the optimum concentration of NPs [125]. In Figure 2-17, the deviation from the straight line begins at 38 vol% of *n*-heptane; this point is considered AOP in the absence of NPs. Figure 2-18 depicts how AOP changes in the presence of different concentrations of NPs. The optimum concentration is 0.1 wt% of NPs as it improves the AOP more than other concentrations. Furthermore, AOP at the higher concentration of 0.5 wt% of NPs decreases compared to 0.1 wt% concentration. In another study by Shojaati et al. [126], UV spectroscopy was used to assess three different nano-inhibitors at 0.01 and 0.1 wt% concentrations of NPs. The results showed that 0.1 wt% concentration is more effective than 0.01 wt%, and alumina oxide improves AOP better than nickel and iron oxide due to its acidic nature.

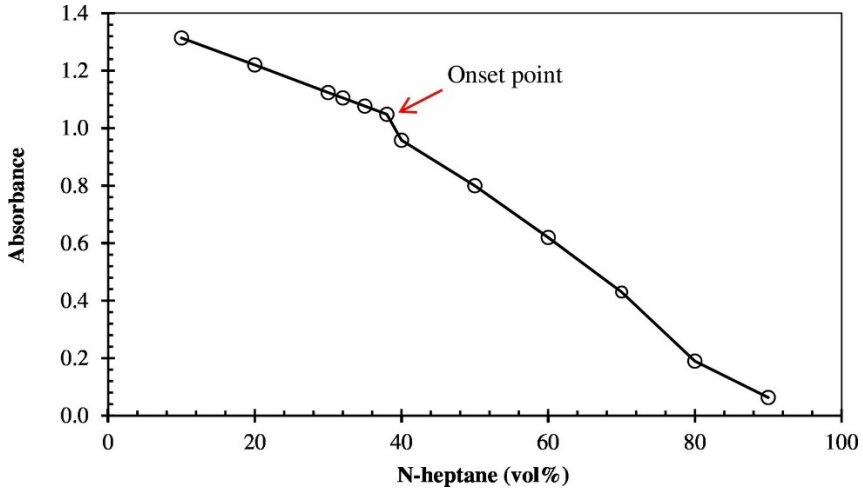

Figure 2-17. Asphaltene onset point in the absence of NPs [125].

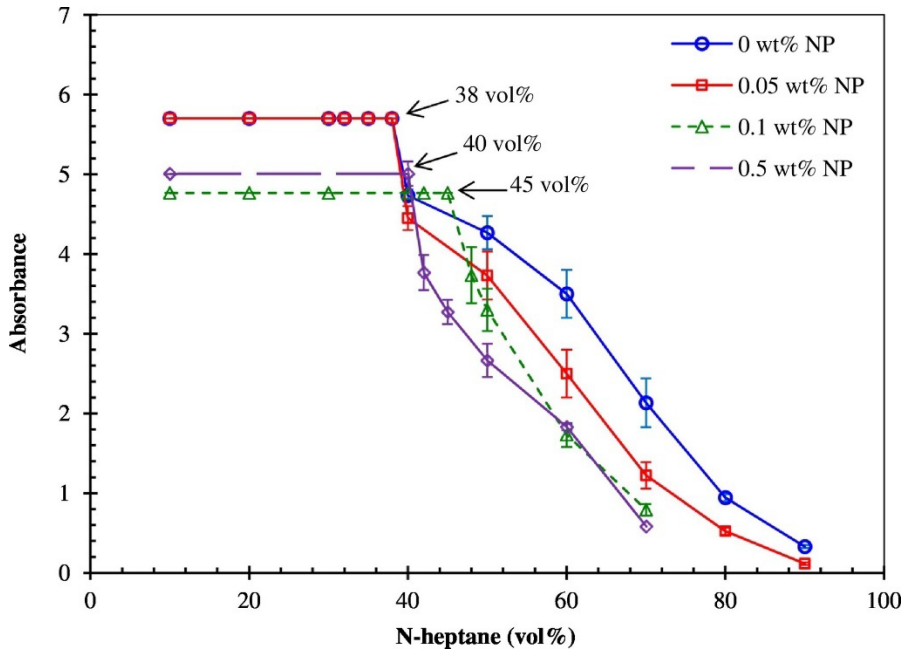

Figure 2-18. Asphaltene onset point for 0.5 wt% synthetic oil with different NPs concentrations [125]

2.3.3 Thermogravimetric analysis (TGA)

Thermogravimetric analysis (TGA) is a method used to study how a material changes weight as it is heated under specific conditions. TGA works by measuring the weight of a sample at different temperatures and times using a thermobalance device. This device has high sensitivity and can detect weight changes as small as one microgram [127]. When the sample is heated in an inert environment, TGA helps assess the material's thermal stability and identify weight changes due to moisture loss and the breakdown of organic compounds. TGA can also be used to understand how the material decomposes over time in an oxidizing or inert atmosphere. The heating rate and sample size are important factors that influence the TGA curve, which shows

how the material changes in weight over time. As the heating rate and sample size increase, the temperature at which the sample decomposes also increases. Factors such as gas flow rate, particle size, and packing can affect the reaction kinetics, so it is essential to keep these variables constant when comparing the thermal stability of different materials [127]. For example, Mahmoudi et al. used TGA to assess the thermal degradation of asphaltene in the absence and presence of NPs [89]. Figure 2-19 shows that the maximum mass loss of asphaltene during adsorption on the surface of NPs decreased by 100 degrees. The author explains this by the fact that asphaltene molecules are adsorbed on the surface of NPs, having more available surface for combustion, accelerating the process of asphaltene decomposition.

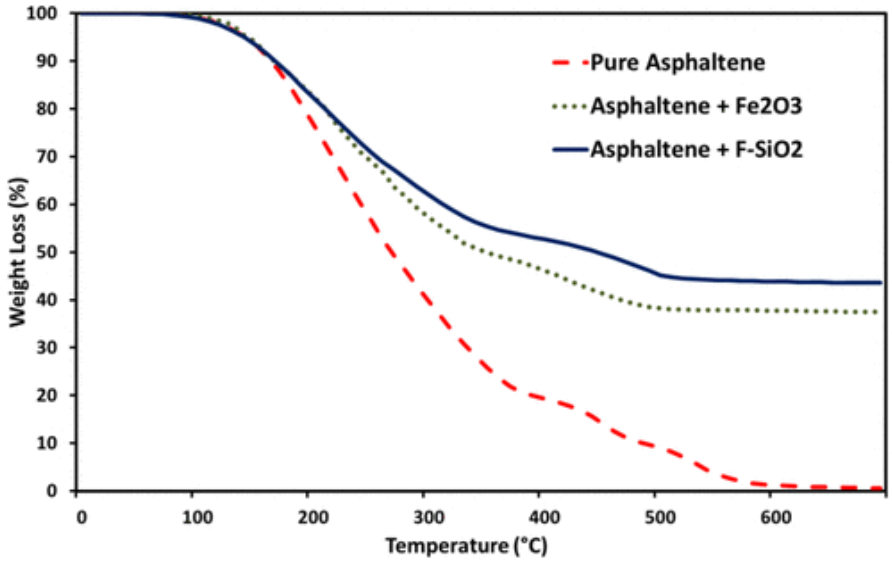

Figure 2-19. TGA mass loss curves for pure asphaltene and asphaltene adsorbed onto the surface of NPs [89].

3 MATERIALS AND METHODS

This chapter details the materials, methodology of asphaltene extraction, techniques of asphaltene characterization, inhibitor characterization, and evaluation to attain the objectives and aim mentioned in Chapters 1 and 2. Then, all methods in Chapter 3 are explained and described in detail along with the experimental setups and procedures of sample preparation and conduction of the experiments.

3.1 Materials

3.1.1 Sample origin

A paraffinic heavy crude oil from West Kazakhstan was used to extract the asphaltene. The SARA analysis results are presented in Table 2-1.

Table 3-1. SARA analysis of the crude oil.

SARA	Content (wt%)
Saturate	37.41
Aromatic	32.07
Resin	24.87
Asphaltene	5.65

3.1.2 Green synthesis of thiazine-Fe_3O_4-TiO_2-SiO_2-Bentonite NCs

Fifty grams of the dried powdered leaf of the *Alocasia macrorrhiza* was extracted using boiling in 400 mL double distilled water for 40 minutes at 80°C. Then the obtained extract was filtered and kept in refrigerator for further use. Two grams of $FeCl_3.6H_2O$, 4 g titanyl hydroxide ($TiO(OH)_2$), and 5 g of sodium metasilicate (Na_2SiO_3) were mixed with 100 ml *Alocasia macrorrhiza* extract in a 250 ml beaker, at 80°C and pH ten under stirring. The stirring was continued until the formation of a black precipitate was observed. The precipitate was separated using filtration. It was then heated at 400°C and washed with hot distilled water to remove the impurities and complete the oxidizing process for each nano fraction. Afterwards, the obtained precipitate was mixed with 3 g of thiazine and 6 g bentonite in 200 mL Ethanol under reflux condition for 8 h at 80°C to form the precipitation of thiazine-Fe_3O4-TiO_2-SiO_2-Bentonite NCs as can be separated using a simple magnet.

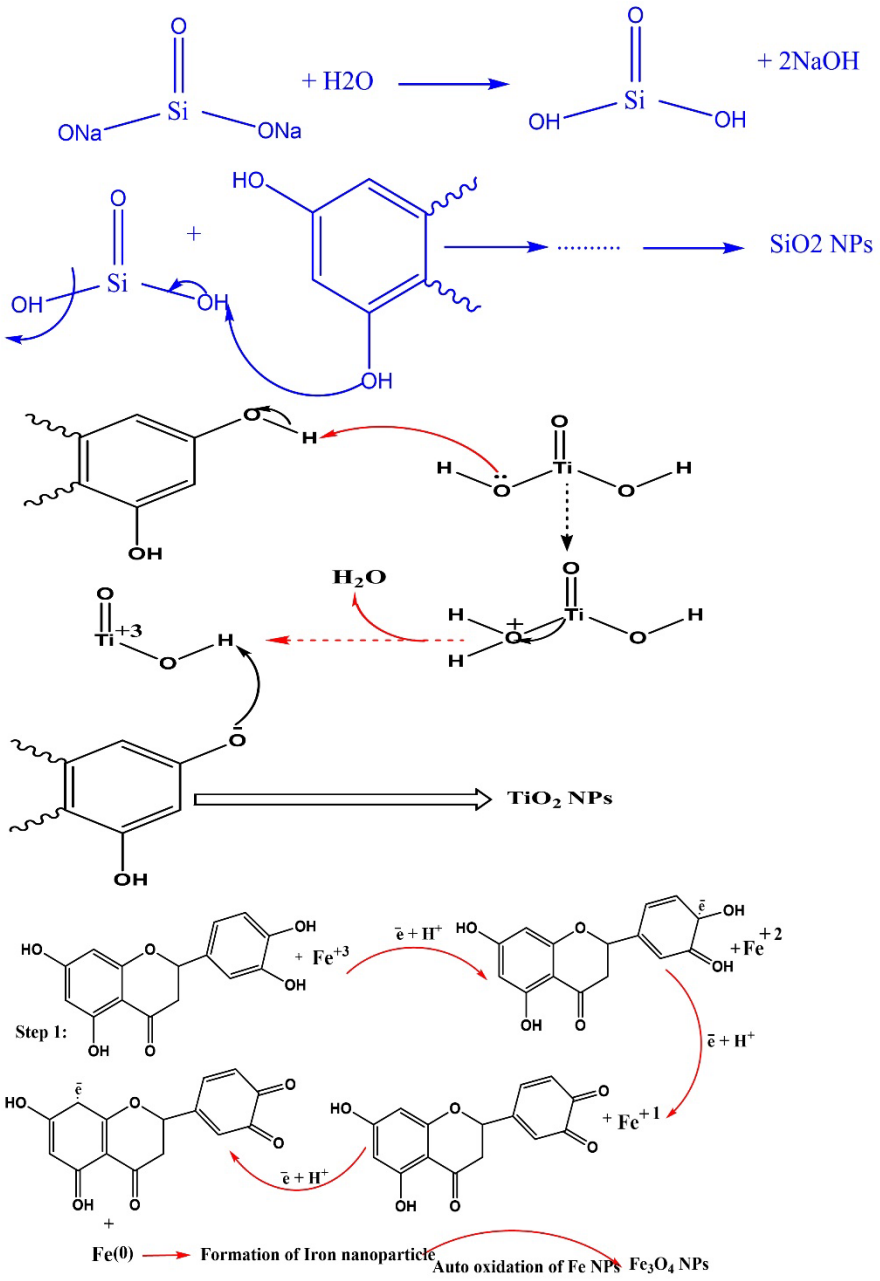

Figure 3-1. Mechanism of nanocomposite synthesis

3.2 Methods

3.2.1 Asphaltene extraction

Asphaltene was extracted using IP143 (Heptane Insoluble) method depicted in Figure 3-1. Crude oil was mixed with *n*-heptane in a 1:40 volume ratio for 4 hours using the digital magnetic stirrer at 600 rpm. *n*-heptane created unstable conditions, and asphaltene started to precipitate. Then the mixture was placed in a dark place overnight to let asphaltene precipitate at the bottom of the beaker. After precipitating the asphaltene fraction, the filter paper Whatman #42 separated the precipitation from the mixture (see Figure 3-2). The Soxhlet extractor was used

for asphaltene purification to eliminate possible oil components. Figure 3-3 represents simple Soxhlet extractor *n*-heptane was added into the distillation flask, and the separated asphaltene fraction was put into the extractor. The heat source set the temperature of the boiling point of *n*-heptane at about 100°C. When the *n*-heptane was heated, it started to vaporize. The vapor went up through the siphon, then it cooled at the condenser, and drops of *n*-heptane went to the Soxhlet chamber and dissolved different impurities. This procedure continued until drops of *n*-heptane from the bottom of the condenser became colorless. Hot n-heptane dissolved waxy substances removing them from the [128]. Then the procedure was repeated with a Soxhlet extractor replacing *n*-heptane with toluene. Toluene was used to dissolve the purified asphaltene in the filter paper, separating them from the inorganic materials until all dissolved asphaltene were moved to the reflux container. Then heat the resulting mixture at about 100 Celsius to evaporate toluene (see Figure 3-4). After that, put the resulting asphaltene into the oven at 80°C for 4 hours to dry and obtain pure asphaltene by measuring the weight of asphaltene three times every 2 hours to ensure the weight is constant.

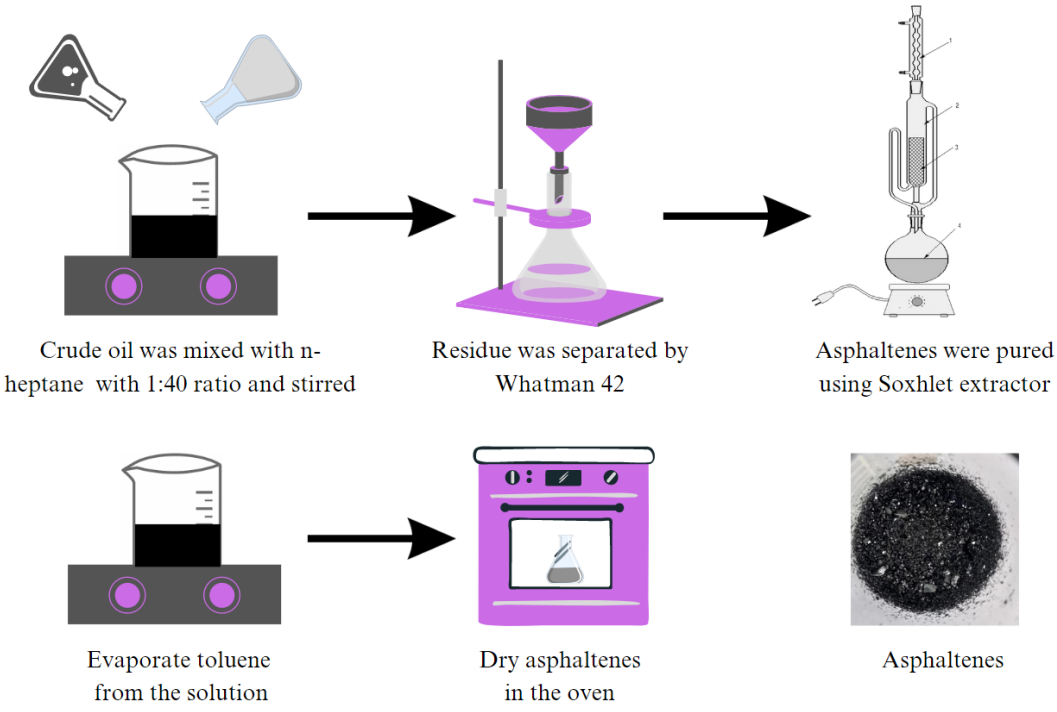

Figure 3-2. Scheme of the asphaltene extraction procedure

Figure 3-3. Filtration of asphaltene using filter paper

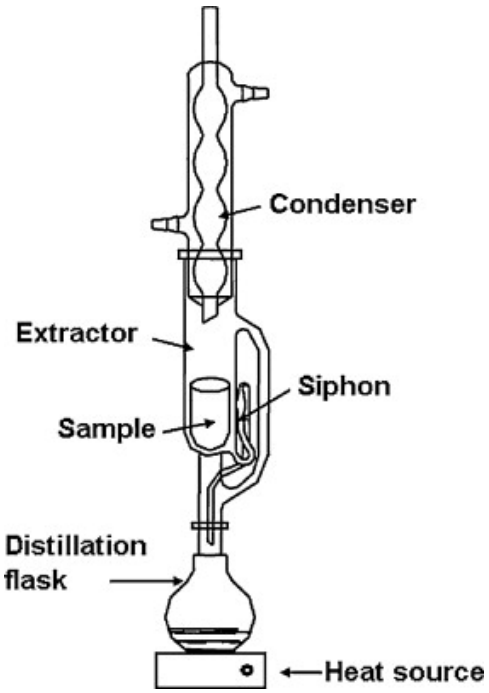

Figure 3-4. Schematic of Soxhlet extraction apparatus

Figure 3-5. Toluene evaporation

After extraction, asphaltene is presented in a solid state; then, it is necessary to prepare synthetic oil-dissolving asphaltene in toluene at specific concentrations for further experiments. Therefore, synthetic oil containing 0.5 wt% of asphaltene was prepared. Knowing the required concentration of asphaltene in the mixture and the mass of the solution, the required mass of asphaltene can be calculated using provided Equation 3-1:

$$C_{asphalt} = \frac{m_{asphalt}}{m_{asphalt}+m_{toluene}} * 100\% = \frac{m_{asphalt}}{m_{asphalt}+V_{toluene}*\rho_{toluene}} * 100\% \qquad \text{Equation 3-1}$$

3.2.2 Asphaltene & nanocomposite characterization

Different characterization techniques were applied to obtain the chemical and structural description of asphaltene and nanocomposite samples. First, asphaltene's chemical composition can be determined using elemental analysis, and Energy Dispersive Spectroscopy (EDAX) determines the elemental composition of the nanocomposite. Then, nuclear magnetic resonance (NMR) spectroscopy was used to obtain the chemical structure and functional groups that makeup asphaltene. H-NMR represented the average length of the side chain to assess the level of asphaltene aromaticity. C-NMR provides information that cannot be studied from H-NMR about the basic structure of carbon molecules in heavy fractions [129]. To identify the intra and intermolecular bonds, Fourier-transform infrared (FTIR) spectroscopy was used for both asphaltene and NC characterization [130]. Usually, NP characterization includes the determination of their size, structure, and charge of the surface. The NPs' physical stability and in vivo distribution is influenced by the average particle diameter, size distribution, and charge.

Electron microscopy techniques are beneficial in assessing the general form of polymeric NPs. Their surface charge affects the NPs' physical stability, dispersibility, and in vivo performance [50].

3.2.2.1 Fourier-transform infrared spectroscopy (FTIR)

Asphaltene and nanocomposites can be identified using the non-destructive analytical method known as FTIR (Fourier Transform Infrared Spectroscopy). Making asphaltene or nanocomposite material involves crushing or grinding the material into a fine powder. First, the powder should be combined with a suitable solvent, such as toluene or chloroform, to create a homogeneous solution. After that, the solution should be put in a suitable cuvette for FT-IR spectrometer analysis. Finally, to ensure accurate results, the spectrometer must be calibrated using a suitable reference material, such as a well-known standard of the same material. Additionally, the instrument must be calibrated for the wavelength range and resolution needed to analyze the material. After that, the various functional groups present in the asphaltene or nanocomposite material can be determined by examining the resulting FTIR spectrum. With the help of this data, it is possible to ascertain the material's structure and chemical makeup and any potential changes by NPs. By contrasting it with well-known reference spectra of related materials or using sophisticated data analysis and interpretation software tools, data from FTIR analysis can be understood. This can enhance the performance of asphaltene or nanocomposites and assist in identifying any potential issues or areas of concern.

Infrared spectroscopy generates an infrared spectrum by passing infrared radiation through a material with a permanent or induced dipole moment. Then the amount of radiation absorbed in a certain energy frequency is recorded. The produced absorption spectrum has energy peaks that correlate to a molecule's vibrational frequency, allowing for qualitative identification of the bond types in the sample. In addition, the IR spectrometer records the energy of electromagnetic radiation transmitted through the sample, which is a function of the wave number or frequency [120].

A FTIR setup, which consists of an infrared source, an interferometer, an infrared detector, and a sample cell, is shown in Figure 3-5 [120]. The interferometer is an optical apparatus comprising a beam splitter, a fixed mirror, and a moving mirror that must always be perfectly oriented because the FTIR's accuracy relies heavily on it. The production of interference in a beam of light is how the FTIR works. First, a light beam from a source is splitted into two, with one of the resultant beams having a changing phase difference. Then,

after measuring the interferogram, the two beams are recombined, and an interferogram is recorded [120].

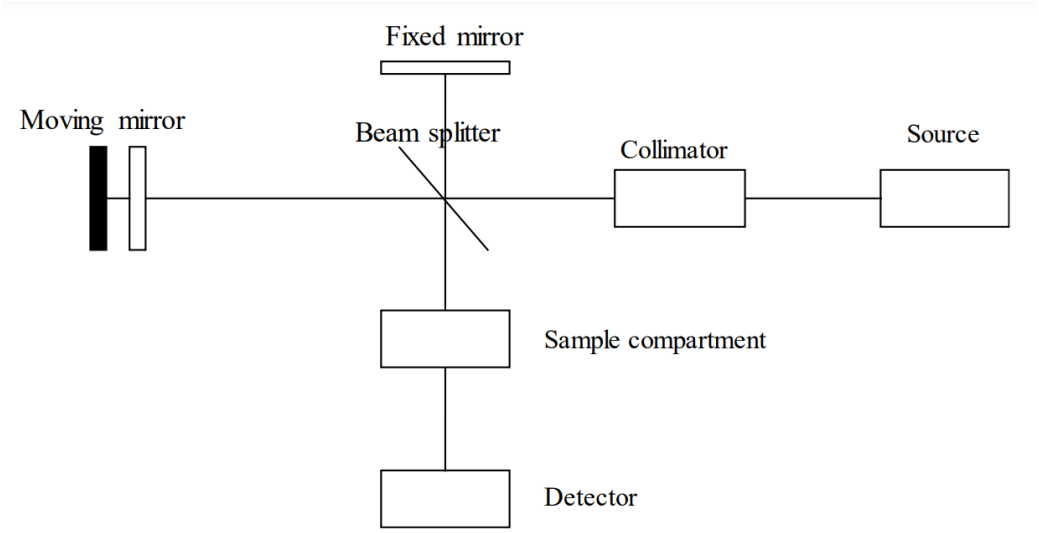

Figure 3-6. The FTIR configuration [131]

3.2.2.2 Scanning electron microscopy (SEM)

Scanning electron microscopy (SEM) is a highly efficient method for characterizing NPs to learn more about their physical and chemical characteristics. Sample preparation, instrument setup, imaging, particle size analysis, elemental analysis, morphological analysis, and data analysis are some of the steps included in the procedure. SEM is used for morphological analysis, which involves examining the NPs' surface structure, morphology, and shape. In addition, SEM can reveal details about a particle's internal structure, such as whether it is hollow or solid [131].

Before the SEM technique characterized the nanocomposite, the nanocomposite sample was cleared of impurities. Next, the necessary amount of sample was heated in the furnace at 400°C for one hour. Then the sample was washed with ethanol 3-5 times using an ultrasonic bath. After that, the nanocomposite was separated from ethanol using a centrifuge and put in the vacuum oven at 60°C overnight to evaporate ethanol. Finally, the dried sample was crushed into the powder. An essential step in the SEM characterization procedure is applying a thin conductivity layer to samples. This is required to stop the sample from charging and enhance the quality of the image. When a sample insulates or has poor electrical conductivity, charging happens, which results in an electrical charge accumulating on the sample's surface. The image may become distorted or lose resolution due to doing this. Using sputtering or carbon coating, a thin layer of a conductive material, such as gold, platinum, or palladium, is applied to the

sample to prevent charging. The electron beam can pass through the sample without experiencing charging effects thanks to the conductive coating's role in facilitating the flow of electrical charge.

SEM works based on a focused electron beam being scanned over a sample and signals being picked up from the sample in response to the beam. The SEM instrument comprises an electron source, electron lenses, a stage, and detectors. The interaction between an electron beam and the sample's atoms releases secondary electrons, backscattered electrons, and X-rays. Detectors pick up these signals, which are then used to build images of the sample. After being bombarded by a primary electron beam, the sample's surface emits secondary electrons. The sample surface can be imaged with high resolution using these low-energy electrons. On the other hand, backscattered electrons are high-energy electrons that scatter back from the sample due to contact with the sample's atomic structure. Images highlighting variations in a sample's atomic number are produced using backscattered electrons, which can be used to distinguish between various materials [132], [133].

Using energy-dispersive X-ray spectroscopy and imaging (EDS), SEM can be used for elemental analysis. When a sample is exposed to an electron beam, EDS picks up the X-rays that are released from the sample. The sample's elemental composition can be ascertained by analyzing the detected x-rays, which indicate the elements present in the sample.

3.2.2.3 Surface area analysis (BET)

A popular technique for characterizing nanoparticle samples is the Brunauer-Emmett-Teller (BET) method (see Figure 3-8). Sample preparation is the first step in the BET method's characterization of NPs. In the same manner, as for SEM measurements, the sample was prepared. To remove any adsorbed gas or moisture from the sample's surface, the sample should be degassed above the boiling point of the adsorbed solvent. Typically, samples are vacuum-degassed for several hours between 150°C and 200°C. The sample is prepared for BET analysis after degassing. BET analysis entails measuring the isotherm of adsorption of a gas, typically nitrogen, on a sample's surface. Plotting the amount of adsorbed gas against the gas's relative pressure (P/Po), where P is the equilibrium pressure, and Po is the gas's saturation pressure at the measurement temperature, is how the BET method works [134], [135]. The BET method calibrates the instrument using a reference material with a known surface area. The specific surface area of a sample can be determined using the BET method. The BET equation, a mathematical formula connecting the volume of gas adsorbed to the sample's surface area, is

used to calculate the surface area from the BET plot [135]. The specific surface area can be calculated by dividing the sample's total surface area by its mass. The data can be analyzed to determine the characteristics of the nanoparticle sample, such as particle size and morphology, once the precise surface area of the sample has been calculated.

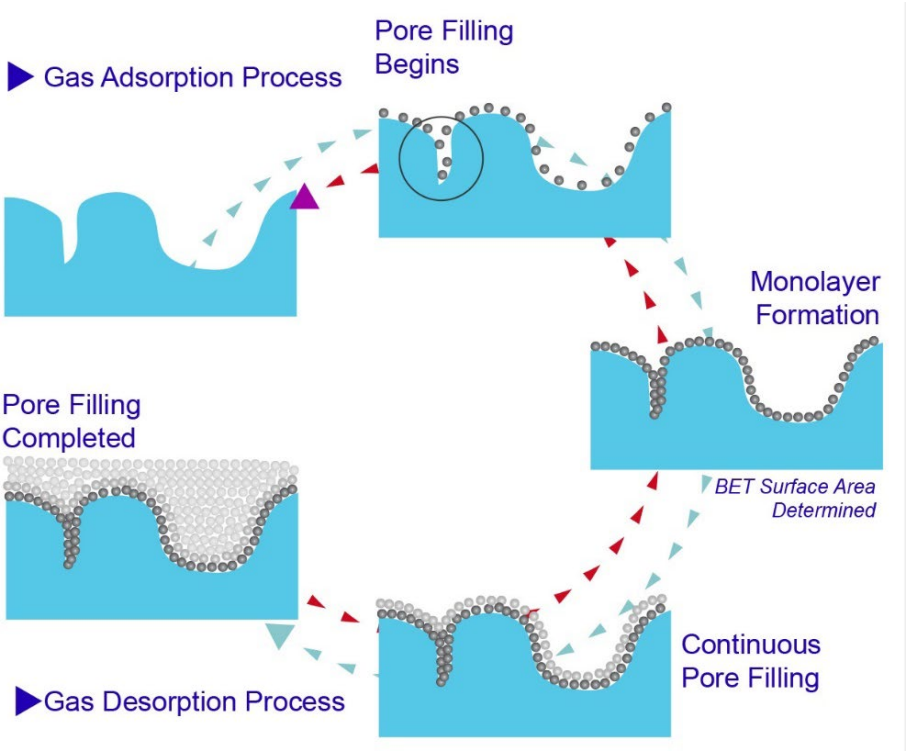

Figure 3-7. Mechanism of BET analysis [133]

3.2.2.4 X-ray diffraction (XRD)

Asphaltene and NP sample diffraction patterns can be deciphered to reveal the crystal structure, lattice parameters, and phase identification. Particle size, morphology, and crystallographic orientation can be determined by analyzing the location and intensity of peaks. X-ray diffraction patterns are frequently used in NP research as the primary characterization tool for acquiring crucial features such as crystal structure, crystallite size, and strain. For example, the diffraction peaks in nano-crystalline materials become broader due to randomly aligned crystals. This is because an X-ray grating with a finite size does not entirely interfere with X-rays in both a constructive and destructive manner.

Diffraction allows studying the crystal lattice of various solid materials [136]. This method is one of the most important for the characterization of asphaltene, showing the arrangement of atoms in a solid sample due to the intensity of refracted rays. XRD is based on Bragg's law of diffraction, illustrated in Figure 3-7 [137]. It shows that the incident beam is

normal to the reflecting plane, and the diffracted beam is normal to the reflecting plane. Furthermore, the angle formed by the incident and dispersed beams is called the scattering angle with a constant value 2θ [137]. An X-ray diffractometer comprises an X-ray source, a goniometer, a counter tube, and counting electronics. A plot of peak intensity versus 2θ is usually applied to acquire XRD data. The angle is then converted to the space between crystallographic planes using Bragg's formula [138].

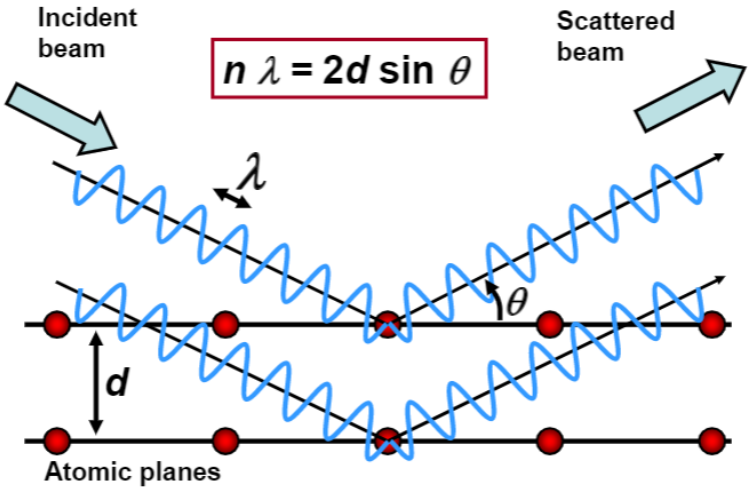

Figure 3-8. Principle of XRD process [137]

3.2.3 Nanocomposite efficiency evaluation

The nanocomposite efficiency evaluation consists of determining the optimum concentration of the novel nanocomposite by comparing the asphaltene onset point at those concentrations. In addition, the thermogravimetric analysis identifies the mechanisms of asphaltene adsorption and provides information about the catalytic activity of asphaltene and NCs.

3.2.3.1 Determination of nanocomposite optimum concentration

One of the methods to assess the NC efficiency is to determine the asphaltene precipitation onset point (AOP). The "indirect method" proposed by Tavakkoli was applied in this research [139]. The main principle of the "indirect technique" is to use supernatant liquid content after the samples of synthetic oil were centrifuged to determine the asphaltene onset point. Asphaltene onset point shows at what *n*-heptane concentration asphaltene starts to precipitate. This method applies to oil samples with different concentrations of asphaltene [139]. It compares AOP curves in the absence and presence of NC at different concentrations. The sample preparation for AOP determination is depicted in Figure 3-10. Initially, different

concentrations of synthetic oil and NC were mixed. After that, the mixture was put into an ultrasonic bath for 25 minutes. Next, *n*-heptane was added to the solution and left for 2 hours at room temperature and pressure. Precipitation was separated from the supernatant liquid using a centrifuge for 15 minutes at 10,000 rpm. If prepared supernatant liquids were too dark for UV spectroscopy, dilution was required. The mixture was diluted with toluene at different concentrations. After that, absorbance for each sample was measured in a range of wavelengths between 500 and 900 nm using a spectrophotometer, using toluene as a blank. Values of absorbance at a wavelength of 700 nm were used. Cuvettes made of quartz were used to measure the absorbance. Then adsorption for each initial concentration was calculated, removing the dilution effect. AOP was defined on the graph of absorbance vs. *n*-heptane concentration. The volume fraction of *n*-heptane at the time of the detection of asphaltene precipitation correlates to the abrupt departure from linear behavior in the data points. AOP is identified as the first deviation from the straight line. The same procedure was repeated, adding nanocomposite at 0.1, 0.3, 0.4, and 0.5 wt% concentrations.

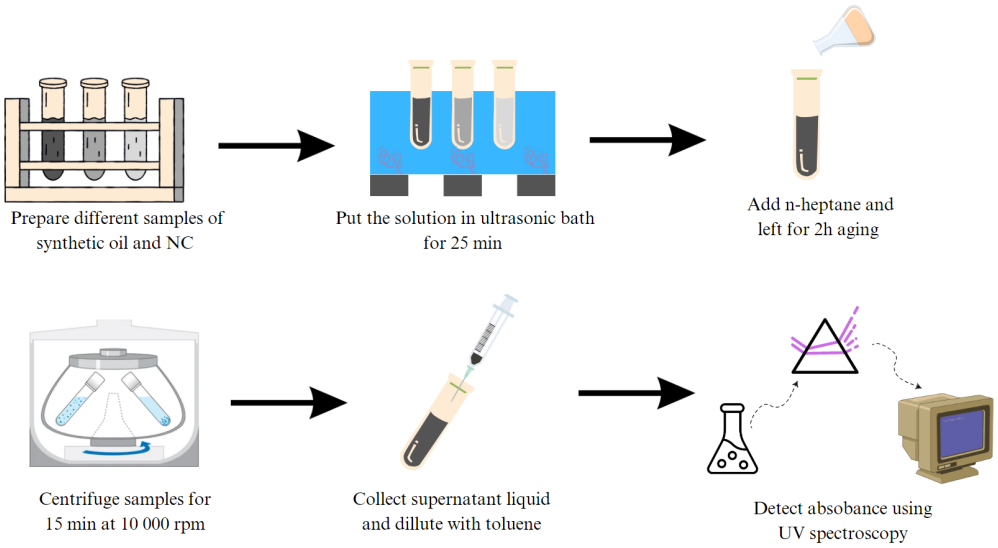

Figure 3-9. Sample preparation for AOP determination

3.2.3.2 Thermogravimetric analysis (TGA)

The thermogravimetric analysis (TGA) technique is a thermal analysis method that uses a beam balance principle to detect changes in the weight of a sample over time and temperature. A thermobalance with a capacity of a few hundred milligrams is used in a TGA device, which measures the amount of sample with an accuracy of roughly 1 g. It also contains a heater between 50°C and 1,000°C, with a heating rate of 100°C per minute [140]. A TGA experiment,

performed in an inert atmosphere, aids in estimating the sample's thermal stability and evaluating weight changes due to moisture evaporation and organic chemical breakdown. TGA provides a curve that aids in understanding the material's degradation mechanism. The heating rate and sample size affect the TGA curve. The heating and sample size rate are proportional to the sample's decomposition temperature changes. The flow rate of gas, the size of particles, and the decomposition temperature may affect the kinetics of the reaction; consequently, while comparing the thermal stability of 2 samples, it is critical to maintaining an identical condition of variables [127].

The sample preparation for TGA analysis and asphaltene adsorption isotherms was described in Figure 3-10. Asphaltene molecules adsorb on the surface of NPs at 25°C temperature. The experiment consisted of adding a certain nanoparticle concentration to synthetic oil in a ratio of 1:10 (g/l) ratio. Then they were tightly closed and stirred at a speed of 200 rpm at a temperature of 25°C. Subsequently, to separate the asphaltene adsorbed on the surface of the NPs using a centrifuge for 15 minutes at a speed of 10,000 rpm. Next, the NPs with asphaltene placed in a vacuum oven for a day at 60°C; the dry finished material is used for thermogravimetric analysis [79]. While, supernatant liquid was used to determine the adsorption isotherms using UV spectroscopy. TGA can be used to evaluate how much asphaltene is adsorbed onto NPs' surfaces by measuring mass loss between 200–800°C. TGA was used to perform a thermogravimetric analysis on asphaltene, NC, and NC with adsorbed asphaltene. The samples were heated in an environment of air for around 5 mg. To get over diffusion constraints, the sample mass was kept low. Airflow was maintained at 100 cm^3/min. Fresh NPs from the original bottle were heated to 1,000°C at a heating rate of 10°C/min to achieve an accurate profile of mass loss and heat changes. Pure asphaltene and asphaltene adsorbed onto NPs were heated to 900°C in the air at a heating rate of 10°C/min for adsorption kinetics and isotherms.

TGA analysis enables determining the amount of adsorbed asphaltene. Firstly, the mass of fresh NPs is analyzed by TGA; then, the final mass is recorded ($m_{TGA(NP)}$). Then NPs with adsorbed asphaltene was analyzed by TGA, then the final mass and mass loss were recorded ($m_{TGA(ads+NP)}$). As a result, the mass of adsorbed asphaltene (m_{ads}) can be calculated using the equation below:

$$m_{ads} = m_{TGA(ads+NP)} - m_{TGA(NP)} \qquad \text{Equation 3-2}$$

Comparing the profiles of fresh NPs and NPs added to the solution, a negligible difference in mass loss between the two profiles led to the conclusion that the adsorption process did not occur. At the same time, the significant change in mass loss between the two profiles represents the adsorption of asphaltene. Since the initial concentration of asphaltene and the mass of NPs are known, the equilibrium concentration of asphaltene in the supernatant, Ce, and the amount adsorbed (Qe, mass of adsorbed asphaltene/mass of NPs), are then estimated from the mass balance [76].

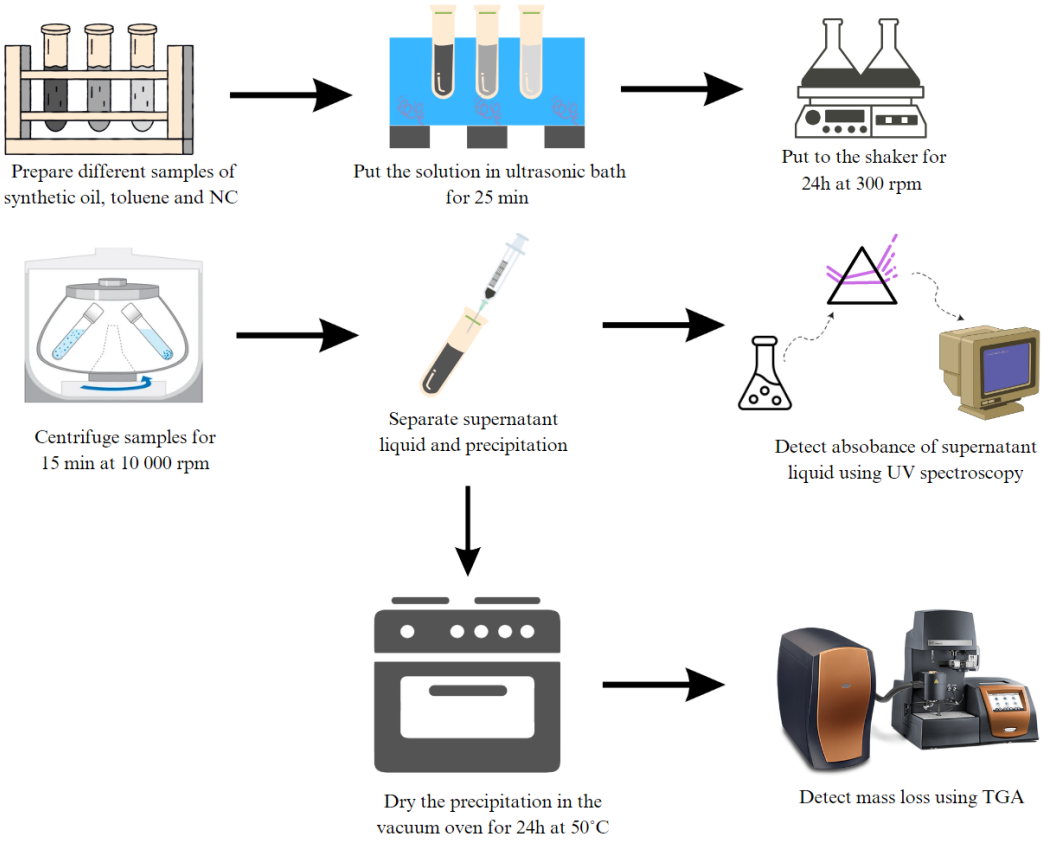

Figure 3-10. Sample preparation for TGA analysis and adsorption isotherm determination

4 RESULTS AND DISCUSSION

This section includes raw data from experiments and an analysis of the results. The result and Discussion chapter is divided into three parts. The first part describes asphaltene samples, their molecular structure, and their chemical composition. The second part analyses nanocomposite properties characterization. In addition, the last part of this chapter represents the results of the interaction between the nanocomposite and asphaltene sample. It evaluates the efficiency of nanocomposite on asphaltene aggregation and adsorption, determining the optimum concentration of nanocomposite.

4.1 Nanocomposite characterization

This section contains results of characterization of the novel NC using different techniques such as scanning electron microscopy (SEM) for morphology, energy dispersive spectroscopy (EDS) for elemental analysis, Brunauer–Emmett–Teller (BET) method for the surface area of the sample, Fourier transform infrared (FTIR) spectroscopy for functional groups, x-ray diffraction (XRD) for the crystal structure of NC and thermogravimetric analysis (TGA) for its thermal stability. For example, Thiazine-Fe_3O_4-TiO_2-SiO_2-Bentonite is a novel NC including the organic compound thiazine, metal oxides, and clays.

4.1.1 Energy dispersive spectroscopy (EDS)

The EDS analysis is incorporated with Scanning Electron Microscope ZEISS Crossbeam 540. EDS analysis is used to characterize nanocomposite in terms of elemental composition and distribution of molecules. Figure 4-1 represents the results of the EDS analysis. Each chemical element has a specific energy level that reflects in peaks at X-ray regions. The EDS confirms the elemental composition of the new nanocomposite [141]. It can be seen from the EDX that oxygen (O) and silicon (Si) elements dominate in the composition of Thiazine-Fe_3O_4-TiO_2-SiO_2-Bentonite 55.1 and 18.9 wt%, respectively. Fe and Ti also contribute to the elemental composition of nanocomposite as 4 and 2.5 wt%, respectively. The Presence of Al, Mg, K, Ca, and Na indicates the presence of bentonite, as these chemical elements form clay. The presence of all elements mentioned above indicates that the novel NC was successfully prepared. This experiment also reveals the relative content of the aforementioned elements in the NC. However, EDS did not detect nitrogen and sulfur even though these elements are present in the composition of the organic compound Thiazine.

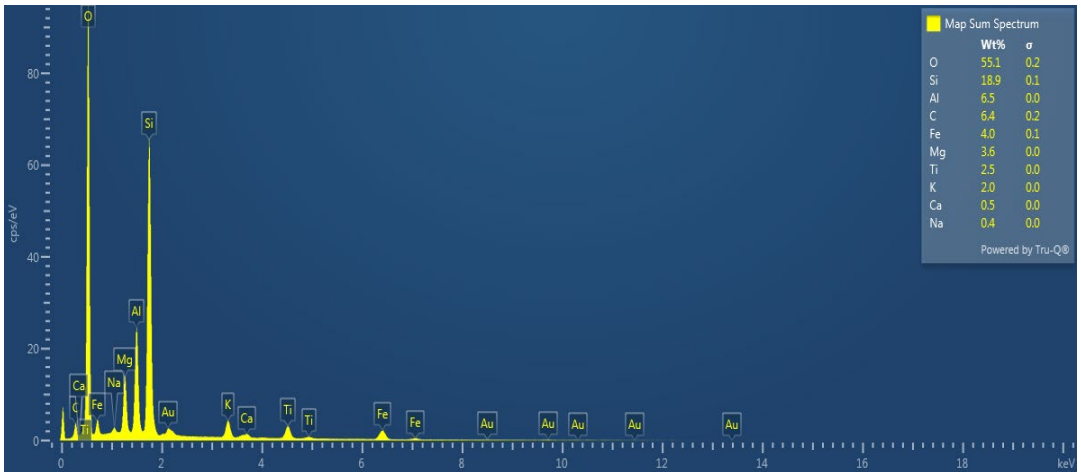

Figure 4-1. EDS of the Thiazine-Fe_3O_4-TiO_2-SiO_2-Bentonite NC

4.1.2 Scanning electron microscopy (SEM)

Scanning Electron Microscope ZEISS Crossbeam 540 was used to study the morphology and size of the nanocomposite. The sample was investigated under two scales. 300 nm scale was used to observe the sample's morphology visually, and the 100 nm scale shows the size of the NC. Morphology of Thiazine-Fe_3O_4-TiO_2-SiO_2-Bentonite NC is presented in Figure 4-2b. It was noticed that the surface of the sample was rough, and its shape was non-uniform and irregular. The average size of the nanocomposite determined from the SEM measurements (Figure 4-2a) was around 38-76 nm. Hence, the NC varies in a wide range of size and is highly agglomerated.

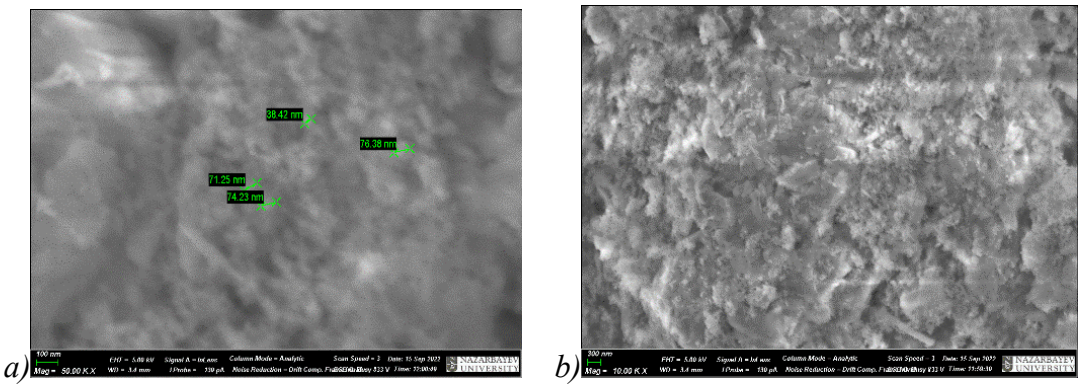

Figure 4-2. SEM of the Thiazine-Fe_3O_4-TiO_2-SiO_2-Bentonite NC a) 100 nm scale b) 300 nm scale

4.1.3 X-ray diffraction (XRD)

SmartLab (Rigaku) X-ray Diffraction System provides XRD patterns for the Thiazine-Fe_3O_4-TiO_2-SiO_2-Bentonite NC. X-ray diffraction (XRD) is a commonly used technique for the characterization of NPs. The XRD pattern can provide information about the crystalline structure, phase composition, and crystallite size of the NPs. When interpreting an XRD pattern of NPs, it is essential to compare the peaks observed in the pattern to the reference patterns of known nanoparticle crystal structures.

The XRD pattern of SiO_2 typically shows several prominent peaks at specific angles, known as 2θ angles, which correspond to the diffraction of X-rays by the crystal lattice of SiO_2. The most prominent peaks in the XRD pattern of SiO_2 are usually observed at around 20.89°, 26.67°, 45.87°, 50.14°, and 59.95° 2θ angles. The peak at around 20.89° corresponds to the (100) plane of the α-quartz structure of SiO_2. The peak at around 26.67° corresponds to the (101) plane of α-quartz. In addition, the peak at around 45.87° corresponds to the (201) plane of α-quartz. Finally, quartz surface 112 and 211 planes refer to the 50.14° and 59.95° 2θ angles, as it was obtained in previous studies by Zhang et al. [142]. Figure 4-3 shows that silicon oxide is present in two phases: quartz and cristobalite. Comparing XRD patterns with patterns obtained by Munasir et al. [143]. From the XRD results, SiO_2 is the dominant NP in the composition of the new NC that is corresponds to the results of the EDS where Si and O constitute the highest weight content in the NC.

The interpretation of XRD patterns for TiO_2 can be complex and depends on several factors, such as the phase of TiO_2 (Anatase, Rutile, or Brookite), the crystal size, and the degree of crystallinity. In many cases, TiO_2 samples may contain a mixture of two or more phases. In such cases, the XRD pattern will show peaks corresponding to the diffraction peaks of each phase present in the sample. For example, in Figure 4-3, intensive peaks of 2 theta values 26.67° and 36.62° identify the Anatase and rutile phases of TiO_2 that were also reported in other studies [143]–[145].

Fe_3O_4 is a compound of iron and oxygen, also known as magnetite. Its XRD pattern typically shows distinctive peaks at specific angles that can be used to identify the material's crystal structure. For example, the XRD pattern of Fe_3O_4 typically displays several peaks corresponding to the (220), (311), (400), (422), (511), and (440) planes, among others. These peaks can be indexed to a face-centered cubic (FCC) crystal structure with lattice parameter a

= 8.397 Å. The most intense peak in the pattern is usually the (311) peak, which appears at around 2θ = 36.62°. Other notable peaks include the (400) peak at around 2θ = 42.49°.

Bentonite is a clay mineral typically exhibiting several X-ray diffraction (XRD) peaks in its XRD pattern. These peaks correspond to specific crystallographic planes within the mineral's crystal lattice. The XRD pattern of montmorillonite typically shows strong peaks at around 19.86°, 23.72°, and 27.77° 2θ angles. The specific 2θ angles and peak intensities can vary depending on factors such as the type of bentonite, the sample preparation, and the XRD instrument used.

The crystallite size of nanocomposite was calculated using the Scherrer equation:

$$D = \frac{k\lambda}{\beta cos\theta} \qquad \text{Equation 4-1}$$

where D is crystallite size in nm, k is Scherrer constant (0.9), λ is X-ray wavelength (0.15406 nm), β is full width at a half maximum (FWHM) in radians, θ is a peak position in radians. FWHM was determined from Origin Pro software and at the maximum peak position of 26.67, it equals to 0.174 rad. The crystallite size is about 46 nm which good corresponds to the measured NC size range using the SEM technique.

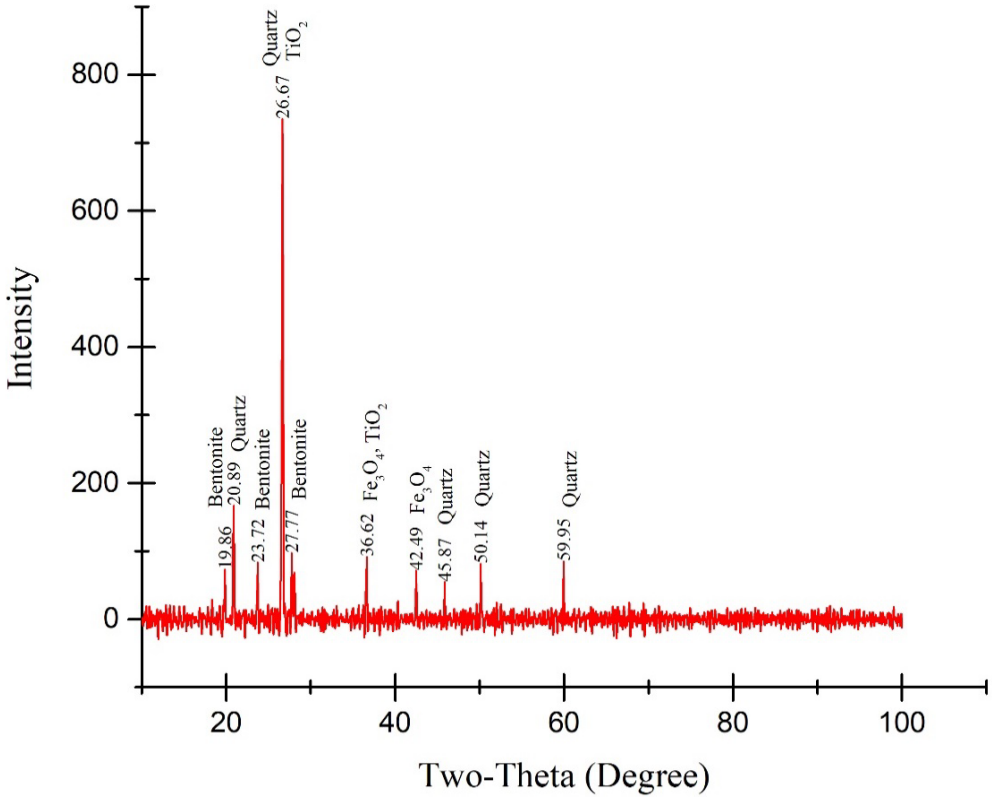

Figure 4-3. XRD of the Thiazine-Fe_3O_4-TiO_2-SiO_2-Bentonite NC

4.1.4 Fourier – transform infrared spectroscopy (FTIR)

FTIR analysis of NC was performed using Nicolet iS10 FT-IR Spectrometer. This analysis characterizes NC in terms of chemical bonds under infrared radiation in a wavelength range from 400 cm^{-1} to 4,000 cm^{-1} that is presented in Figure 4-4. IR radiation may cause atomic vibrations reflected in different peaks of transmission energy. 3,620 cm^{-1} peak is located in a single bond region with a frequency between 2,500 and 4,000 cm^{-1}, confirming the presence of hydrate and hydroxyl groups (OH) in the NC [146]. 1640 cm^{-1} peak refers to a double bond region from 1,500 cm^{-1} to 2,000 cm^{-1} frequency proving the existence of unsaturated bonds (C=C or C=O) or aromatic compounds [146]. The 1000 cm^{-1} peak corresponds to Si – O – Si stretching bond, while the 797 and 692 cm^{-1} frequency peaks refer to Si – O – Ti stretching and Al – O – Si stretching, respectively. Peaks at lowest frequencies 418 and 522 cm^{-1} correspond to the Ti – O stretching and Fe – O vibrations, respectively.

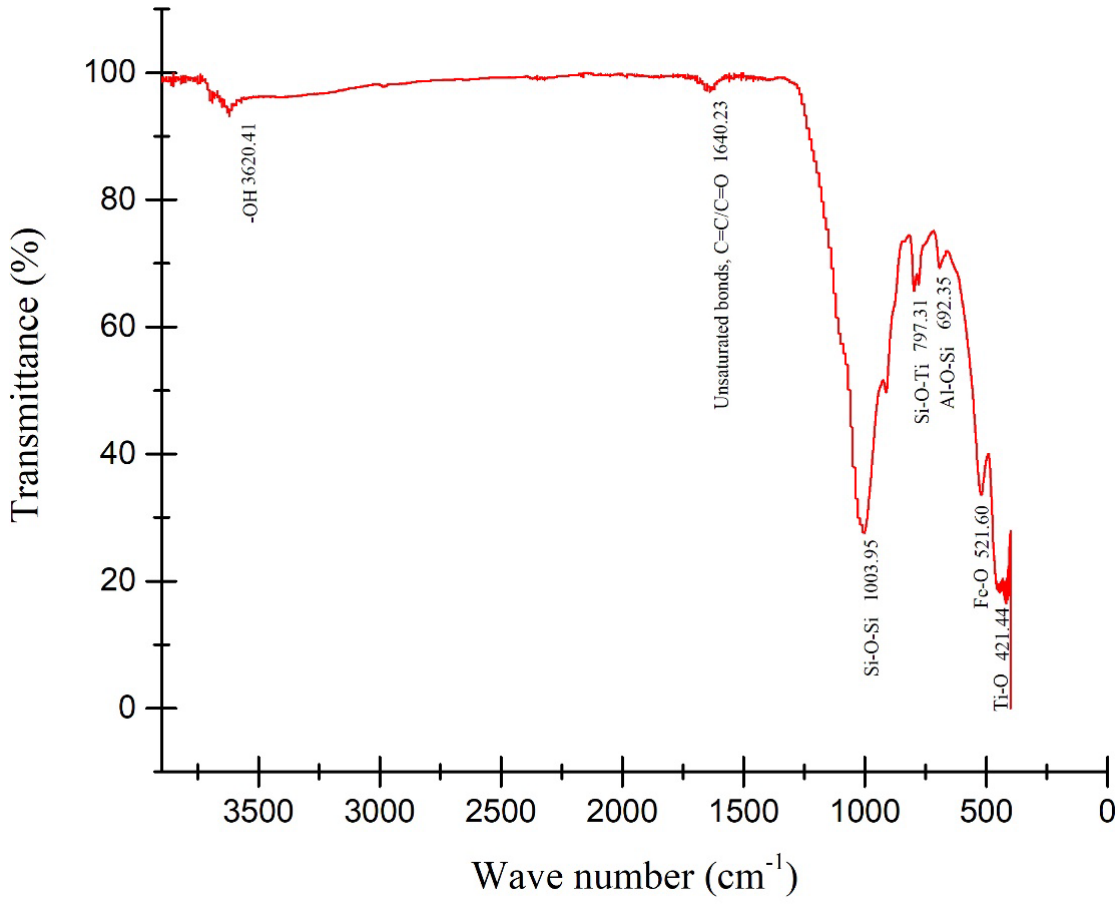

Figure 4-4. FTIR of the Thiazine-Fe_3O4-TiO_2-SiO_2-Bentonite NC

4.1.5 Thermogravimetric analysis (TGA)

TGA was performed using Simultaneous Thermal Analyzer (STA) 6000, which records the weight alteration with temperature increasing at a constant rate. It allows evaluation of the sample's thermal stability and volatile components' existence. The sample was heated from 30°C to 800°C at a constant rate of 10°C/min. Initially, 24 mg of the NC was taken for characterization. After heating the sample to 800°C, the mass of the sample decreased to 21.9 mg. Figure 4-5 represents the relation between mass loss and its derivative with temperature changes. From Figure 5, it can be seen that Thiazine-Fe_3O_4-TiO_2-SiO_2-Bentonite NC has three stages of weight loss. The first stage is between 30 and 195°C and refers to NC thermal dehydration. The sample's mass loss due to the water content reduction was 2.71%. The second stage was from 195°C to 490°C, corresponding to the thermal decomposition of organic material and decarboxylation, where the mass loss was 3.6% out of the total mass [147]. The first peak of the mass loss rate refers to evaporation of the volatile components; while, the second peak refers to the burning of non-volatile components of the NC [148]. Combustion of organic polymers and aromatic structures describes the third stage of NC mass loss at a temperature range between 490 and 800°C. During the heating of the sample from 30 to 800°C, the mass loss was only about 10%, indicating the new NC's high thermal stability.

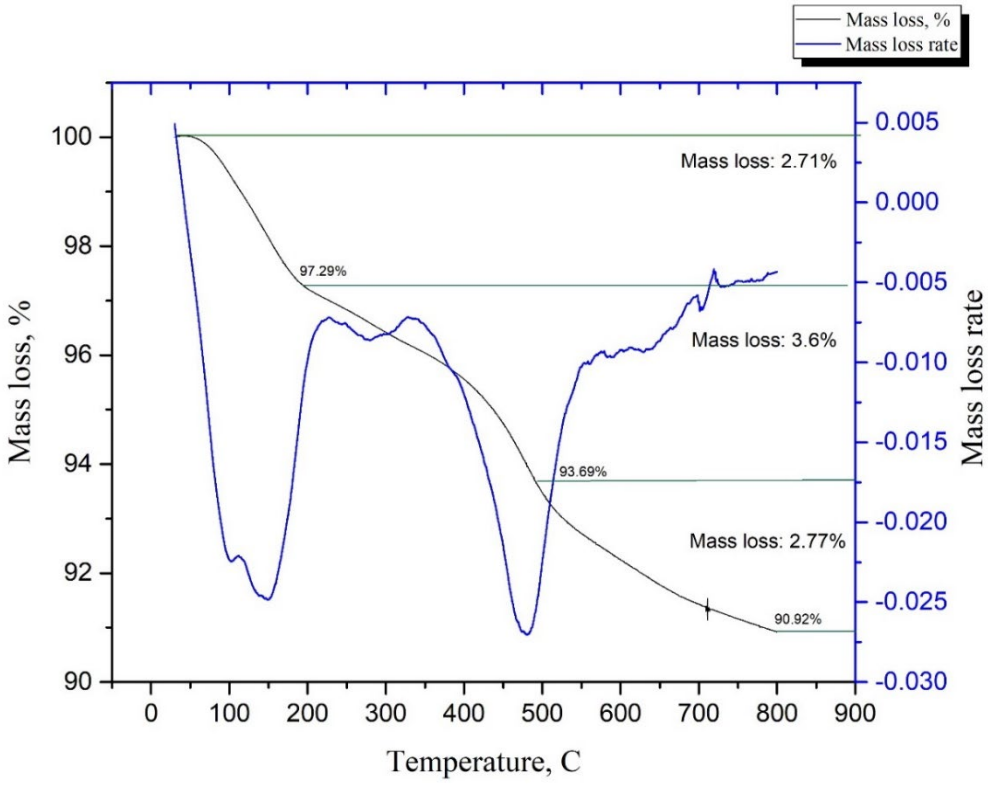

Figure 4-5. Thermogravimetric analysis of the Thiazine-Fe_3O_4-TiO_2-SiO_2-Bentonite NC

4.2 Evaluation of the efficiency of nanocomposite

4.2.1 Asphaltene onset point (AOP)

The asphaltene onset point was analyzed to assess the efficacy of the NC and establish the optimal concentration. Asphaltene onset point curves were compared in the absence and presence of the NC at a particular concentration, as illustrated in Figures 4-6, 4-7, 4-8, and 4-9. The absorbance value decreases as the concentration of asphaltene decreases with an increase in *n*-heptane volume in the mixture. As per the Beer-Lambert law, the absorbance is directly proportional to the concentration. Therefore, a deviation from the linear relationship indicates the onset of asphaltene precipitation. After this, the asphaltene absorbance value drops sharply in the solution, significantly reducing asphaltene concentration. Notably, a linear correlation between optical density and solution concentration was found when plotting the dependence of optical density values on asphaltene concentration. This outcome indicates that the Beer-Lambert law governs the system.

The black graph in Figure 4-6 depicts the solution without the NC. The precipitation of asphaltene commenced at a concentration of 40 vol% *n*-heptane, resulting in an abrupt reduction in optical density. Consequently, the validity of linear orientation was compromised. The absorption drop can be observed between 40 and 50 vol% *n*-heptane in the detailed view provided in Figure 4-6. Three midpoints were selected from the intervals above to precisely determine the deviation point and the exact percentage of *n*-heptane responsible for the onset of precipitation. These midpoints had precipitation contents of 42, 45, and 47 vol%, respectively. Thus, the asphaltene onset point in the absence of NC was determined to be 40% of the *n*-heptane volume serving as a reference point for evaluating the influence of NPs on asphaltene onset point. This signifies the point at which the synthetic oil containing 0.5 wt% asphaltene begins to solidify and enables the assessment of the potency of their inhibitory effect. The NC was added to the synthetic oil at 4 different weight percentages. Its impact on AOP was examined after establishing the onset point for the synthetic oil. Four different weight percentages of NPs, namely 0.1, 0.3, 0.4, and 0.5, were tested. In presence of the NC at each concentration, the deviation from the straight line occurred between 40 vol% and 50 vol%, similar to the condition without NPs. Several midpoints within the ranges where the deviation from a straight line occurred were selected to determine the exact starting point for each nanoparticle.

The results of calculating the asphaltene onset point (AOP) of synthetic oil in the presence of a NC at concentrations of 0.1 wt%, 0.3 wt%, 0.4 wt%, and 0.5 wt% are presented in Figures 4-6, 4-7, 4-8, and 4-9, respectively. As indicated in Figure 4-6, a concentration of 0.5 wt% had no significant effect on the AOP, which remained at 40 wt%, the same as in the absence of the NC. Decreasing the concentration from 0.5 wt% to 0.4 wt% increased the AOP from 40 to 45 wt%, as shown in Figure 4-7. However, there was no further increase in AOP when the concentration was decreased from 0.4 wt% to 0.3 wt%, as seen in Figure 4-8. The AOP for the 0.1 wt% concentration, as determined from Figure 4-9, was determined to be 40 wt%. The effect of the NC concentration on the AOP was not significant. Therefore, the maximum AOP was achieved with 0.3 wt% and 0.4 wt% of the NC. However, the optimum concentration of the NC for reaching the maximum AOP value was determined to be 0.3 wt% as this concentration required the minimum amount of NC.

Compared to synthetic oil, a reduction in absorbance was observed due to removing asphaltene from the system. This decrease in absorbance value can be attributed to the removal of asphaltene from the oil system and the subsequent formation of a bond between NC and asphaltene molecules, which delays the onset of precipitation. The elimination of asphaltene from a petroleum system occurs by adhering to the NC. Both types of NPs reduce the absorption capacity of synthetic oil. It is therefore suggested that asphaltene molecules should adsorb onto nanoparticle surfaces and be centrifuged out of the system to decrease the absorption capacity. This decline was observed both before and after the asphaltene onset point. Since the likelihood of asphaltene precipitation increases with increasing asphaltene content, reducing the number of asphaltene in the synthetic oil solution through the adsorption mechanism can be considered one of the primary factors in preventing asphaltene precipitation. Consequently, the number of asphaltene and the asphaltene onset point are inversely related.

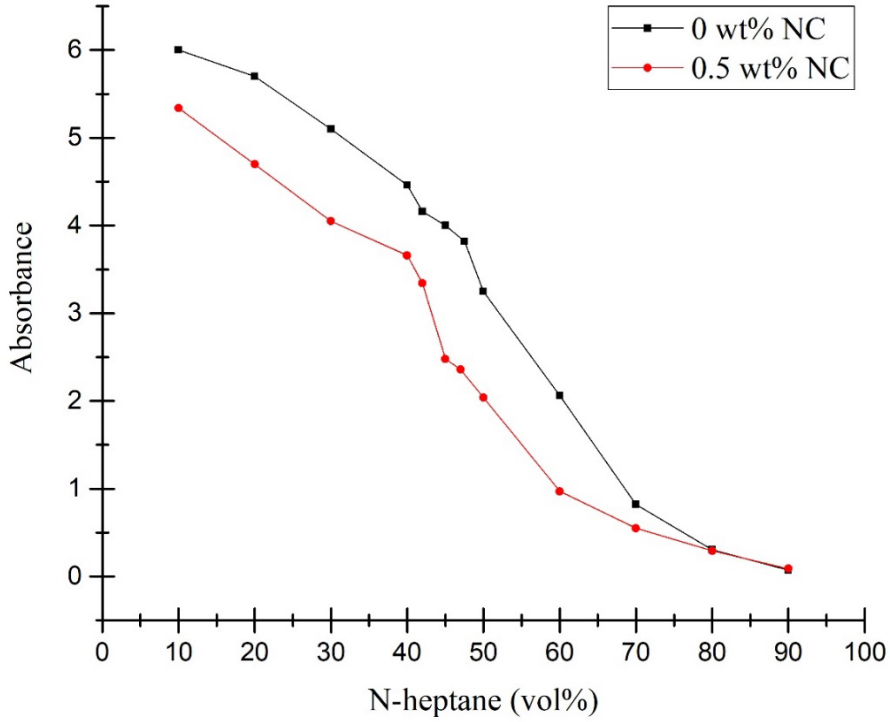

Figure 4-6. Asphaltene onset point determination in the presence of 0.5% of Thiazine-Fe_3O_4-TiO_2-SiO_2-Bentonite NC

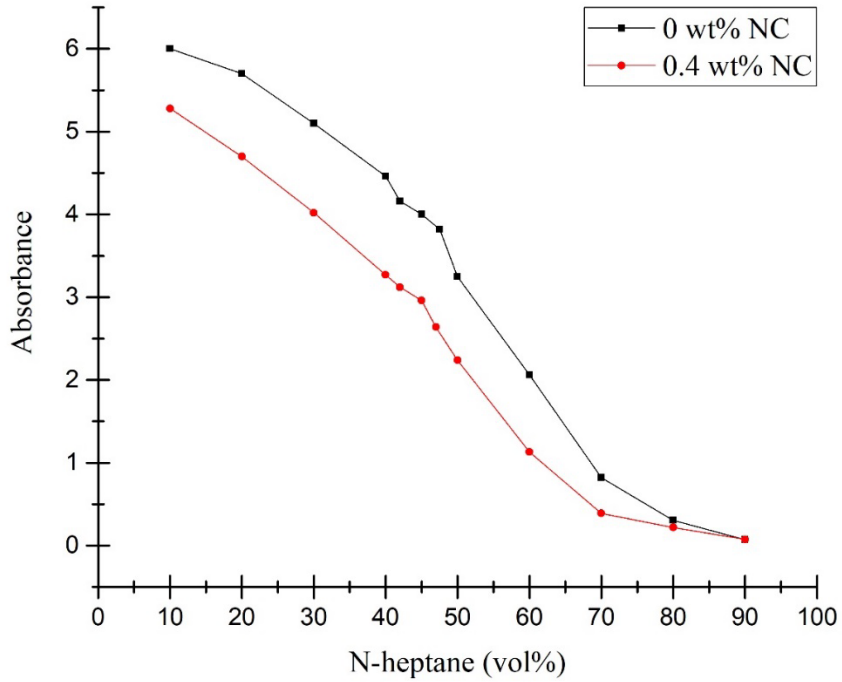

Figure 4-7. Asphaltene onset point determination in the presence of 0.4% of Thiazine-Fe_3O_4-TiO_2-SiO_2-Bentonite NC

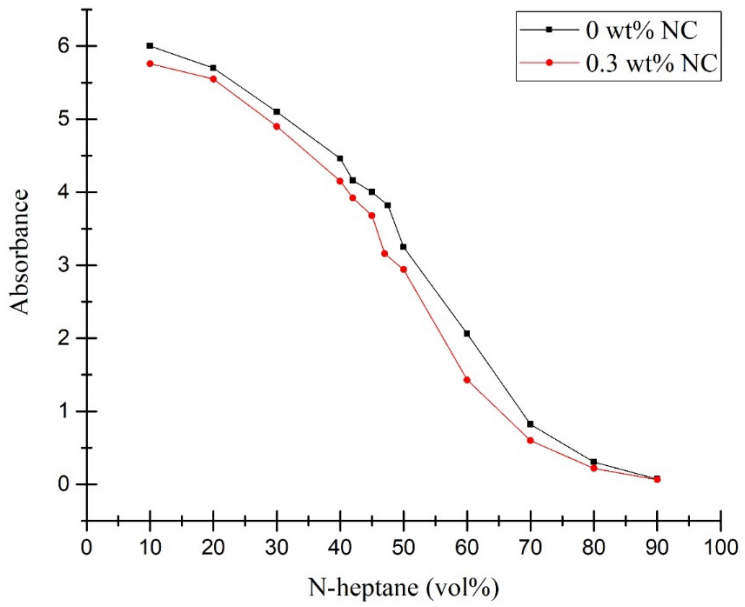

Figure 4-8. Asphaltene onset point determination in the presence of 0.3% of Thiazine-Fe_3O_4-TiO_2-SiO_2-Bentonite NC

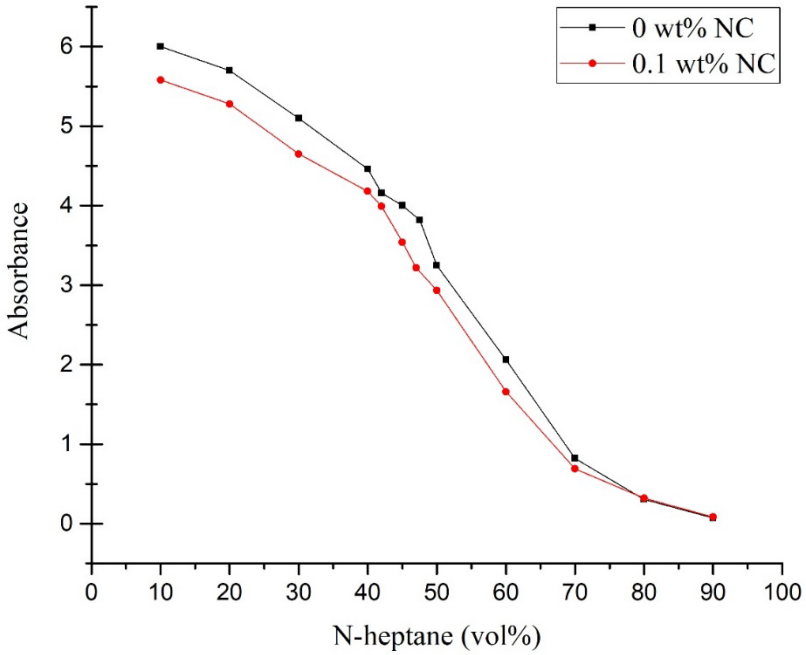

Figure 4-9. Asphaltene onset point determination in the presence of 0.1% of Thiazine-Fe_3O_4-TiO_2-SiO_2-Bentonite NC

4.2.2 TGA analysis

TGA (thermogravimetric analysis) was used to evaluate the catalytic impact of the NC on oxidation of asphaltene and asphaltene adsorption onto the surface of the NC. The method involved comparing the combustion behavior of pure asphaltene and asphaltene that was adsorbed onto the surface of a NC, as depicted by the mass loss profiles in Figure 4-10. The mass loss behavior of virgin asphaltene, which occurs in two stages, is presented in Figure 4-11. The first stage occurs between 350°C and 470°C and is attributed to the thermal degradation of aliphatic side chains. The second stage takes place above 470°C and a high-temperature mass loss peak is observed, which is associated with the degradation of polynuclear aromatic sheets [149]. At 800°C pure asphaltene lose their mass by 55% but are not fully burned, while asphaltene adsorbed onto the NC are burned fully at 550°C to 600°C as shown in Figure 4-10. Therefore, maximum weight loss temperature shifted from 800°C to 550°C. This shift in maximum weight loss temperature is attributed to the high adsorption of asphaltene on to the surfaces of the NC, which results in more asphaltene-accessible surface for burning. Consequently, it accelerates the asphaltene degradation/combustion process.

It can be seen from Figure 4-10 that the mass loss of pure nanocomposite was only about 10% due to the presence of sorbed moisture, impurities, and presence of organic materials. The data presented in Figure 4-12 depicts the variation of conversion factor as a function of temperature for different concentrations of synthetic oil, with the addition of 0.15 grams of NC. The conversion factor was calculated using Equation 4-2:

$$\alpha = \frac{m_0 - m_t}{m_0 - m_f} \qquad \text{Equation 4-2}$$

The catalytic effect of the NC on oxidation diminishes with an increase in the initial concentration of asphaltene in the model solution, resulting in a higher uptake until Q_{max} is achieved. In reactions performed under non-isothermal conditions using a catalyst, an increase in reactant mass is expected to lead to longer reaction times and higher temperatures. However, in solution-based reactions, the initial concentration is not an independent variable for fractional conversion, and therefore cannot be used to obtain reaction kinetics using the iso-conversational method [150]. Consequently, the conversion factor can only be used to compare the kinetics of condensed-phase reactions when the same initial and final masses are achieved. The best way to assess the kinetics of adsorbed species in condensed phases is through the mass reaction per unit area, as suggested by Abu Tarboush and Husein [83].

According to the results obtained from TGA analysis, the role of the NC in oxidation of asphaltene is to facilitate the process by means of surface exposure, rather than serving as catalysts. The efficacy of NC in oxidizing adsorbed asphaltene demonstrated an inverse correlation with their Q_{max} in mg/g. Specifically, greater asphaltene adsorption leads to reduced exposure to the air stream, which results in a slower oxidation rate [147].

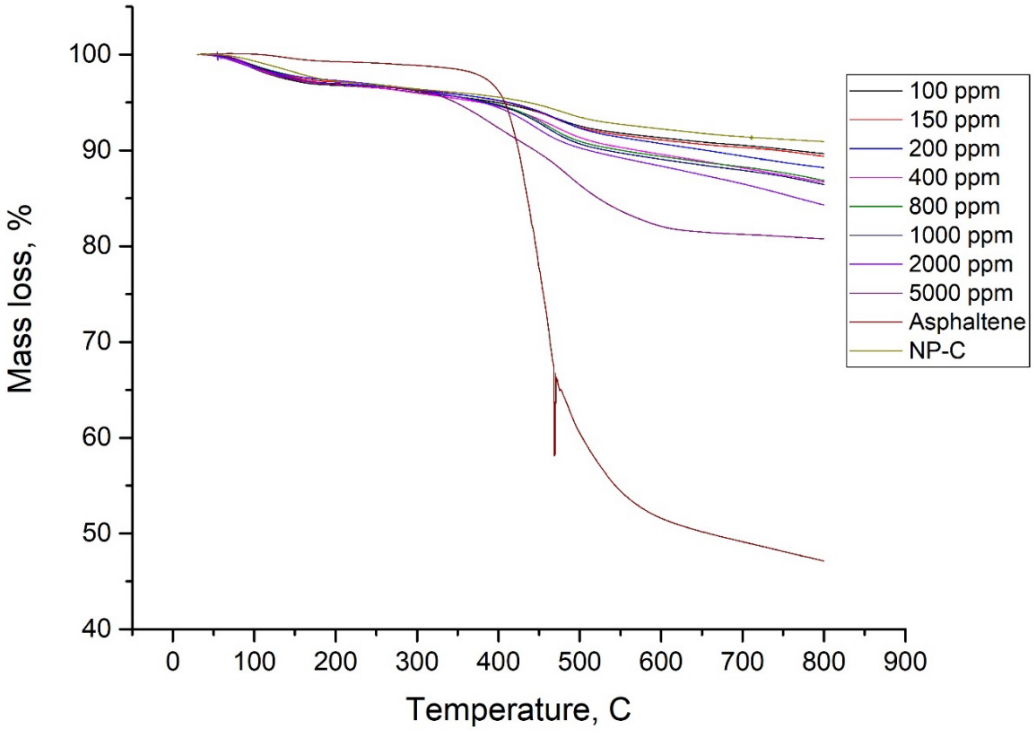

Figure 4-10. The mass loss of adsorbed asphaltene onto the Thiazine-Fe_3O_4-TiO_2-SiO_2-Bentonite NC

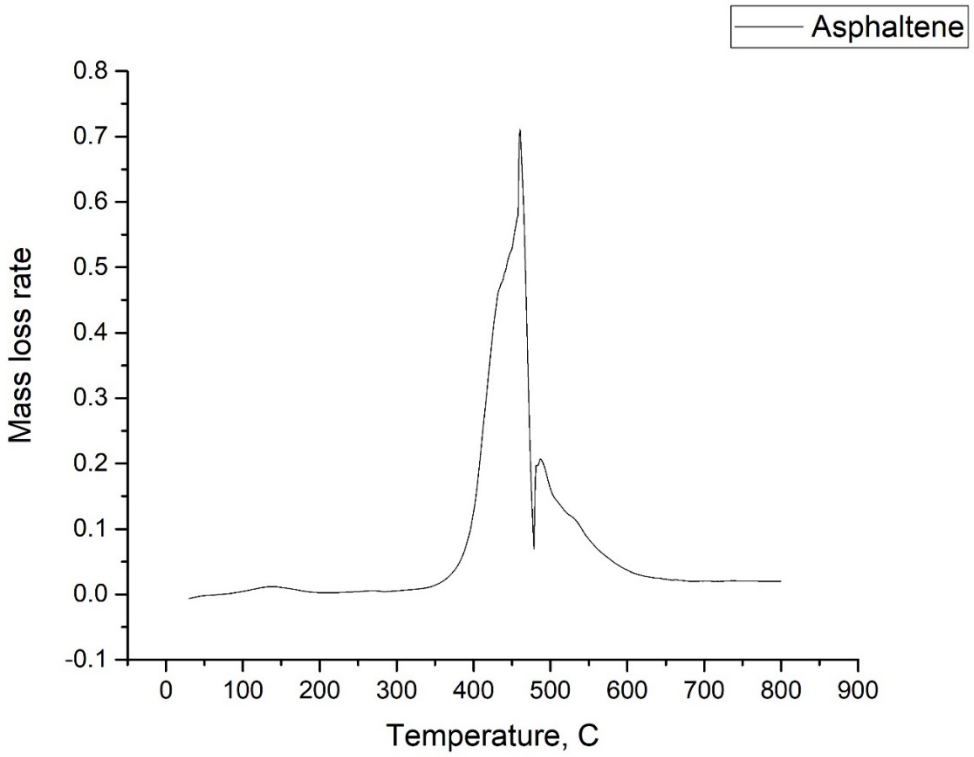

Figure 4-11. The mass loss rate of virgin asphaltene

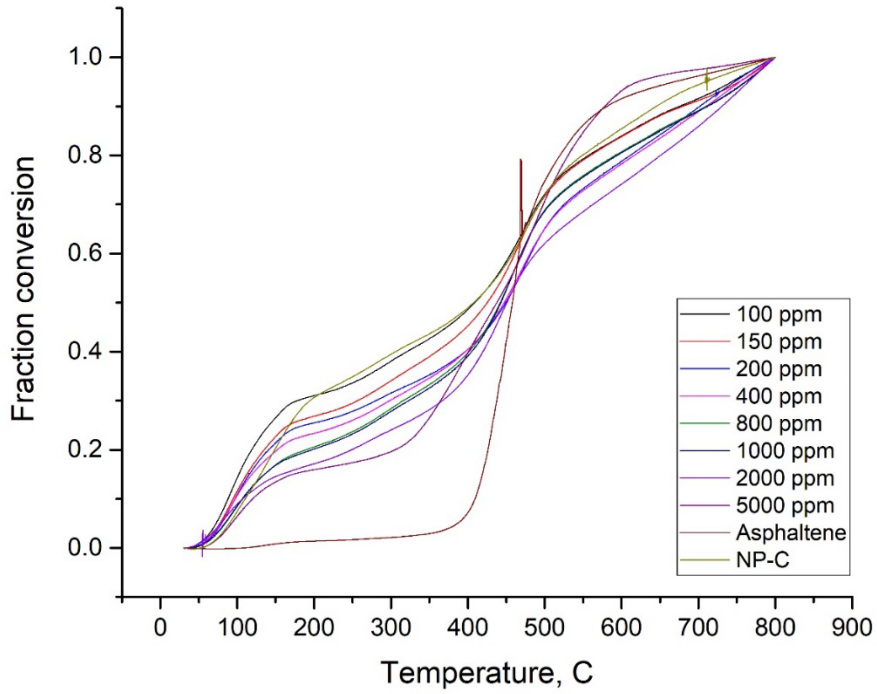

Figure 4-12. Fraction conversion of adsorbed asphaltene onto the Thiazine-Fe_3O_4-TiO_2-SiO_2-Bentonite NC

4.2.3 Asphaltene adsorption isotherms

Various concentrations of asphaltene solutions ranging from 100 to 5,000 ppm were used to prepare adsorption isotherms at a temperature of 25°C. The optimal concentration of the NC in the solution was determined to be 5,000 ppm. The relationship between the surface area of the NC and the amount of adsorbed asphaltene was demonstrated through the plot of Qe vs. Ce with the Langmuir fitting model, where Qe refers to the mass of asphaltene adsorbed on the surface of the NC and Ce is the equilibrium concentration. The adsorption isotherm, which shows asphaltene precipitation patterns, is produced by the relationship between Qe and Ce. A sharp increase in the amount of adsorbed asphaltene is observed at low equilibrium concentrations, and after a concentration of around 700 ppm, Qe stabilizes, indicating the behavior of asphaltene following the Langmuir monolayer model of asphaltene adsorption. The amount of adsorbate (Qe) was calculated using Equation 4-3 below:

$$Q_e = \frac{M(C_0 - C_e)}{mA} \qquad \text{Equation 4-3}$$

where M is a mass of asphaltene in mg, C_0 is the initial concentration of asphaltene in the model solution in ppm, Ce is the equilibrium concentration of supernatant in ppm, m is the mass of NC in g, A is the surface area of NC in m^2/g.

The experimental data were analyzed to fit both the Langmuir and Freundlich models of adsorption isotherms. The Freundlich and Langmuir models are presented in Equations 2-4 and 2-2, respectively. The linearized Freundlich and Langmuir models are represented in Equations 2-5 and 2-3, respectively. The linear Langmuir fitting model with experimental data and the coefficient of determination $R^2 = 0.999$ is shown in Figure 4-14; while, the Freundlich fitting model with experimental data is shown in Figure 4-15, where $R^2 = 0.84$. Both models exhibit high values of R^2.

Table 4-1. Langmuir and Freundlich parameters

Langmuir model			Freundlich model		
K_L (kg/mg)	Q_{max} (mg/m^2)	R^2	K_F ($(mg/m^2)(L/mg)^{1/n}$)	n	R^2
0.0028	0.75	0.99	0.38	1.03	0.84

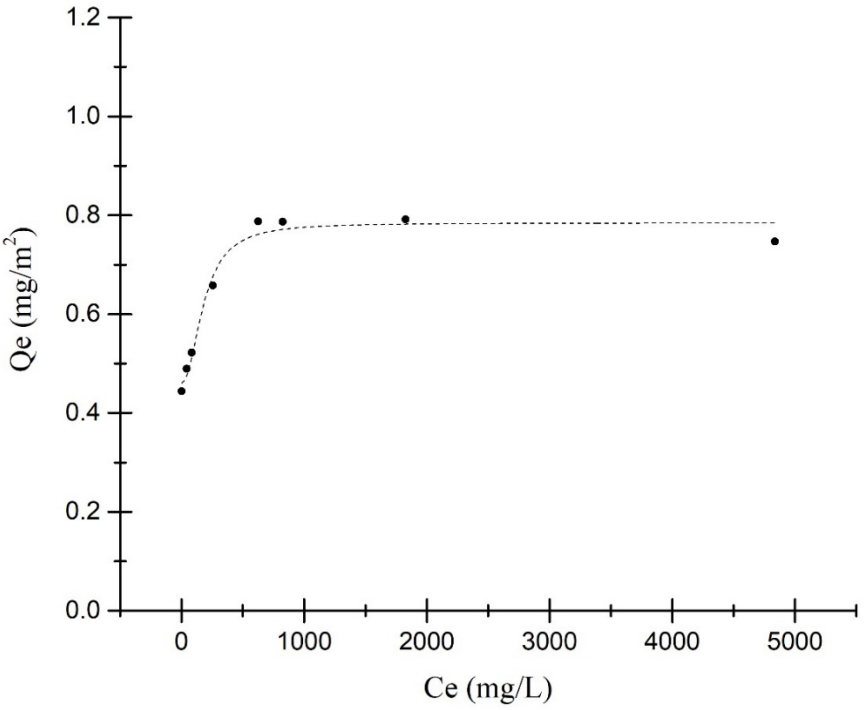

Figure 4-13. Asphaltene adsorption isotherm onto Thiazine-Fe_3O_4-TiO_2-SiO_2-Bentonite NC. The dots represent experimental data; the dashed line represents the Langmuir model.

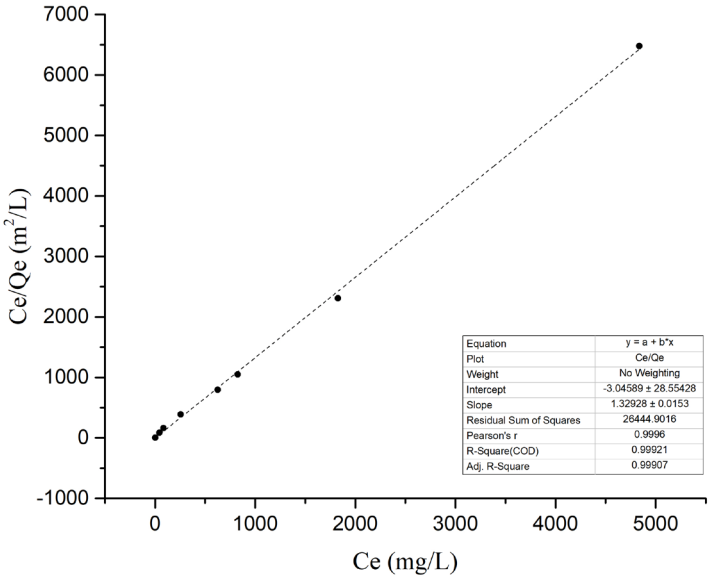

Figure 4-14. Langmuir model of asphaltene adsorption isotherm onto Thiazine-Fe_3O_4-TiO_2-SiO_2-Bentonite NC. The dots represent experimental data; the dashed line represents the Langmuir model's linear fitting.

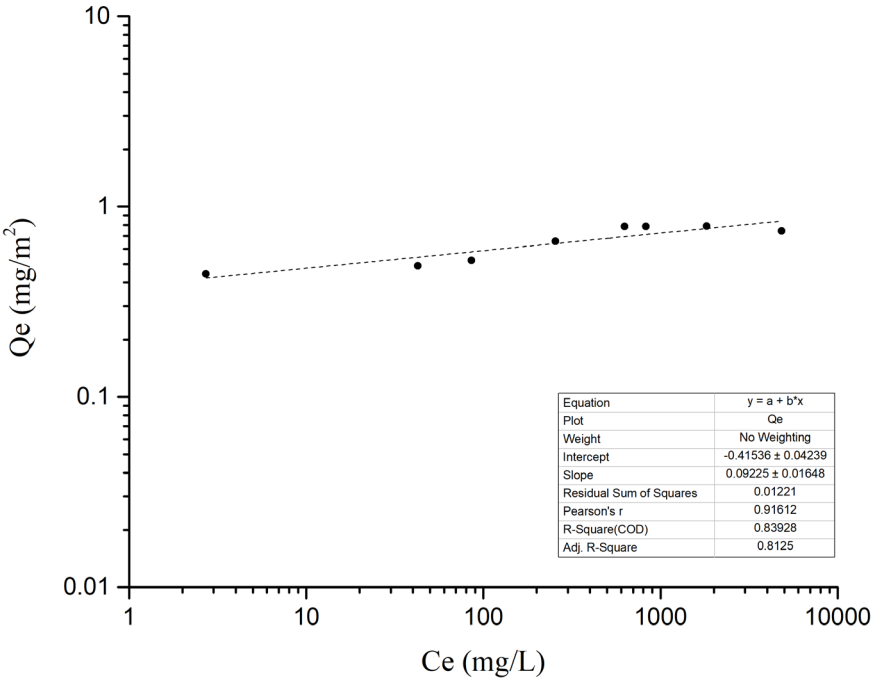

Figure 4-15. Freundlich model of asphaltene adsorption isotherm onto Thiazine-Fe_3O_4-TiO_2-SiO_2-Bentonite NC. The dots represent experimental data; the dashed line represents the Freundlich model's linear fitting.

5 CONCLUSIONS AND RECOMMENDATIONS

The main objective of this research work was to assess how a newly synthesized sophisticated NC (Thiazine-Fe_3O_4-SiO_2-TiO_2-Bentonite) performs as an asphaltene precipitation inhibitor. For this purpose, several techniques such as SEM, EDX, BET, XRD, FTIR, and TGA were used to first characterize the NC, to determine its surface area, morphology, particle size and distribution, elemental composition, functional groups, structure, and catalytic impact of the NC on oxidation of asphaltene and asphaltene adsorption onto the NC. Based on the findings of the current research work, the following 4 major conclusions can be drawn:

1. The NC's morphology is rough and non-uniform. Oxygen and Silicon are the main elements that compose NC in 55.1 and 18.9 wt% respectively obtained from the EDAX. The size of NC determined from SEM is in between 38-74 nm. Crystal size 46 nm was calculated from the XRD analysis, showing good matching with SEM results. The interpretation of the XRD data shows that quartz dominates in NC composition.
2. The asphaltene was adsorbed onto the surface of the NC, which significantly postponed the asphaltene onset point in a 0.5 wt% synthetic oil. The optimal NC concentration for postponing the AOP was determined as 0.3 wt%.
3. Experimental adsorption isotherms fitted well to the Langmuir adsorption isotherm with the determination coefficient of 99% rather than to the Freundlich model with the 83.92% coefficient of determination suggesting a monolayer asphaltene adsorption.
4. The absence of NPs during the oxidation of asphaltene resulted in two distinct regions indicating the oxidation of different carbon types in the system. However, the presence of NC caused a significant reduction in the oxidation temperature. When Thiazine-Fe_3O_4-SiO_2-TiO_2-Bentonite NC was added, it significantly lowered the temperature at which asphaltene oxidizes proving that the novel NC has a catalytic effect.

This research work demonstrated great potential of the novel Thiazine-Fe_3O_4-TiO_2-SiO_2-Bentonite NC as a new asphaltene precipitation agent. Overall, the results showed that the novel NC performed well under laboratory conditions and prevented asphaltene precipitation effectively. These findings demonstrate that the novel NC can help to control asphaltene precipitation effectively. However, further investigation on performance assessment of the NC under reservoir conditions is recommended.

REFERENCES

[1] Z. Hongjun, J. Jiaqiang, L. Qingping, Y. Xichong, and C. Junwen, "Simulations of Asphaltene Deposition in Submarine Pipelines by CFD," in *All Days*, SPE, Jun. 2010. doi: 10.2118/130949-MS.

[2] M. Z. Hasanvand, M. A. Ahmadi, and R. M. Behbahani, "Solving asphaltene precipitation issue in vertical wells via redesigning of production facilities," *Petroleum*, vol. 1, no. 2, pp. 139–145, Jun. 2015, doi: 10.1016/j.petlm.2015.07.002.

[3] N. D. McMullen, "Flow-Assurance Field Solutions (Keynote)," in *Offshore Technology Conference*, Offshore Technology Conference, Apr. 2006. doi: 10.4043/18381-MS.

[4] T. M. Vargas Francisco M., *Asphaltene Deposition Fundamentals, Prediction, Prevention, and Remediation*, 1st ed. Boca Raton, 2018.

[5] A. Hammami and J. Ratulowski, "Precipitation and Deposition of Asphaltenes in Production Systems: A Flow Assurance Overview," in *Asphaltenes, Heavy Oils, and Petroleomics*, O. C. Mullins, E. Y. Sheu, A. Hammami, and A. G. Marshall, Eds., New York, NY: Springer New York, 2007, pp. 617–660. doi: 10.1007/0-387-68903-6_23.

[6] K. Gharbi, K. Benyounes, and M. Khodja, "Removal and prevention of asphaltene deposition during oil production: A literature review," *J Pet Sci Eng*, vol. 158, pp. 351–360, Sep. 2017, doi: 10.1016/j.petrol.2017.08.062.

[7] P. Chunsheng, S. Daohan, Z. Shushan, X. Hongxing, and S. Hua'nan, "Foundation item: National High-tech R&D Program of China," 2007.

[8] R. Rezaei Dehshibi, A. Mohebbi, M. Riazi, and M. Niakousari, "Experimental investigation on the effect of ultrasonic waves on reducing asphaltene deposition and improving oil recovery under temperature control," *Ultrason Sonochem*, vol. 45, pp. 204–212, Jul. 2018, doi: 10.1016/j.ultsonch.2018.03.023.

[9] X. Sun, Y. Zhang, G. Chen, and Z. Gai, "Application of Nanoparticles in Enhanced Oil Recovery: A Critical Review of Recent Progress," *Energies (Basel)*, vol. 10, no. 3, p. 345, Mar. 2017, doi: 10.3390/en10030345.

[10] C. A. Franco, N. N. Nassar, M. A. Ruiz, P. Pereira-Almao, and F. B. Cortés, "Nanoparticles for Inhibition of Asphaltenes Damage: Adsorption Study and Displacement Test on Porous Media," *Energy & Fuels*, vol. 27, no. 6, pp. 2899–2907, Jun. 2013, doi: 10.1021/ef4000825.

[11] N. N. Shayan and B. Mirzayi, “Adsorption and Removal of Asphaltene Using Synthesized Maghemite and Hematite Nanoparticles,” *Energy & Fuels*, vol. 29, no. 3, pp. 1397–1406, Mar. 2015, doi: 10.1021/ef502494d.

[12] N. N. Nassar, “Asphaltene Adsorption onto Alumina Nanoparticles: Kinetics and Thermodynamic Studies,” *Energy & Fuels*, vol. 24, no. 8, pp. 4116–4122, Aug. 2010, doi: 10.1021/ef100458g.

[13] N. N. Nassar, A. Hassan, and P. Pereira-Almao, “Comparative oxidation of adsorbed asphaltenes onto transition metal oxide nanoparticles,” *Colloids Surf A Physicochem Eng Asp*, vol. 384, no. 1–3, pp. 145–149, Jul. 2011, doi: 10.1016/j.colsurfa.2011.03.049.

[14] U.S. Energy Information Administration Office of Energy Analysis U.S. Department of Energy Washington, “International Energy Outlook,” 2019.

[15] Hussein Alboudwarej *et al.*, “Highlighting Heavy Oil,” *Oilfield Review*, pp. 34–53, 2006.

[16] K. Akbarzadeh *et al.*, “Asphaltenes - problematic but rich in potential,” *Oilfield Review*, vol. 19, pp. 22–43, Jun. 2007.

[17] K. J. Leontaritis, “The Asphaltene and Wax Deposition Envelopes,” *Fuel Science and Technology International*, vol. 14, no. 1–2, pp. 13–39, Jan. 1996, doi: 10.1080/08843759608947560.

[18] A. Alhosani and N. Daraboina, “Effect of multi-phase flow on asphaltene deposition: Field case application of integrated simulator,” *J Pet Sci Eng*, vol. 206, p. 108972, Nov. 2021, doi: 10.1016/j.petrol.2021.108972.

[19] J. G. Speight, “Petroleum Asphaltenes - Part 1: Asphaltenes, Resins and the Structure of Petroleum,” *Oil & Gas Science and Technology*, vol. 59, no. 5, pp. 467–477, Sep. 2004, doi: 10.2516/ogst:2004032.

[20] F. Zheng, Q. Shi, G. S. Vallverdu, P. Giusti, and B. Bouyssiere, “Fractionation and Characterization of Petroleum Asphaltene: Focus on Metalopetroleomics,” *Processes*, vol. 8, no. 11, p. 1504, Nov. 2020, doi: 10.3390/pr8111504.

[21] E. Rogel, T. Miao, J. Vien, and M. Roye, “Comparing asphaltenes: Deposit versus crude oil,” *Fuel*, vol. 147, pp. 155–160, May 2015, doi: 10.1016/j.fuel.2015.01.045.

[22] K. Indo, J. Ratulowski, B. Dindoruk, J. Gao, J. Zuo, and O. C. Mullins, “Asphaltene Nanoaggregates Measured in a Live Crude Oil by Centrifugation,” *Energy & Fuels*, vol. 23, no. 9, pp. 4460–4469, Sep. 2009, doi: 10.1021/ef900369r.

[23] D. Molina V., E. Ariza, and J. C. Poveda, “Structural Differences among the Asphaltenes in Colombian Light Crudes from the Colorado Oil Field,” *Energy & Fuels*, vol. 31, no. 1, pp. 133–139, Jan. 2017, doi: 10.1021/acs.energyfuels.6b01887.

[24] H. W. Yarranton, “Asphaltene Self-Association,” *J Dispers Sci Technol*, vol. 26, no. 1, pp. 5–8, Jan. 2005, doi: 10.1081/DIS-200040234.

[25] D. M. Sztukowski, “ Asphaltene and solids-stabilized water-in-oil emulsions,” University of Calgary, Canada, 2005.

[26] O. P. Strausz, T. W. Mojelsky, and E. M. Lown, “The molecular structure of asphaltene: an unfolding story,” *Fuel*, vol. 71, no. 12, pp. 1355–1363, Dec. 1992, doi: 10.1016/0016-2361(92)90206-4.

[27] T. Fu. Yen, J. G. Erdman, and S. S. Pollack, “Investigation of the Structure of Petroleum Asphaltenes by X-Ray Diffraction,” *Anal Chem*, vol. 33, no. 11, pp. 1587–1594, Oct. 1961, doi: 10.1021/ac60179a039.

[28] M. L. Chacón-Patiño, S. M. Rowland, and R. P. Rodgers, “Advances in Asphaltene Petroleomics. Part 1: Asphaltenes Are Composed of Abundant Island and Archipelago Structural Motifs,” *Energy & Fuels*, vol. 31, no. 12, pp. 13509–13518, Dec. 2017, doi: 10.1021/acs.energyfuels.7b02873.

[29] V. G. Santos *et al.*, “Fullerenes in asphaltenes and other carbonaceous materials: natural constituents or laser artifacts,” *Analyst*, vol. 141, no. 9, pp. 2767–2773, 2016, doi: 10.1039/C5AN02333E.

[30] K. J. Leontaritis and G. Ali Mansoori, “Asphaltene deposition: a survey of field experiences and research approaches,” *J Pet Sci Eng*, vol. 1, no. 3, pp. 229–239, Aug. 1988, doi: 10.1016/0920-4105(88)90013-7.

[31] S. Ashoori, M. Sharifi, M. Masoumi, and M. Mohammad Salehi, “The relationship between SARA fractions and crude oil stability,” *Egyptian Journal of Petroleum*, vol. 26, no. 1, pp. 209–213, Mar. 2017, doi: 10.1016/j.ejpe.2016.04.002.

[32] M. R. Gray, R. R. Tykwinski, J. M. Stryker, and X. Tan, “Supramolecular Assembly Model for Aggregation of Petroleum Asphaltenes,” *Energy & Fuels*, vol. 25, no. 7, pp. 3125–3134, Jul. 2011, doi: 10.1021/ef200654p.

[33] O. C. Mullins, “The Modified Yen Model,” *Energy & Fuels*, vol. 24, no. 4, pp. 2179–2207, Apr. 2010, doi: 10.1021/ef900975e.

[34] M. H. Schneider, A. B. Andrews, S. Mitra-Kirtley, and O. C. Mullins, “Asphaltene Molecular Size by Fluorescence Correlation Spectroscopy,” *Energy & Fuels*, vol. 21, no. 5, pp. 2875–2882, Sep. 2007, doi: 10.1021/ef700216r.

[35] G. Javanbakht, M. Sedghi, W. R. W. Welch, L. Goual, and M. P. Hoepfner, “Molecular polydispersity improves prediction of asphaltene aggregation,” *J Mol Liq*, vol. 256, pp. 382–394, Apr. 2018, doi: 10.1016/j.molliq.2018.02.051.

[36] M. H. Khalaf and G. A. Mansoori, “A new insight into asphaltenes aggregation onset at molecular level in crude oil (an MD simulation study),” *J Pet Sci Eng*, vol. 162, pp. 244–250, Mar. 2018, doi: 10.1016/j.petrol.2017.12.045.

[37] Z. Rashid, C. D. Wilfred, N. Gnanasundaram, A. Arunagiri, and T. Murugesan, “A comprehensive review on the recent advances on the petroleum asphaltene aggregation,” *J Pet Sci Eng*, vol. 176, pp. 249–268, May 2019, doi: 10.1016/j.petrol.2019.01.004.

[38] K. A. Ferworn, “Thermodynamic and kinetic modelling of asphaltene precipitation from heavy oils and bitumens,” University of Calgary, Calgary, 1995.

[39] A. Hammami, D. Chang-Yen, J. A. Nighswander, and E. Stange, “AN EXPERIMENTAL STUDY OF THE EFFECT OF PARAFFINIC SOLVENTS ON THE ONSET AND BULK PRECIPITATION OF ASPHALTENES,” *Fuel Science and Technology International*, vol. 13, no. 9, pp. 1167–1184, Sep. 1995, doi: 10.1080/08843759508947730.

[40] A. B. Demir, “Effect of clay and salinity on asphaltene stability ,” West Virginia University, 2016.

[41] L. Loeber, G. Muller, J. Morel, and O. Sutton, “Bitumen in colloid science: a chemical, structural and rheological approach,” *Fuel*, vol. 77, no. 13, pp. 1443–1450, Oct. 1998, doi: 10.1016/S0016-2361(98)00054-4.

[42] S. L. Kokal and S. G. Sayegh, “Asphaltenes: The Cholesterol Of Petroleum,” in *All Days*, SPE, Mar. 1995. doi: 10.2118/29787-MS.

[43] N. B. Joshi, O. C. Mullins, A. Jamaluddin, J. Creek, and J. McFadden, “Asphaltene Precipitation from Live Crude Oil,” *Energy & Fuels*, vol. 15, no. 4, pp. 979–986, Jul. 2001, doi: 10.1021/ef0100471.

[44] C. E. Haskett and M. Tartera, “A Practical Solution to the Problem of Asphaltene Deposits-Hassi Messaoud Field, Algeria,” *Journal of Petroleum Technology*, vol. 17, no. 04, pp. 387–391, Apr. 1965, doi: 10.2118/994-PA.

[45] T. Maqbool, “ Understanding the Kinetics of Asphaltene Precipitation from Crude Oils,” University of Michigan, 2011.

[46] A. Hammami, C. H. Phelps, T. Monger-McClure, and T. M. Little, “Asphaltene Precipitation from Live Oils: An Experimental Investigation of Onset Conditions and Reversibility,” *Energy & Fuels*, vol. 14, no. 1, pp. 14–18, Jan. 2000, doi: 10.1021/ef990104z.

[47] S. Iar Andersen, “HYSTERESIS IN PRECIPTIATION AND DISSOLUTION OF PETROLEUM ASPHALTENES.,” *Fuel Science and Technology International*, vol. 10, no. 10, pp. 1743–1749, Jan. 1992, doi: 10.1080/08843759208905371.

[48] P. F. Clarke and B. B. Pruden, “Heat Transfer Analysis For Detection of Asphaltene Precipitation And Resuspension,” in *Annual Technical Meeting*, Petroleum Society of Canada, Apr. 1996. doi: 10.2118/96-112.

[49] R. S. Mohamed, W. Loh, A. C. S. Ramos, C. C. Delgado, and V. R. Almeida, “REVERSIBILITY AND INHIBITION OF ASPHALTENE PRECIPITATION IN BRAZILIAN CRUDE OILS,” *Pet Sci Technol*, vol. 17, no. 7–8, pp. 877–896, Aug. 1999, doi: 10.1080/10916469908949754.

[50] S. Lal, U. Jana, P. K. Manna, G. P. Mohanta, R. Manavalan, and S. L. Pal, “Nanoparticle: An overview of preparation and characterization,” *J Appl Pharm Sci*, vol. 2011, no. 06, pp. 228–234.

[51] S. Khan and M. K. Hossain, “Classification and properties of nanoparticles,” in *Nanoparticle-Based Polymer Composites*, Elsevier, 2022, pp. 15–54. doi: 10.1016/B978-0-12-824272-8.00009-9.

[52] S. Khan *et al.*, “A review on nanotechnology: Properties, applications, and mechanistic insights of cellular uptake mechanisms,” *Journal of Molecular Liquids*, vol. 348. Elsevier B.V., Feb. 15, 2022. doi: 10.1016/j.molliq.2021.118008.

[53] B. J. Stephen, S. Suchanti, R. Mishra, and A. Singh, “Cancer Nanotechnology in Medicine: A Promising Approach for Cancer Detection and Diagnosis,” *Crit Rev Ther Drug Carrier Syst*, vol. 37, no. 4, pp. 375–405, 2020, doi: 10.1615/CritRevTherDrugCarrierSyst.2020032634.

[54] Z. Lin, C. Zhi, and L. Qu, “ Nano Research Energy : An interdisciplinary journal centered on nanomaterials and nanotechnology for energy ,” *Nano Research Energy*, vol. 1, p. e9120005, Jun. 2022, doi: 10.26599/nre.2022.9120005.

[55] G. Ali Mansoori, T. R. Bastami, A. Ahmadpour, and Z. Eshaghi, “ENVIRONMENTAL APPLICATION OF NANOTECHNOLOGY,” 2008, pp. 439–493. doi: 10.1142/9789812790248_0010.

[56] P. I. Dolez, “Nanomaterials Definitions, Classifications, and Applications,” in *Nanoengineering: Global Approaches to Health and Safety Issues*, Elsevier, 2015, pp. 3–40. doi: 10.1016/B978-0-444-62747-6.00001-4.

[57] M. G. Lines, “Nanomaterials for practical functional uses,” *J Alloys Compd*, vol. 449, no. 1–2, pp. 242–245, Jan. 2008, doi: 10.1016/j.jallcom.2006.02.082.

[58] M. T. Rahman, M. Asadul Hoque, G. T. Rahman, M. A. Gafur, R. A. Khan, and M. K. Hossain, “Study on the mechanical, electrical and optical properties of metal-oxide nanoparticles dispersed unsaturated polyester resin nanocomposites,” *Results Phys*, vol. 13, Jun. 2019, doi: 10.1016/j.rinp.2019.102264.

[59] U. Farooq, A. Patil, B. Panjwani, and G. Simonsen, “Review on Application of Nanotechnology for Asphaltene Adsorption, Crude Oil Demulsification, and Produced Water Treatment,” *Energy & Fuels*, vol. 35, no. 23, pp. 19191–19210, Dec. 2021, doi: 10.1021/acs.energyfuels.1c01990.

[60] M.-A. Ahmadi, Z. Ahmad, L. T. K. Phung, T. Kashiwao, and A. Bahadori, “Evaluation of the ability of the hydrophobic nanoparticles of SiO_2 in the EOR process through carbonate rock samples,” *Pet Sci Technol*, vol. 34, no. 11–12, pp. 1048–1054, Jun. 2016, doi: 10.1080/10916466.2016.1148052.

[61] S. I. Ali, S. M. Lalji, J. Haneef, U. Ahsan, M. A. Khan, and N. Yousaf, “Estimation of asphaltene adsorption on MgO nanoparticles using ensemble learning,” *Chemometrics and Intelligent Laboratory Systems*, vol. 208, Jan. 2021, doi: 10.1016/j.chemolab.2020.104220.

[62] I. Nowrouzi, A. Khaksar Manshad, and A. H. Mohammadi, “Effects of TiO2, MgO and γ-Al2O3 nano-particles on wettability alteration and oil production under carbonated nano-fluid imbibition in carbonate oil reservoirs,” *Fuel*, vol. 259, Jan. 2020, doi: 10.1016/j.fuel.2019.116110.

[63] M. Mohammadi, M. Dadvar, and B. Dabir, “TiO2/SiO2 nanofluids as novel inhibitors for the stability of asphaltene particles in crude oil: Mechanistic understanding, screening, modeling, and optimization,” *J Mol Liq*, vol. 238, pp. 326–340, Jul. 2017, doi: 10.1016/j.molliq.2017.05.014.

[64] N. N. Nassar, A. Hassan, and G. Vitale, “Comparing kinetics and mechanism of adsorption and thermo-oxidative decomposition of Athabasca asphaltenes onto TiO2, ZrO2, and CeO2 nanoparticles,” *Appl Catal A Gen*, vol. 484, pp. 161–171, Aug. 2014, doi: 10.1016/j.apcata.2014.07.017.

[65] F. Mahmoudi Alemi, S. A. Mousavi Dehghani, A. Rashidi, N. Hosseinpour, and S. Mohammadi, “Potential Application of Fe2O3and Functionalized SiO2Nanoparticles for Inhibiting Asphaltene Precipitation in Live Oil at Reservoir Conditions,” *Energy and Fuels*, vol. 35, no. 7, pp. 5908–5924, Apr. 2021, doi: 10.1021/acs.energyfuels.1c00060.

[66] M. Razavifar and J. Qajar, “Synergistic effects of ultrasonic irradiation and α-Fe2O3 nanoparticles on the viscosity and thermal properties of an asphaltenic crude oil and their application to in-situ combustion EOR,” *Ultrasonics*, vol. 120, Mar. 2022, doi: 10.1016/j.ultras.2021.106655.

[67] E. I. Mikhienkova, S. V. Lysakov, A. L. Neverov, V. A. Zhigarev, A. V. Minakov, and V. Y. Rudyak, “Experimental study on the influence of nanoparticles on oil-based drilling fluid properties,” *J Pet Sci Eng*, vol. 208, Jan. 2022, doi: 10.1016/j.petrol.2021.109452.

[68] F. Farahbod, “Experimental investigation of thermo-physical properties of drilling fluid integrated with nanoparticles: Improvement of drilling operation performance,” *Powder Technol*, vol. 384, pp. 125–131, May 2021, doi: 10.1016/j.powtec.2021.02.002.

[69] S. Kumar and J. Foroozesh, “Application of nanotechnology in hydrocarbon reservoir exploration and characterization,” in *Emerging Nanotechnologies for Renewable Energy*, Elsevier, 2021, pp. 115–134. doi: 10.1016/B978-0-12-821346-9.00015-8.

[70] S. Murugesan, R. Suresh, D. Agrawal, Q. Darugar, V. Khabashesku, and B. Hughes, "IPTC-19600-MS Unconventional Nanotechnology-Based Tracers for Drilling and Completion Applications," 2020. [Online]. Available: http://onepetro.org/IPTCONF/proceedings-pdf/20IPTC/2-20IPTC/D021S025R002/2285472/iptc-19600-ms.pdf/1

[71] M. Mohajeri, M. Hemmati, and A. S. Shekarabi, "An experimental study on using a nanosurfactant in an EOR process of heavy oil in a fractured micromodel," *J Pet Sci Eng*, vol. 126, pp. 162–173, Feb. 2015, doi: 10.1016/j.petrol.2014.11.012.

[72] F. Sagala and N. N. Nassar, "Nanoparticles for Drilling, Cementing, Hydraulic Fracturing, and Well Stimulation Fluids," 2021, pp. 359–380. doi: 10.1007/978-3-319-12051-5_10.

[73] H. Ehtesabi, M. M. Ahadian, and V. Taghikhani, "Enhanced Heavy Oil Recovery Using TiO 2 Nanoparticles: Investigation of Deposition during Transport in Core Plug," *Energy & Fuels*, vol. 29, no. 1, pp. 1–8, Jan. 2015, doi: 10.1021/ef5015605.

[74] R. D. Shah, "Application of Nanoparticle Saturated Injectant Gases for EOR of Heavy Oils," in *All Days*, SPE, Oct. 2009. doi: 10.2118/129539-STU.

[75] M. Y. Kanj, Md. H. Rashid, and E. P. Giannelis, "Industry First Field Trial of Reservoir Nanoagents," in *All Days*, SPE, Sep. 2011. doi: 10.2118/142592-MS.

[76] D. López, L. J. Giraldo, E. F. Lucas, M. Riazi, C. A. Franco, and F. B. Cortés, "Cardanol/SiO 2 Nanocomposites for Inhibition of Formation Damage by Asphaltene Precipitation/Deposition in Light Crude Oil Reservoirs. Part I: Novel Nanocomposite Design Based on SiO 2 –Cardanol Interactions," *Energy & Fuels*, vol. 34, no. 6, pp. 7048–7057, Jun. 2020, doi: 10.1021/acs.energyfuels.0c01114.

[77] Y. Kazemzadeh, S. E. Eshraghi, K. Kazemi, S. Sourani, M. Mehrabi, and Y. Ahmadi, "Behavior of Asphaltene Adsorption onto the Metal Oxide Nanoparticle Surface and Its Effect on Heavy Oil Recovery," *Ind Eng Chem Res*, vol. 54, no. 1, pp. 233–239, Jan. 2015, doi: 10.1021/ie503797g.

[78] R. Parsaei, Y. Kazemzadeh, and M. Riazi, "Study of Asphaltene Precipitation during CO2 Injection into Oil Reservoirs in the Presence of Iron Oxide Nanoparticles by Interfacial Tension and Bond Number Measurements," *ACS Omega*, vol. 5, no. 14, pp. 7877–7884, Apr. 2020, doi: 10.1021/acsomega.9b04090.

[79] N. N. Nassar, A. Hassan, and P. Pereira-Almao, “Metal Oxide Nanoparticles for Asphaltene Adsorption and Oxidation,” *Energy & Fuels*, vol. 25, no. 3, pp. 1017–1023, Mar. 2011, doi: 10.1021/ef101230g.

[80] O. E. Medina, C. Olmos, S. H. Lopera, F. B. Cortés, and C. A. Franco, “Nanotechnology Applied to Thermal Enhanced Oil Recovery Processes: A Review,” *Energies (Basel)*, vol. 12, no. 24, p. 4671, Dec. 2019, doi: 10.3390/en12244671.

[81] M. Alhreez and D. Wen, “Controlled releases of asphaltene inhibitors by nanoemulsions,” *Fuel*, vol. 234, pp. 538–548, Dec. 2018, doi: 10.1016/j.fuel.2018.06.079.

[82] J. J. Adams, “Asphaltene Adsorption, a Literature Review,” *Energy & Fuels*, vol. 28, no. 5, pp. 2831–2856, May 2014, doi: 10.1021/ef500282p.

[83] B. J. Abu Tarboush and M. M. Husein, “Adsorption of asphaltenes from heavy oil onto in situ prepared NiO nanoparticles,” *J Colloid Interface Sci*, vol. 378, no. 1, pp. 64–69, Jul. 2012, doi: 10.1016/j.jcis.2012.04.016.

[84] N. Setoodeh, P. Darvishi, and A. Lashanizadegan, “Enhancing of asphaltene adsorption onto Fe3O4 nanoparticles coated with metal-organic framework Mil-101 (Cr) for the inhibition of asphaltene precipitation,” *J Dispers Sci Technol*, vol. 39, no. 3, pp. 452–459, Mar. 2018, doi: 10.1080/01932691.2017.1326310.

[85] N. N. Nassar, A. Hassan, L. Carbognani, F. Lopez-Linares, and P. Pereira-Almao, “Iron oxide nanoparticles for rapid adsorption and enhanced catalytic oxidation of thermally cracked asphaltenes,” *Fuel*, vol. 95, pp. 257–262, May 2012, doi: 10.1016/j.fuel.2011.09.022.

[86] S. Betancur, J. C. Carmona, N. N. Nassar, C. A. Franco, and F. B. Cortés, “Role of Particle Size and Surface Acidity of Silica Gel Nanoparticles in Inhibition of Formation Damage by Asphaltene in Oil Reservoirs,” *Ind Eng Chem Res*, vol. 55, no. 21, pp. 6122–6132, Jun. 2016, doi: 10.1021/acs.iecr.6b01187.

[87] N. S. Rayeni, M. Imanivarnosfaderani, A. Rezaei, and S. Rezaei Gomari, “An experimental study of the combination of smart water and silica nanoparticles to improve the recovery of asphaltenic oil from carbonate reservoirs,” *J Pet Sci Eng*, vol. 208, Jan. 2022, doi: 10.1016/j.petrol.2021.109445.

[88] M. A. Ahmadi, Z. Ahmad, L. T. K. Phung, T. Kashiwao, and A. Bahadori, “Evaluation of the ability of the hydrophobic nanoparticles of SiO2 in the EOR process through carbonate rock samples,” *Pet Sci Technol*, vol. 34, no. 11–12, pp. 1048–1054, Jun. 2016, doi: 10.1080/10916466.2016.1148052.

[89] F. Mahmoudi Alemi, S. A. Mousavi Dehghani, A. Rashidi, N. Hosseinpour, and S. Mohammadi, “Potential Application of Fe2O3and Functionalized SiO2Nanoparticles for Inhibiting Asphaltene Precipitation in Live Oil at Reservoir Conditions,” *Energy and Fuels*, vol. 35, no. 7, pp. 5908–5924, Apr. 2021, doi: 10.1021/acs.energyfuels.1c00060.

[90] C. J. Jia *et al.*, “Co3O4 - SiO2 Nanocomposite: A very active catalyst for co oxidation with unusual catalytic behavior,” *J Am Chem Soc*, vol. 133, no. 29, pp. 11279–11288, Jul. 2011, doi: 10.1021/ja2028926.

[91] J. V. Clavijo, I. Moncayo-Riascos, M. Husein, S. H. Lopera, C. A. Franco, and F. B. Cortés, “Theoretical and Experimental Approach for Understanding the Interactions among SiO2Nanoparticles, CaCO3, and Xanthan Gum Components of Water-Based Mud,” *Energy and Fuels*, vol. 35, no. 6, pp. 4803–4814, Mar. 2021, doi: 10.1021/acs.energyfuels.0c03898.

[92] A. K. Manshad, J. A. Ali, O. M. Haghighi, S. Mohammad Sajadi, and A. Keshavarz, “Oil recovery aspects of ZnO2/SiO2 nano-clay in the carbonate reservoir,” *Fuel*, vol. 307, Jan. 2022, doi: 10.1016/j.fuel.2021.121927.

[93] N. N. Nassar, A. Hassan, and P. Pereira-Almao, “Metal oxide nanoparticles for asphaltene adsorption and oxidation,” *Energy and Fuels*, vol. 25, no. 3, pp. 1017–1023, Mar. 2011, doi: 10.1021/ef101230g.

[94] M. Mohammadi, M. Dadvar, and B. Dabir, “TiO2/SiO2 nanofluids as novel inhibitors for the stability of asphaltene particles in crude oil: Mechanistic understanding, screening, modeling, and optimization,” *J Mol Liq*, vol. 238, pp. 326–340, Jul. 2017, doi: 10.1016/j.molliq.2017.05.014.

[95] S. Ansari *et al.*, “Experimental measurement and modeling of asphaltene adsorption onto iron oxide and lime nanoparticles in the presence and absence of water,” *Sci Rep*, vol. 13, no. 1, Dec. 2023, doi: 10.1038/s41598-022-27335-z.

[96] Y. Kazemzadeh, M. R. Malayeri, M. Riazi, and R. Parsaei, “Impact of Fe3O4 nanoparticles on asphaltene precipitation during CO2 injection,” *J Nat Gas Sci Eng*, vol. 22, pp. 227–234, Jan. 2015, doi: 10.1016/j.jngse.2014.11.033.

[97] N. Setoodeh, P. Darvishi, and F. Esmaeilzadeh, “Adsorption of asphaltene from crude oil by applying polythiophene coating on Fe3O4 nanoparticles,” *J Dispers Sci Technol*, vol. 39, no. 4, pp. 578–588, Apr. 2018, doi: 10.1080/01932691.2017.1339607.

[98] K. Jlassi, S. Chandran, M. A. Poothanari, M. Benna-Zayani, S. Thomas, and M. M. Chehimi, “Clay/Polyaniline Hybrid through Diazonium Chemistry: Conductive Nanofiller with Unusual Effects on Interfacial Properties of Epoxy Nanocomposites,” *Langmuir*, vol. 32, no. 14, pp. 3514–3524, Apr. 2016, doi: 10.1021/acs.langmuir.5b04457.

[99] A. Heydari and H. Sheibani, “Fabrication of poly(β-cyclodextrin-co-citric acid)/bentonite clay nanocomposite hydrogel: thermal and absorption properties,” *RSC Adv*, vol. 5, no. 100, pp. 82438–82449, Sep. 2015, doi: 10.1039/c5ra12423a.

[100] J. Nones, H. G. Riella, A. G. Trentin, and J. Nones, “Effects of bentonite on different cell types: A brief review,” *Applied Clay Science*, vol. 105–106. Elsevier Ltd, pp. 225–230, Mar. 01, 2015. doi: 10.1016/j.clay.2014.12.036.

[101] N. G. Almstead *et al.*, “Design, synthesis, and biological evaluation of potent thiazine- and thiazepine-based matrix metalloproteinase inhibitors,” *J Med Chem*, vol. 42, no. 22, pp. 4547–4562, Nov. 1999, doi: 10.1021/jm990330y.

[102] S. D. Chaudhari *et al.*, “Engineering of heterojunction TiO2/CaIn2S4@rGO novel nanocomposite for rapid photodegradation of toxic contaminants,” *Journal of Industrial and Engineering Chemistry*, vol. 114, pp. 305–316, Oct. 2022, doi: 10.1016/j.jiec.2022.07.020.

[103] T. Jafari Behbahani and Z. Behbahani, “A new study on asphaltene adsorption in porous media,” *Petroleum and Coal*, vol. 56, pp. 459–466, Jan. 2014.

[104] R. B. Long and J. Griffel, “Selective Removal of Coke Precursor from Hydrocarbon Feedstock,” 4624776, Nov. 25, 1986

[105] G. González and M. B. C. Moreira, “The wettability of mineral surfaces containing adsorbed asphaltene,” *Colloids and Surfaces*, vol. 58, no. 3, pp. 293–302, Sep. 1991, doi: 10.1016/0166-6622(91)80229-H.

[106] T. Pernyeszi, Á. Patzkó, O. Berkesi, and I. Dékány, “Asphaltene adsorption on clays and crude oil reservoir rocks,” *Colloids Surf A Physicochem Eng Asp*, vol. 137, no. 1–3, pp. 373–384, Jun. 1998, doi: 10.1016/S0927-7757(98)00214-3.

[107] A. W. Marczewski and M. Szymula, “Adsorption of asphaltenes from toluene on mineral surface,” *Colloids Surf A Physicochem Eng Asp*, vol. 208, no. 1–3, pp. 259–266, Aug. 2002, doi: 10.1016/S0927-7757(02)00152-8.

[108] J. S. Buckley, “WETTING ALTERATION OF SOLID SURFACES BY CRUDE OILS AND THEIR ASPHALTENES,” 1998.

[109] S. T. Dubey and M. H. Waxman, “Asphaltene Adsorption and Desorption From Mineral Surfaces,” *SPE Reservoir Engineering*, vol. 6, no. 03, pp. 389–395, Aug. 1991, doi: 10.2118/18462-PA.

[110] F. Melo Faus, P. Grange, and B. Delmon, “Influence of asphaltene deposition on catalytic activity of cobalt molybdenum on alumina catalysts,” *Appl Catal*, vol. 11, no. 2, pp. 281–293, Jan. 1984, doi: 10.1016/S0166-9834(00)81886-2.

[111] A. D. Olaitan *et al.*, “Transition metal oxide nanoparticles as surfaces for surface-assisted laser desorption/ionization mass spectrometry of asphaltenes,” *Pet Sci Technol*, vol. 35, no. 19, pp. 1917–1924, Oct. 2017, doi: 10.1080/10916466.2017.1370476.

[112] S. Kokal, T. Tang, L. Schramm, and S. Sayegh, “Electrokinetic and adsorption properties of asphaltenes,” *Colloids Surf A Physicochem Eng Asp*, vol. 94, no. 2–3, pp. 253–265, Jan. 1995, doi: 10.1016/0927-7757(94)03007-3.

[113] D. M. Clementz, “Interaction of Petroleum Heavy Ends with Montmorillonite,” *Clays Clay Miner*, vol. 24, no. 6, pp. 312–319, 1976, doi: 10.1346/CCMN.1976.0240607.

[114] H. Labrador, Y. Fernández, J. Tovar, R. Muñoz, and J. C. Pereira, “Ellipsometry Study of the Adsorption of Asphaltene Films on a Glass Surface,” *Energy & Fuels*, vol. 21, no. 3, pp. 1226–1230, May 2007, doi: 10.1021/ef060375r.

[115] F. Melo Faus, P. Grange, and B. Delmon, “Influence of asphaltene deposition on catalytic activity of cobalt molybdenum on alumina catalysts,” *Appl Catal*, vol. 11, no. 2, pp. 281–293, Jan. 1984, doi: 10.1016/S0166-9834(00)81886-2.

[116] M. Thommes *et al.*, “Physisorption of gases, with special reference to the evaluation of surface area and pore size distribution (IUPAC Technical Report),” *Pure and Applied Chemistry*, vol. 87, no. 9–10, pp. 1051–1069, Oct. 2015, doi: 10.1515/pac-2014-1117.

[117] Rahman, Muttakin, Pal, Shafiullah, and Saha, “A Statistical Approach to Determine Optimal Models for IUPAC-Classified Adsorption Isotherms,” *Energies (Basel)*, vol. 12, no. 23, p. 4565, Nov. 2019, doi: 10.3390/en12234565.

[118] D. Dudášová, S. Simon, P. V. Hemmingsen, and J. Sjöblom, “Study of asphaltenes adsorption onto different minerals and clays,” *Colloids Surf A Physicochem Eng Asp*, vol. 317, no. 1–3, pp. 1–9, Mar. 2008, doi: 10.1016/j.colsurfa.2007.09.023.

[119] N. Hosseinpour, A. A. Khodadadi, A. Bahramian, and Y. Mortazavi, “Asphaltene Adsorption onto Acidic/Basic Metal Oxide Nanoparticles toward in Situ Upgrading of Reservoir Oils by Nanotechnology,” *Langmuir*, vol. 29, no. 46, pp. 14135–14146, Nov. 2013, doi: 10.1021/la402979h.

[120] N. L. Ezeonyeka, “Evaluation of Measurement Techniques for the Adsorption of Asphaltenes onto Metal Oxide Nanoparticles.” 2018. doi: http://dx.doi.org/10.11575/PRISM/31961.

[121] B. Irvinq Langmuir, “ADSORPTION OF GASBS ON GLASS, MICA AND PLATINUM. THE ADSORPTION OF GASES ON PLANE SURFACES OF GLASS, MICA AND PLATINUM.” [Online]. Available: https://pubs.acs.org/sharingguidelines

[122] P. J. Quinlan, “The design and optimization of sustainable biopolymer-based adsorbents for the removal of a model aromatic naphthenic acid from aqueous solution Asphalt rejuvenators View project”, doi: 10.13140/RG.2.1.4268.1448.

[123] G. Verma and M. Mishra, “DEVELOPMENT AND OPTIMIZATION OF UV-VIS SPECTROSCOPY-A REVIEW,” *Govinda et al. World Journal of Pharmaceutical Research*, vol. 7, 2018, doi: 10.20959/wjpr201811-12333.

[124] “Mechanisms of UV Stabilization.”

[125] S. Tazikeh, J. Sayyad Amin, and S. Zendehboudi, “Experimental study of asphaltene precipitation and metastable zone in the presence of polythiophene-coated Fe3O4 nanoparticles,” *J Mol Liq*, vol. 301, Mar. 2020, doi: 10.1016/j.molliq.2019.112254.

[126] F. Shojaati, M. Riazi, S. H. Mousavi, and Z. Derikvand, “Experimental investigation of the inhibitory behavior of metal oxides nanoparticles on asphaltene precipitation,” *Colloids Surf A Physicochem Eng Asp*, vol. 531, pp. 99–110, Oct. 2017, doi: 10.1016/j.colsurfa.2017.07.087.

[127] M. Kutz, “TGA,” in *Handbook of Measurement in Science and Engineering*, John Wiley & Sons, 2013, pp. 744–747.

[128] “Designation: D 6560-00 Designation: IP 143/01 Standard Test Method for Determination of Asphaltenes (Heptane Insolubles) in Crude Petroleum and Petroleum Products 12.”

[129] J.-C. Poveda, D.-R. Molina, and E.-F. Pantoja-Agreda, “H-AND 13 C-NMR STRUCTURAL CHARACTERIZATION OF ASPHALTENES FROM VACUUM RESIDUA MODIFIED BY THERMAL CRACKING,” 2014.

[130] I. Zojaji, A. Esfandiarian, and J. Taheri-Shakib, “Toward molecular characterization of asphaltene from different origins under different conditions by means of FT-IR spectroscopy,” *Adv Colloid Interface Sci*, vol. 289, p. 102314, 2021, doi: https://doi.org/10.1016/j.cis.2020.102314.

[131] M. M. Modena, B. Rühle, T. P. Burg, and S. Wuttke, “Nanoparticle Characterization: What to Measure?,” *Advanced Materials*, vol. 31, no. 32, p. 1901556, Aug. 2019, doi: https://doi.org/10.1002/adma.201901556.

[132] S. Rades *et al.*, “High-resolution imaging with SEM/T-SEM, EDX and SAM as a combined methodical approach for morphological and elemental analyses of single engineered nanoparticles,” *RSC Adv.*, vol. 4, no. 91, pp. 49577–49587, Oct. 2014, doi: 10.1039/C4RA05092D.

[133] “BET Specific Surface Area.”

[134] F. Ambroz, T. J. Macdonald, V. Martis, and I. P. Parkin, “Evaluation of the BET theory for the characterization of meso and microporous MOFs,” *Small Methods*, vol. 2, no. 11. John Wiley and Sons Inc, 2018. doi: 10.1002/smtd.201800173.

[135] J. Zou *et al.*, “A preliminary study on assessing the Brunauer-Emmett-Teller analysis for disordered carbonaceous materials,” *Microporous and Mesoporous Materials*, vol. 327, Nov. 2021, doi: 10.1016/j.micromeso.2021.111411.

[136] B. Akbari, M. Pirhadi Tavandashti, and M. Zandrahimi, “PARTICLE SIZE CHARACTERIZATION OF NANOPARTICLES – A PRACTICALAPPROACH,” 2011.

[137] J. Epp, “X-Ray Diffraction (XRD) Techniques for Materials Characterization,” in *Materials Characterization Using Nondestructive Evaluation (NDE) Methods*, Elsevier Inc., 2016, pp. 81–124. doi: 10.1016/B978-0-08-100040-3.00004-3.

[138] K. Thamaphat, P. Limsuwan, and B. Ngotawornchai, “Phase Characterization of TiO 2 Powder by XRD and TEM,” 2008.

[139] M. Tavakkoli *et al.*, “Indirect method: A novel technique for experimental determination of asphaltene precipitation,” *Energy and Fuels*, vol. 29, no. 5, pp. 2890–2900, May 2015, doi: 10.1021/ef502188u.

[140] R. B. P. Joseph D. Menczel, *Thermal analysis of polymers. Fundamentals and applications*. John Wiley & Sons, 2009.

[141] S. Subhapriya and P. Gomathipriya, “Green synthesis of titanium dioxide (TiO2) nanoparticles by Trigonella foenum-graecum extract and its antimicrobial properties,” *Microb Pathog*, vol. 116, pp. 215–220, Mar. 2018, doi: 10.1016/j.micpath.2018.01.027.

[142] C. Zhang *et al.*, “Novel insights into the hydroxylation behaviors of α-quartz (101) surface and its effects on the adsorption of sodium oleate,” *Minerals*, vol. 9, no. 7, Jul. 2019, doi: 10.3390/min9070450.

[143] Munasir, Triwikantoro, M. Zainuri, and Darminto, “Synthesis of SiO2 nanopowders containing quartz and cristobalite phases from silica sands,” *Materials Science- Poland*, vol. 33, no. 1, pp. 47–55, Mar. 2015, doi: 10.1515/msp-2015-0008.

[144] J. Abisharani and Rd. Kumar, “Green synthesis of TiO 2 Nanoparticles using Cucurbita pepo seeds extract,” 2019. [Online]. Available: www.sciencedirect.comwww.materialstoday.com/proceedings2214-7853

[145] N. K. Sethy, Z. Arif, P. K. Mishra, and P. Kumar, “Green synthesis of TiO_2 nanoparticles from Syzygium cumini extract for photo-catalytic removal of lead (Pb) in explosive industrial wastewater,” *Green Processing and Synthesis*, vol. 9, no. 1, pp. 171–181, Feb. 2020, doi: 10.1515/gps-2020-0018.

[146] A. B. D. Nandiyanto, R. Oktiani, and R. Ragadhita, “How to read and interpret ftir spectroscope of organic material,” *Indonesian Journal of Science and Technology*, vol. 4, no. 1, pp. 97–118, 2019, doi: 10.17509/ijost.v4i1.15806.

[147] M. J. Díaz, M. Ruiz-Montoya, A. Palma, and M. V. de-Paz, “Thermogravimetry applicability in compost and composting research: A review,” *Applied Sciences (Switzerland)*, vol. 11, no. 4, pp. 1–15, Feb. 2021, doi: 10.3390/app11041692.

[148] D. Eliche-Quesada, F. A. Corpas-Iglesias, L. Pérez-Villarejo, and F. J. Iglesias-Godino, “Recycling of sawdust, spent earth from oil filtration, compost and marble residues for brick manufacturing,” *Constr Build Mater*, vol. 34, pp. 275–284, Sep. 2012, doi: 10.1016/j.conbuildmat.2012.02.079.

[149] N. Hosseinpour, Y. Mortazavi, A. Bahramian, L. Khodatars, and A. A. Khodadadi, “Enhanced pyrolysis and oxidation of asphaltenes adsorbed onto transition metal oxides nanoparticles towards advanced in-situ combustion EOR processes by nanotechnology,” *Appl Catal A Gen*, vol. 477, pp. 159–171, May 2014, doi: 10.1016/j.apcata.2014.03.017.

[150] J. H. Flynn, “The isoconversional method for determination of energy of activation at constant heating rates,” *Journal of Thermal Analysis*, vol. 27, no. 1, pp. 95–102, May 1983, doi: 10.1007/BF01907325.